THEORY OF LOW ENERGY

ELECTRON DIFFRACTION

by

A. M. GIBBONS

A dissertation submitted

to the University of Warwick for

admission to the degree of

Doctor of Philosophy

MEMORANDUM

This dissertation is submitted to the University of Warwick in support of my application for admission to the degree of Doctor of Philosophy. It contains an account of my own work performed at the School of Physics of the University of Warwick in the period October 1965 to October 1968 under the general supervision of Doctor B. W. Holland. No part of it has been used previously in a degree thesis submitted to this or any other university. The work described in this thesis is the result of my own independent research except where specifically acknowledged in the text. Parts of this thesis will be shortly submitted for publication in the journal 'Surface Science'.

A. M. Gibbons

MAY, 1969. A. M. Gibbons

ACKNOWLEDGEMENTS

I am extremely grateful to Doctor B. W. Holland for his continued interest and encouragement throughout the course of this work and in the preparation of this thesis. I wish to thank also Professor A. J. Forty for making the facilities of the School of Physics at the University of Warwick available to me. Furthermore, I would like to thank all those members of the School of Physics, and in particular, the members of the surface physics group, who have been available for discussion.

My thanks are due to the Science Research Council for providing the financial support of a Research Studentship.

Finally, I wish to thank Miss M. Burton for her skill and great patience in the typing of this thesis and Miss C. A. Phillips for her careful preparation of the diagrams.

ABSTRACT

An understanding of Low Energy Electron Diffraction has been sought using an energy band structure formalism. The approach, which matches wavefunctions at the vacuum/crystal interface, is similar to that first used by Sommerfeld and Bethe (5). However, following Heine (8), we have included complete sets of matching functions at the crystal boundary and on this basis derived formal expressions for the reflected intensities.

Previous theories have tended to ignore the inner potential as a source of internal reflections. Not accepting the usual rationale that the inner potential merely requires us to apply an energy correction to the observed peak positions, we have shown that its inclusion in the formalism leads to a modification of the relative intensities of the diffraction spots and to additional scattering mechanisms. In particular it has been shown that the presence of the inner potential leads to a particularly simple mechanism for the production of pronounced secondary Bragg peaks. On the grounds that the inelastic scattering would damp out processes of high order in the multiple scattering this particular mechanism has been assumed to be the most dominant. Some justification has been found in a discussion of Taylor's (28) results for Cu (111). This discussion demonstrates that the mechanism for secondary Bragg peaks proposed by Boudreaux and Heine (14) predicts too

many peaks in practice. It has also been shown that their mechanism is inappropriate in a large number of cases where the inner potential does not even approximately allow a single Bloch function to describe the total wavefunction in the crystal.

A calculation has been performed which demonstrates that the particular surface resonance mechanism of Boudreaux and Heine (14) is likely to be unimportant in practice. This is of course in accordance with the emphasis of these authors. The work of Duke and Tucker (4) has shown that, in any case, the surface resonances should be damped out by the inelastic scattering. We have tentatively suggested an alternative mechanism for the peaks observed by McRae and Caldwell (16) which they interpret as resonance peaks.

Our qualitative and quantitative results obtained by using our formalism and by taking the Bloch states in the crystal to zero order haveled us to develop a simple theory for predicting the positions of intensity peaks in the specular reflectivity. This theory is closely related to that of Marcus/Jona and Jepsen (20) but specifically incorporates our ideas onwhich secondary Bragg peaks will be appreciably intense. The theory has been used in an attempt to interpret the experimental results of McRae and Caldwell for lithium fluoride (9) and sodium fluoride (16). From the misfit in this comparison between theory and experiment we have suggested that our initial assumption (that the NFE approximation may be a reasonable first approach at the energies of LEED) is not correct.

Finally, although we believe that the band-structure approach gives a good 'physical feel' for the LEED problem, we give reasons which suggest that ultimately it will not provide the best means of calculating LEED intensities with any accuracy. The most important of these is that we believe the elastic and inelastic scattering should be treated on an equal basis, and, as Duke and Tucker (4) have indicated, the inelastic scattering makes a Bloch wave description inappropriate at the energies in LEED.

CONTENTS

CHAPTER I

Introduction

A. Low Energy Electron Diffraction (LEED): Idealised and Real Experiments

LEED is the elastic back-scattering of low energy electrons by crystals. In this context low-energy denotes electron energies of 100 eV or less.

The discovery that diffraction patterns are produced when low-energy electrons are scattered by crystals was made by Davisson and Germer (1) in 1927. The technical difficulties of performing LEED experiments led to a postponement of activity until fairly recent years. Consequently the vast bulk of the literature concerned with electron diffraction is devoted to high energy, transmission, electron microscopy.

Many experiments have shown that LEED phenomena are sensitive to the nature of the crystal surface under investigation (2). The strong inelastic scattering processes confine the incident electrons with the incident energy to within a few atomic layers of the crystal surface (2). Thus, in principle, LEED can be used to determine the average surface structure of crystals just as X-rays are used to determine the average bulk structure. The chief limitation of the usefulness of LEED is that the interaction of low energy electrons with crystal surfaces is not well understood. In the next section we outline some current theories.

In an idealised LEED experiment a monoenergetic and perfectly collinated beam of electrons impinges on a crystal surface which has perfect periodicity in two dimensions. The elastically back-scattered electrons form a diffraction pattern. The quantities measured are the diffracted directions and the flux densities associated with diffracted beams as the energy and angle of incidence are varied.

In real LEED experiments the crystal surface is usually prepared so as to approximate as closely as possible to the ideal, perfectly periodic, structure. Experimentally one cannot prepare surfaces which are atomically flat. Surfaces may also exhibit faceting; and of course, dislocations of the bulk crystal with edge components in the surface will disrupt the surface periodicity. Finally, as far as the surface is concerned, it is only quite recently that the advent of Auger spectroscopy has allowed the chemical purity of the surface to be known with any certainty.

As far as the electron beam is concerned, it can at worst, contain an energy spread of ten percent and a divergence of about one degree. The crystal surface area over which the primary beam is coherent is the so-called coherence zone. In an ideal experiment the coherence zone is the same as the cross-sectional area of the primary beam. In practice, however, the time incoherence (brought about by the energy spread in the incident beam) and the space incoherence (divergence in the incident beam) reduce the coherence zone to about 10^{6}Å^{2} (3). Typically, the cross-sectional

area of the beam at the crystal is $10^{14}\,\text{Å}^2$. One then has to imagine each coherence zone in the cross-sectional area of the beam producing its own diffraction pattern. A superposition of such patterns forms the observed pattern which is consequently a blurred edition of the ideal pattern.

B. Current Theories

We now present a synopsis of LEED theory. No pretence is made that this is an exhaustive survey. Only those theories, which have an historical pertinence or are at the centre of current trends, are discussed.

The most recent theories can, in general, be placed into one of two groups: those which use a band-structure formalism or those which use the so-called multiple scattering approach. The underlying theme in both is that the large elastic scattering cross-sections, associated with the electrons incident on a crystal in LEED, make it highly probable that an incident electron suffers several collisions in the crystal before being ejected. The incorporation of such effects is accomplished in the band-structure approach by describing the electrons in the crystal by Bloch waves, which are produced when the periodic potential multiply-scatters a plane-wave. In the multiple scattering approach, the crystal is considered to be the sum of individual scatterers; the electron field incident on an individual scatterer is described as the addition of the incident wave and the sum of all the waves scattered from the other scatterers in the crystal.

Apart from the theory of Duke and Tucker (4), it is a common assumption that, in the crystal, the electron moves in a static periodic potential where the electron-ion-core interaction dominates all the other interactions. Clearly the periodicity of the ion-core lattice is an essential requirement for the prediction of a diffraction pattern, but it is not at all clear that the exclusion, for example, of the electron-electron interaction will allow the theories to predict correctly the behaviour of the intensity of a particular diffracted beam as a function of incident energy and angle of incidence. As Duke and Tucker (4) have pointed out, the motivation for excluding inelastic scattering processes is provided by the idea proposed in the early years of the quantum theory of solids that the strong scattering of electrons by atoms, as opposed to the weak atomic scattering of X-rays, is the physical origin of the qualitative difference between the observed LEED and X-ray scattered intensities. Results obtained since 1950, using many-body theories of the electron-electron interaction render the assumption invalid for a modern theory. The present discussion provides what is probably the severest criticism that can be levelled at current theories. It is clear, however, that the exclusion of inelastic scattering still allows qualitative predictions to be made which are empirically confirmed.

We now proceed to look in more detail at particular theories.

The first proponents of an electron diffraction theory were essentially Sommerfeld and Bethe (5), although certain expositions had already been given by Bethe (6) and Morse (7). A model was chosen in which the crystal

consisted of a rigid, perfectly periodic potential contained between two planes at $z = 0$ and $z = D$. For $z < 0$ and $z > D$, the vacuum was represented by a constant potential. The basic idea was to write down the physically appropriate solutions of the Schrödinger equation in the regions $z < 0$, $0 < z < D$, $z > D$, then by requiring the wavefunctions to be smooth and continuous at $z = 0$ and $z = D$, to find the amplitudes of the reflected and transmitted waves.

Taking the incident-wave to be a plane-wave, a formal solution for the intensities was found. The first major result contained in the formalism is that the geometry of the diffraction pattern is completely determined by the energy and the reduced value of the wave-vector parallel to the crystal surface, which are both constants of the motion.

However, the formalism does have one defect, Sommerfeld and Bethe recognised that the boundary conditions at $z = 0$ and $z = D$ are unlikely to be satisfied by taking a single Bloch function in the metal, and thus took a linear combination of such functions. However, it is claar that they did not realise that such a sum, for real wave-vector, contains a small number of terms. Indeed they were not aware of how to construct a complete set of states for matching at $z = 0$ and $z = D$. Heine (8), in a paper on the general theory of surface states and the scattering of electrons in solids, has now resolved this problem.

The rest of the qualitative, and quantitative results obtained by Sommerfeld and Bethe were obtained when they used a particular model

in which the crystal potential was separable. Then, as an approximation, they described the wavefunction for $z < 0$, by an incident plus a specularly reflected plane-wave, while for $z > D$ they took a single specularly transmitted plane-wave. This description essentially involves the Born approximation which inhibits multiple scattering and thus the analysis is inappropriate for the energies of interest in LEED. This analysis did, however, provide a description of Bragg peaks in the specular reflectivity and of anomalous dispersion reported by Davisson and Germer. We note, however, that much more structure is seen in the reflectivity curves than that due to Bragg peaks.

Before going on to discuss more recent theories, we make some brief remarks concerning the kinematical theory. Despite the obvious limitation through the Born approximation, it has been suggested that LEED intensities can be related to the crystal surface structure through simple modifications of the kinematical theory (2). One finds, for example, a modified structure factor:

$$F_{hk}(\lambda,\theta) = \sum_j t_j(\tau)\, f_j \exp 2\pi i \left[hx_j + ky_j + \{1+\cos\theta_{hk}\}\frac{z_j}{\lambda}\right] \qquad 1.1$$

where j labels atoms in a column perpendicular to the crystal surface with a cross-sectional area equal to that of the unit mesh. This equation is shown for the situation of normal incidence. It does not require periodicity in the z-direction. The factor $t_j(\tau)$ accounts for absorption phenomenalogically and depends on the 'visibility' of the j^{th} atom from above the surface. Such a structure factor has been used to predict fractional order peaks (see (2)). Several authors ((11) and (12) for

example), have used the modified kinematical theory with apparent success, others (9) and (10) for example) have shown that it is not capable of accounting for the detailed variation of the intensity versus energy curves.

We come now to the more recent theories. These account for the multiple scattering in a consistent manner. We start with the work of McRae (13).

McRae's theory ((13) - 1966) is formulated on the basis of Lax's (35) multiple scattering equations. The formulation is self consistent and is thus applicable regardless of the magnitude of the atomic scattering factors. Lax's equations describe the total field as an addition of the incident wave and the fields emitted by all the atoms. The formal algebra of McRae ((13) - 1966) is essentially, to determine the total field at a distance remote from the crystal. The final outcome is a dynamical structure factor of the form:

$$F(\underline{k}_r^- + \underline{k}) = \sum_s \alpha^s \langle f^s(\underline{k}_r^- + \underline{k})\rangle \exp i(\underline{k}-\underline{k}_r^-).\underline{R}_s \qquad 1.2$$

where the sum over s means the same as the sum over j in 1.1. We see that 1.1 and 1.2 are of the same form. The attenuation coefficient $t_j(\tau)$, is replaced by the ratio of the reduced effective field to the primary field at the s^{th} atom, α^s. The optical theorem in general scattering theory provides that the forward scattered wave always interferes with the incident wave in a destructive manner (a necessary condition for flux conservation). Thus, there is always attenuation of the elastic field in the forward direction whether or not inelastic scattering is considered. Also, in

1.2, the effective atomic scattering factor, $\langle f^s(\underline{k}' \leftarrow \underline{k})\rangle$, replaces the atomic scattering factor, f_j, of 1.1. This effective atomic scattering factor has to be evaluated self-consistently along with the effective and total fields.

McRae finds that, for small atomic scattering cross-sections, the theory gives the same results as the kinematical theory. For large atomic scattering cross-sections two new types of peaks are obtained. The first is a specular reflectivity peak at an energy less than that at which the first non-specular reflected beam is allowed. This peak is associated with a multiple scattering resonance in a single atomic layer and is referred to as a resonance peak. Secondly, McRae finds what he terms sequencies of secondary Bragg peaks. These arise out of the interference (beating) between plane-wave components of the effective field, the resulting modulation of the wave-field can be though of, kinematically, as superimposing a dynamical potential upon the crystal potential.

McRae and Caldwell (16) have been able to detect peaks in specular reflectivity curves which have locations depending on the primary beam orientation in precisely the manner predicted by McRae ((13) - 1966) for resonance peaks. As McRae points out there is a basic difficulty in understanding the presence of such peaks because his analysis depends essentially on there being coherent contributions to the effective field from a large number of atoms in a layer parallel to the crystal surface. In actual experiments, the so-called coherence-zone area should not enclose a sufficiently large number of atoms to give rise to the resonance effects predicted theoretically.

McRae also demonstrates (36) that not all the sequencies of secondary Bragg peaks are seen in practice. He does this by an inspection of Taylor's results (28) for Cu (111). In each sequence of the secondary Bragg peaks (which are fractional-order Bragg peaks at normal incidence), the order numbers are integer multiples of $\frac{1}{t}$, where t is a fixed integer. The first sequence is characterised by a value of t equal to the ratio, t_1, of the spacing of equivalent atomic layers to the spacing of adjacent atomic layers parallel to the crystal surface. Other sequencies are characterised by $t > t_1$. On the basis that the period of the modulation of the wave-field must be much smaller than the depth of penetration of the incident electrons, McRae suggests that the sequence characterised by t_1 will be most prominent. His comparison with Taylor's results shows that the great majority of the peaks can be interpreted as either fractional order peaks characterised by t_1 or integer order peaks.

Boudreaux and Heine (14) have demonstrated how secondary Bragg peaks and surface resonance peaks can arise on a band-structure formalism of LEED. Their approach is similar to that of Sommerfeld and Bethe (5), except that their 'crystal' is semi-infinite in extent and they take account of the lines of real energy with complex wave-vector described by Heine (8) in the band-structure. They are also able to clear up one point of detail unanswered by McRae ((13) - 1966). For a given surface reciprocal lattice vector, $\underline{g}$, and away from normal incidence, one in principle expects two resonance peaks corresponding to the surface waves: $\exp i (\underline{p}'' \pm \underline{g}).\underline{r}$. However, as Boudreaux and Heine indicate, the amplitude of one of these waves is negligible if the coupling matrix element, $|V_{2\underline{g}}|$,

is larger than the difference in kinetic energy between the two surface waves.

As Heine and Boudreaux stress, the particular surface resonance mechanism they discuss in detail, may not be observed in practice. The presence of a non-zero inner-potential removes the singularity in the amplitude of the propagating Bloch wave in the crystal which occurs in their analysis. It is just this zero in that amplitude which allows complete reflection of the incident flux at the energy of the resonance. Also their mechanism for the secondary Bragg peaks appears to predict far too much structure in the reflectivity curves. This is most easily realised by recollecting McRae's (36) discussion of Taylor's results for Cu (111).

Incidentally, Capart (15) has shown, at least for a cubic array of s-wave scatterers, that the band-structure formalism gives identical results to McRae's formalism. He is also able to correct a wrong assignment by McRae, of the type of mechanism producing a certain peak in McRae's computations ((13) - 1966). Evaluation of the band-structure as a natural step in evaluating LEED intensities ensures that the band-structure approach provides an easier means of indentifying the physical processes in LEED.

Other authors have presented formalisms of the problem which are closely related to those already discussed. The 'propagator-matrix' method of Marcus and Jepsen (19) is essentially a band-structure approach.

The central feature is the setting up of a 'propagation-matrix' which is defined so that its eigenvectors are the complete set of matching wavefunctions required at the crystal boundary. Thus a systematic computational procedure using familiar computing techniques is achieved. The outcome of such calculations shows a strong correlation between the reflectivity and the band-structure, which of course Boudreaux and Heine predict. Marcus/Jona and Jepsen (20) take advantage of this correlation in the development of their 'energy-diagram' technique. They qualitatively predict the occurrence of Bragg and secondary Bragg peaks through the free electron bands. We reserve further comment on this theory until Chapter IV of this thesis where a closely related theory is developed and tested.

Our comments so far have been essentially concerned with the treatment of LEED for crystals with clean, perfect surfaces. The present thesis is solely concerned with this aspect. We note, however, that McRae ((13) 1968a) has extended his work to include a treatment of crystal 'selvedge' effects through a generalisation of Darwin's (25) theory of X-ray scattering. The treatment by Marus/Jona and Jepsen is also easily extended to deal with a crystal selvedge. In fact, (19), they demonstrate that the propagation-matrix is closely related to the reduced transfer matrix of McRae ((13) - 1968a). We note also that Kambe (18) has derived the properties of the reduced transfer matrix (termed the scattering matrix in his more general treatment).

Another formalism of the LEED problem has been given by Beeby (21). His approach is closely related to McRae's (13), and is a T-matrix approach.

It contains the obvious advantage of flexibility in dealing with crystal selvedge effects by separating out the contributions to the reflection amplitudes from the individual atomic planes (actually the 'sub-planes') parallel to the crystal surface. Beeby shows that his formal solution embodies the results of McRae ((13) - 1966). We note that the numerical evaluation of intensities according to Beeby's formalism requires an evaluation of structure factors similar to those found in Kohn-Rostoker band-structure theory.

In conclusion, we briefly report the very recent work of Duke and Tucker (4). Their approach is essentially of the multiple scattering variety, in the same vein as that of Beeby (21), but at the same time involving completely new conceptual ideas. They reject the idea that the interaction of the incident electrons with the ion-cores of the crystal dominate all the other interactions. Rather, they base their model on the observation that, in the energy range of LEED, the electrons are poorly described by Bloch waves. They incorporate this concept in a many body propagator formalism, in which single electron propagators characteristic of an interacting electron fluid are utilised in the description of the electron-lattice interaction. The immediate advantage is that the propagator for an electron in a uniform electron fluid (which is well known from many-body theory) can be used directly in Beeby's (21) theory.

In its present form, Duke and Tucker's theory contains a serious deficiency. It implicity assumes that all diffraction inside the crystal occurs in a uniformelectron fluid which terminates outside the potential

of the outermost ion core. This assumption is clearly inadequate to describe scattering from the first few atomic planes and from localised excitations like surface plasmons.

For our purposes we wish to note two results of Duke and Tucker. First, the mean-free-path, of the incident electrons in LEED, for bulk-plasmon excitation and incoherent particle-hole pair creation is equivalent to only a few lattice spacings. From this we deduce that multiple-scattering phenomena involving many inter-layer collisions are damped out. Secondly, we note that the damping of the elastic wave field removes the singularities in the sub-plane propagators of Beeby (21). These singularities are responsible for the prediction of strong surface resonances. Thus, the resonance phenomenum may not be as pronounced as previously predicted by McRae ((13) - 1966).

C. The Purpose and Content of the Thesis

It is felt that the band-structure approach can provide a good physical understanding of the basic elastic-scattering processes in LEED, and that this aspect has not been fully exploited. An expansion of the Bloch states into plane waves should provide the basis for our comprehension of the physics, this is because one has an intuitive feel for the scattering of plane waves from a 'plane of potential.' Such a 'plane' may be an atomic plane of the bulk crystal or perhaps the inner potential.

Previous theories have tended to ignore the inner potential as far as it may provide a source of internal reflection. Such reflections should not only provide new processes which operate through several reflections between 'potential planes', but should also modify the intensities of the back-scattered beams. An extreme case which emphasises the latter is the phemonenon of total internal reflection. Thus we cannot accept the usual rationale that the inner potential merely requires us to apply an energy correction to the observed peak positions and that it only serves to enhance the specular intensity.

Our first steps are then to develop a formalism embodying the ideas expressed above. The model is necessarily similar to those used previously by Sommerfeld and Bethe (5), and Boudreaux and Heine (14). Indeed, we also use the procedure of matching wavefunctions utilised by these authors. Naturally we include complete sets of matching functions, a necessity emphasised by Heine (8).

Subsequent to our formalism we shall make approximations to the Bloch states in order to make qualitative investigations into the back-scattered intensities. Of course, the mechanism producing Bragg peaks in the specular intensity is well understood. We feel, however, that the production of secondary Bragg peaks requires clarification. The inner potential may play a role in the production of such peaks. We must also emphasise that the mechanisms outlined by other authors ((13) and (14)) predict far too many intensity peaks. We can now, however, exclude those processes of high order in multiple scattering because of the work

of Duke and Tucker (4), which demonstrates the short mean free path of the incident electrons in which the elastic scattering must take place. There is also a difficulty concerning the surface resonance peaks. Despite the remarks of Boudreaux and Heine (14) that their mechanism would probably not operate in practice, and the work of Duke and Tucker (4) which shows that the inelastic scattering should inhibit the resonance, McRae and Caldwell (16) claim to have observed such peaks.

We thus set out with the purpose of establishing a physical understanding of LEED and with a desire to clarify those particular points outlined. We shall find that our initial investigations, both qualitative and quantitative, will suggest a simple formulation of the problem which is similar to that proposed by Marcus/Jona and Jepsen (20). In the penultimate chapter we test our formulation of this simple approach and in the final chapter we provide a synopsis and criticism of our work. Finally, we will outline our suggestions for proceeding with the theoretical investigation of LEED.

CHAPTER II

General Formalism and a Qualitative Discussion of the Structure in LEED Intensities

In section A of this chapter we describe the model appropriate to the formalism of section B, which, in the absence of inelastic scattering, should give an account of the intensities of diffracted beams relative to one another in LEED. In section C, we discuss, in a qualitative way, the structure one might expect to observe in LEED intensities.

A. The Model

The model we choose is described below. We point out the assumptions involved, the most questionable of these are really inherent in any model which excludes inelastic scattering.

(a) We hope the model will provide an account of the relative intensities of the back-scattered beams. No assertion is made regarding the absolute values of the intensities. Inherent in this hope is that the inelastic scattering removes, in proportion, the same amount of flux from all the diffracted beams. Obviously, this is a questionable assumption, but if the elastic scattering model is to be regarded as useful, it must be made.

(b) In LEED, the large inelastic scattering cross-sections confine the volume of crystal, which the incident electrons sample, to

a region close to the face of the crystal upon which the electrons are incident. The presence of the other faces of the crystals does not play a role in the scattering. We therefore choose our model of the crystal to fill a semi-infinite volume. We are thus led to another assumption: that the electron flux which is elastically transmitted by our model crystal must be inelastically scattered in practice.

It seems that, if one is seeking a simple elastic scattering model of LEED, the assumptions embodied in (a) and (b) are inevitable.

We also adopt assumptions concerning the rigid potential making up the vacuum and crystal boundary region in our model.

(c) We take the vacuum to be a region of constant potential filling the half space $x < \alpha$. The crystal has perfect periodicity throughout the region $x > \alpha$. The boundary plane, $x = \alpha$, contains a step in the potential between the vacuum level and the average value in the model crystal; this is equivalent to the inner potential of the real crystal. It is thus assumed that the form (but not the value of the inner potential) that the crystal takes in the boundary region does not unduly effect the relative intensities of the back-scattered beams.

We can now treat the problem as one of solving the Schrödinger equation in both regions and requiring that the solutions join smoothly on to one another at the plane $x = \alpha$. This method of matching the

solutions in both regions was first used, long ago, by Bethe (6); it has recently been revived by Boudreaux and Heine (14).

We could use the NFE-pseudopotential method to determine the solutions of the Schrödinger equation in the crystal. As is well known, the wavefunctions so obtained only approximate to the real wavefunctions outside the ion cores of the atoms of the crystal. We can adjust the position of the matching plane, $x = \alpha$, so that it would lie between two atomic planes in the infinite crystal. In this way we match on to the NFE-pseudo wavefunctions where they best approximate to the real wavefunctions. Then the calculated intensities of the backscattered beams will be unaffected by the poor approximation to the wavefunctions at the ion cores.

B. Formalism

In this section we find expressions for the intensities of the backscattered beams associated with the model described in section A. In appendix II, the forms of the physically appropriate solutions of the Schrödinger equation in the regions $x > \alpha$ and $x < \alpha$ are found.

For $x < \alpha$, we have, from A2.8:

$$\psi_{o,\underline{p}} = A \exp i(\underline{p}+\underline{g}_o'').\underline{r} + \sum_{\underline{g}_m} A(\underline{p}''+\underline{g}_m'')\exp i\left[(\underline{p}''+\underline{g}_m'') - \underline{n}\sqrt{\frac{2mE}{\hbar^2} - (\underline{p}''+\underline{g}_m'')^2}\right].\underline{r} \qquad 2.1$$

where we have now written the wave-vector of the incident wave in the form $(\underline{p} + \underline{g}_o'')$, where $\underline{g}_o''$ is the component of some reciprocal lattice vector parallel to the crystal surface such that $\underline{p}$ is reduced with respect to its surface projection.

Equation A2.14 gives, for $x > \alpha$:

$$\psi_{i,\underline{p}} = \sum_{\underline{g}_m''} D(\underline{p}''+\underline{g}_m'') \, e^{i\underline{k}_m \cdot \underline{r}} \sum_{\underline{g}_n} U_{\underline{g}_n}^{\underline{g}_m} e^{i\underline{g}_n \cdot \underline{r}} \qquad 2.2$$

where, for each Bloch type of solution with coefficient $D(\underline{P}''+\underline{g}_m'')$, equations A2.10 and A2.11 hold. Also $\underline{k}_m''=\underline{p}''$.

If we join $\psi_{o,\underline{p}}$ and $\psi_{i,\underline{p}}$ smoothly on to one another at the crystal boundary, $x = \alpha$, then the requirement that the solution of the Schrödinger equation be everywhere finite and continuous in value and slope will be satisfied. We imagine $x = \alpha$ to lie between two atomic planes in accordance with our previous remarks. The positions of the atomic planes are inherently contained in 2.2 because the $U_{\underline{g}_n}^{\underline{g}_m}$ involve matrix elements of the potential defined by A2.3. It would be most convenient if the Fourier coefficients of this potential, $V_{\underline{g}}$, were determined with $x = 0$ coinciding with one of the atomic planes. Thus a convenient value for α, for example, would be $\alpha = -\frac{d}{2}$, where d is the spacing between adjacent planes in the x-direction.

The smooth joining is ensured by the boundary conditions:

$$\psi_{o,\underline{p}}\Big|_{x=\alpha} = \psi_{i,\underline{p}}\Big|_{x=\alpha} \qquad 2.3$$

and

$$\frac{d\psi_{o,\underline{p}}}{dx}\Big|_{x=\alpha} = \frac{d\psi_{i,\underline{p}}}{dx}\Big|_{x=\alpha} \qquad 2.4$$

Equation 2.3, of course, not only ensures continuity in value, but also in slope in the surface plane.

We now insert 2.1 and 2.2 into 2.3 and 2.4. Equation 2.3 gives

$$A\, e^{i\underline{g}_o''\cdot\underline{r}}\, e^{i\alpha p^{\perp}} + \sum_{\underline{g}_m''} A(\underline{p}''+\underline{g}_n'')\, e^{i\underline{g}_m''\cdot\underline{r}}\, e^{-i\sqrt{\frac{2mE}{\hbar^2} - (\underline{p}''+\underline{g}_n'')^2}\,\alpha}$$

$$= \sum_{\underline{g}_m''} D(\underline{p}''+\underline{g}_m'') \sum_{\underline{g}_n} U_{\underline{g}_n}^{\underline{g}_m}\, e^{i\underline{g}_n''\cdot\underline{r}}\, e^{i(k_m^{\perp}+g_n^{\perp})\alpha} \qquad 2.5$$

where we have divided through by expi $\underline{p}''\cdot\underline{r}$. From 2.4 we obtain:

$$A\, p^{\perp}\, e^{i\underline{g}_o''\cdot\underline{r}}\, e^{i\alpha p^{\perp}} - \sum_{\underline{g}_m''} A(\underline{p}''+\underline{g}_m'')\sqrt{\frac{2mE}{\hbar^2} - (\underline{p}''+\underline{g}_m'')^2}\, e^{i\underline{g}_m''\cdot\underline{r}}\, e^{-i\sqrt{\frac{2mE}{\hbar^2} - (\underline{p}''+\underline{g}_n'')^2}\,\alpha}$$

$$= \sum_{\underline{g}_m''} D(\underline{p}''+\underline{g}_m'') \sum_{\underline{g}_n} U_{\underline{g}_n}^{\underline{g}_m} (k_m^{\perp}+g_n^{\perp})\, e^{i\underline{g}_n''\cdot\underline{r}}\, e^{i(k_m^{\perp}+g_n^{\perp})\alpha} \qquad 2.6$$

where, again, we have divided through by expi $\underline{p}''\cdot\underline{r}$.

We multiply 2.5 and 2.6 through by $(\exp i\, \underline{g}_r \cdot \underline{r})^*$ and integrate over all $\underline{r}^3$. Equation 2.5 gives:

$$A\, e^{ip^{\pm}\alpha}\delta(\underline{g}''-\underline{g}_r'') + A(\underline{p}''+\underline{g}_r'')\, e^{-i\sqrt{\frac{2mE}{\hbar^2} - (\underline{p}''+\underline{g}_r'')^2}\,\alpha}$$

$$= \sum_{\underline{g}_m''} D(\underline{p}''+\underline{g}_m'') \sum_{\substack{\underline{g}_n^{\pm} \\ \underline{g}_n''=\underline{g}_r''}} U_{\underline{g}_n}^{\underline{g}_m}\, e^{i(k_m^{\pm}+g_n^{\pm})\alpha} \qquad 2.7$$

while from 2.6 we obtain:

$$A\, p^{\pm}\, e^{ip^{\pm}\alpha}\, \delta(\underline{g}_o''-\underline{g}_r'') - \sqrt{\frac{2mE}{\hbar^2} - (\underline{p}''+\underline{g}_r'')^2}\, e^{-i\sqrt{\frac{2mE}{\hbar^2} - (\underline{p}''+\underline{g}_r'')^2}\,\alpha} A(\underline{p}''+\underline{g}_r'')$$

$$= \sum_{\underline{g}_m''} D(\underline{p}''+\underline{g}_m'') \sum_{\substack{\underline{g}_n^{\pm} \\ \underline{g}_n''=\underline{g}_r''}} U_{\underline{g}_n}^{\underline{g}_m}\, (k_n^{\pm}+g_n^{\pm})\, e^{i(k_m^{\pm}+g_n^{\pm})\alpha} \qquad 2.8$$

We can divide equation 2.8 by $\sqrt{\frac{2mE}{\hbar^2} - (\underline{p}''+\underline{g}_r'')^2}$, and noting that:

$$\frac{p^{\pm}}{\sqrt{\frac{2mE}{\hbar^2} - (\underline{p}''+\underline{g}_r'')^2}}\, \delta(\underline{g}_o''-\underline{g}_r'') = \delta(\underline{g}_o''-\underline{g}_r''), \qquad 2.9$$

we obtain:

$$A\, e^{ip^{\pm}\alpha}\delta(\underline{g}_o''-\underline{g}_r'') - A(\underline{p}''+\underline{g}_r'')\, e^{-i\sqrt{\frac{2mE}{\hbar^2} - (\underline{p}''+\underline{g}_r'')^2}\,\alpha}$$

$$= \sum_{\underline{g}_m''} D(\underline{p}''+\underline{g}_m'') \sum_{\substack{\underline{g}_t^{\pm} \\ \underline{g}_t''=\underline{g}_r''}} U_{\underline{g}_n}^{\underline{g}_m} \frac{(k_m^{\pm}+g_n^{\pm})\, e^{i(k_m^{\pm}+g_n^{\pm})\alpha}}{\sqrt{\frac{2mE}{\hbar^2} - (\underline{p}''+\underline{g}_r'')^2}} \qquad 2.10$$

In both 2.8 and 2.10:

$$\delta(\underline{g}_o''-\underline{g}_r'') = 1, \qquad \underline{g}_o''=\underline{g}_r''$$

$$= 0, \qquad \underline{g}_o''\neq\underline{g}_r''$$

We can now add equation 2.7 and 2.10, so eliminating $A(\underline{p}''+\underline{g}_r'')$:

$$\sum_{\underline{g}_m''} D(\underline{p}''+\underline{g}_m'') \sum_{\substack{\underline{g}_n \\ \underline{g}_n''=\underline{g}_r''}} U_{\underline{g}_n}^{\underline{g}_m} \left[1 + \frac{k_m^{\pm}+k_n^{\pm}}{\sqrt{\frac{2mE}{\hbar^2} \cdot (\underline{p}''+\underline{g}_r'')^2}}\right] e^{i(k_m^{\pm}+g_n^{\pm})\alpha} = 2A\, e^{i\alpha p^{\pm}} \delta(\underline{g}_o''-\underline{g}_r'') \qquad 2.12$$

Equation 2.12 represents a set of coupled equations in the $D(\underline{p}''+\underline{g}_r'')$. Each equation is characterized by $\underline{g}_r''$. The coefficient of each $D(\underline{p}''+\underline{g}_r'')$, for fixed $\underline{g}_r''$, is characterized by $\underline{g}_m''$.

In matrix form we write 2.12:

$$\begin{pmatrix} \\ \Gamma \\ \\ \end{pmatrix} \begin{pmatrix} \\ D(\underline{p}''+\underline{g}_m'') \\ \\ \end{pmatrix} = \begin{pmatrix} 0 \\ 0 \\ \vdots \\ 0 \\ 2A\, e^{i\alpha p^{\pm}} \\ 0 \\ \vdots \\ 0 \end{pmatrix} \leftarrow \text{row } \underline{g}_o'' \qquad 2.13$$

The elements of the matrix (Γ) are given by:

$$\Gamma_{\underline{g}_r'',\underline{g}_m''} = \sum_{\substack{\underline{g}_n \\ \underline{g}_n''=\underline{g}_r''}} U_{\underline{g}_n}^{\underline{g}_m} \left[1 + \frac{\{k_m^{\pm}+g_n^{\pm}\}}{\sqrt{\frac{2mE}{\hbar^2} - (\underline{p}''+\underline{g}_r'')^2}}\right] e^{i(k_m^{\pm}+g_n^{\pm})\alpha} \qquad 2.14$$

$(D(\underline{p}''+\underline{g}_m''))$ is a column matrix whose elements are the unknown coefficients $D(\underline{p}''+\underline{g}_m'')$. The matrix on the right hand side of 2.13 is a column whose elements are zero except the one in the row denoted by $\underline{g}_r'' = \underline{g}_o''$.

The theory of simultaneous linear equations then gives us:

$$D(\underline{p}''+\underline{g}_r'') = 2A\, e^{i\alpha p^{\perp}} \frac{\det(\Gamma)_{\underline{g}_o''\underline{g}_s''}}{\det(\Gamma)} \qquad 2.15$$

where $(\Gamma)_{\underline{g}_o''\underline{g}_s''}$ is the cofactor of the element in the $\underline{g}_o''$ row and $\underline{g}_s''$ column of (Γ).

We can now substitute equation 2.15 into equation 2.7, we obtain:

$$\frac{A(\underline{p}''+\underline{g}_r'')}{A} = e^{i\left[p^{\perp}+\sqrt{\frac{2mE}{\hbar^2}-(\underline{p}''+\underline{g}'')^2}\right]\alpha} \times \left[\sum_{\underline{g}_m''} \frac{2\det(\Gamma)_{\underline{g}_o''\underline{g}_m''}}{\det(\Gamma)} \sum_{\substack{\underline{g}_n^{\perp} \\ \underline{g}_n''=\underline{g}_r''}} U_{\underline{g}_n}^{\underline{g}_m} e^{i(k_m^{\perp}+g_n^{\perp})\alpha} - \delta(\underline{g}_o''-\underline{g}_r'')\right] \qquad 2.17$$

Thus, in principle, we have found the intensities, $I(\underline{p}''+\underline{g}_r'')$, of all the back-scattered beams:

$$I(\underline{p}''+\underline{g}_r'') = \left|\frac{A(\underline{p}''+\underline{g}_r'')}{A}\right|^2 \qquad 2.18$$

where the intensity of the incident wave is unity. Of course, the intensity of the specularly reflected beam is associated with $\underline{g}_o''$.

In section C(b), we will see how A2.35 (i.e. approximation of the wavefunctions) allows us to solve 2.17. The difficulty is that the determinants in 2.17 are of infinite dimensions. This could be attended to by truncating the series 2.1 and 2.2 in some way. However, as far as an understanding of the physics is concerned, it is more desirable that the approximate wavefunctions should determine the solutions.

C. Qualitative Discussion of the Structure in LEED Intensities

(a) The geometry of the diffraction pattern

Before looking at the qualitative behaviour of the intensities, $I(\underline{p}''+\underline{g}_r'')$, we discuss the geometry of the diffraction pattern.

In our model the energy is a constant of the motion determined by the energy of the incident wave. In appendix II we see that $\underline{k}''$, the reduced component of the wave-vector parallel to the crystal surface, is also a constant of the motion fixed by the incident wave. The goemetry of the diffraction pattern is uniquely fixed by these two constants.

In our model the back-scattered flux is carried by plane waves with wave-vectors given by:

$$(\underline{p}''+\underline{g}'') - \underline{n}\sqrt{\frac{2mE}{\hbar^2} - (\underline{p}''+\underline{g}'')^2} \qquad 2.19$$

which, in accordance with the previous paragraph, are uniquely determined by $\underline{p}''$ and E. The symmetry of the crystal surface is built into the diffraction pattern via the $\underline{g}''$. The number of diffraction spots seen in practice is determined by the number of $\underline{g}''$ for which:

$$(\underline{p}''+\underline{g}'')^2 < \frac{2mE}{\hbar^2} \qquad 2.20$$

All the other $\underline{g}''$, not satisfying 2.20, correspond to waves localised in the crystal surface.

(b) Qualitative behaviour of the $I(\underline{p}''+\underline{g}_r'')$

In this section we will refer repeatedly to the specularly transmitted beam. In our notation this is the plane wave, $\exp i\,(\underline{k}_o+\underline{g}_o).\underline{r}$, in the crystal. If we turn off the crystal potential this becomes the only beam in the crystal (see appendix I).

The discussion proceeds along particularly simple lines if we decouple, as much as possible, equations 2.12. We accomplish this by letting most of the $U_{\underline{g}_n}^{\underline{g}_m}$ go to zero (by taking β large); that is, we will only consider the wavefunctions to zero-order perturbation. Although we expect such an approximation to give the qualitative behaviour of the dominant effects in LEED, we would not now expect to obtain the relative intensities of the spots correctly. In this context therefore, we allow ourselves to choose the position of the matching plane in a way which aids the discussion. The best simplification of 2.16 and the preceeding equations results if we put $\alpha = 0$, that is, the matching plane is $x = 0$.

In this situation we have:

$$\frac{A(\underline{p}''+\underline{g}_r'')}{A} = \left[\sum_{\underline{g}_m''} \frac{2\ \det\ (\Gamma)_{\underline{g}_o''\underline{g}_m''}}{\det\ (\Gamma)} \sum_{\substack{\underline{g}_n^{+} \\ \underline{g}_n''=\underline{g}_r''}} U_{\underline{g}_n}^{\underline{g}_m} - \delta(\underline{g}_o''-\underline{g}_r'')\right] \qquad 2.21$$

where the elements of (Γ) are now given by:

$$\Gamma_{\underline{g}_r''\underline{g}_m''} = \sum_{\substack{\underline{g}_n^{\pm} \\ \underline{g}_n''=\underline{g}_r''}} U_{\underline{g}_n}^{\underline{g}_m} \left[1 + \frac{\{\underline{k}_m^{\pm}+\underline{g}_n^{\pm}\}}{\sqrt{\frac{2mE}{\hbar^2} - (\underline{p}''+\underline{g}_r'')^2}} \right] \qquad 2.22$$

We shall see, in the approximation to the wavefunctions taken, that the back-scattered intensities are largely determined by the orientation of the wave-vector of the specularly transmitted beam, in k-space, with respect to the Bragg scattering planes.

(i) <u>The wave-vector of the specularly transmitted beam not lying near a Bragg condition</u>

In our present approximation the specularly transmitted beam will not be mixed with other beams by the potential in this situation. So that we can write:

$$U_{\underline{g}_t}^{\underline{g}_o} = 0, \quad \underline{g}_o \neq \underline{g}_t; \quad U_{\underline{g}_o}^{\underline{g}_o} = 1 \qquad 2.23$$

(Here and elsewhere we can take the normalisation constant into the coefficients $D(\underline{p}''+\underline{g}_m'')$ so that we can always put one of the $U_{\underline{g}_n}^{\underline{g}_m}$ equal to unity provided the others are found relative to it.)

We now look at the column of (Γ) denoted by $\underline{g}_o''$. The elements in this column are given, from 2.22, by:

$$\Gamma_{\underline{g}_r''\underline{g}_o''} = \sum_{\substack{\underline{g}_t^{\pm} \\ \underline{g}_t''=\underline{g}_r''}} U_{\underline{g}_t}^{\underline{g}_o} \left[1 + \frac{(\underline{k}_o^{\pm}+\underline{g}_t^{\pm})}{\sqrt{\frac{2mE}{\hbar^2} - (\underline{p}''+\underline{g}_r'')^2}} \right] \qquad 2.24$$

Using 2.23 in 2.24 we see that:

$$\Gamma_{g_r'' g_o''} = 0, \quad g_o'' \neq g_r''; \quad \Gamma_{g_o'' g_o''} = \left[1 + \frac{k_o^+ + g_o^+}{p^+}\right] \tag{2.25}$$

where we have written:

$$p^+ = \sqrt{\frac{2mE}{\hbar^2} - (\underline{p}'' + \underline{g}_o'')^2} \tag{2.26}$$

Hence the $\underline{g}_o''$ column of (Γ) consists of zeros except the element in the $\underline{g}_o''$ row. The determinant of the cofactor, $(\Gamma)_{\underline{g}_o'' \underline{g}_s''}$ thus has, unless $\underline{g}_s'' = \underline{g}_o''$, all the elements in its $\underline{g}_o''$ column equal to zero, and hence is zero itself.

Now 2.15, with $\alpha = 0$, is:

$$D(\underline{p}'' + \underline{g}_s'') = \frac{2A \det (\Gamma)_{\underline{g}_o'' \underline{g}_s''}}{\det (\Gamma)} \tag{2.27}$$

so that we obtain:

$$D(\underline{p}'' + \underline{g}_s'') = 0, \quad \underline{g}_s'' \neq \underline{g}_o''; \quad D(\underline{p}'' + \underline{g}_o'') = \frac{2A \det (\Gamma)_{\underline{g}_o'' \underline{g}_o''}}{\det (\Gamma)} \tag{2.28}$$

We expand $\det (\Gamma)$ by the $\underline{g}_o''$ column, so that:

$$\det (\Gamma) = \Gamma_{\underline{g}_o'' \underline{g}_o''} \det (\Gamma)_{\underline{g}_o'' \underline{g}_o''}$$

Hence 2.28 becomes:

$$D(\underline{p}'' + \underline{g}_o'') = \frac{2A}{\Gamma_{\underline{g}_o'' \underline{g}_o''}} \tag{2.29}$$

We substitute the $D(\underline{p}'' + \underline{g}_s'')$ and $U_{\underline{g}_t}^{\underline{g}_s}$ for this situation into 2.21 and obtain:

$$\left.\begin{aligned} &\frac{A(\underline{p}''+\underline{g}_r'')}{A} = 0 \qquad \underline{g}_r'' \neq \underline{g}_o'' \qquad \text{(i)} \\ &\frac{A(\underline{p}''+\underline{g}_o'')}{A} = \frac{2}{\Gamma_{\underline{g}_o''\underline{g}_o''}} - 1 \qquad \text{(ii)} \end{aligned}\right\} \qquad 2.30$$

If we substitute 2.25 into 2.30(ii) we obtain:

$$\frac{A(\underline{p}''+\underline{g}_o'')}{A} = \left(\frac{p^{\pm} - \{k_o^{\pm}+g_o^{\pm}\}}{p^{\pm} + \{k_o^{\pm}+g_o^{\pm}\}}\right) \qquad 2.31$$

The coefficients $A(\underline{p}''+\underline{g}_o'')$ and $D(\underline{p}''+\underline{g}_o'')$ obtained give the wavefunctions A1.1 and A1.2. In that Appendix it is shown that these wavefunctions are just those one obtains in the problem of scattering from a potential step. Diagram A1.3 then shows the behaviour of $I(\underline{p}''+\underline{g}_o'')$ as a function of energy.

(ii) <u>The wave-vector of the specularly transmitted beam lying near one Bragg condition</u>

In this situation we can write:

$$\left.\begin{aligned} &U_{\underline{g}_o}^{\underline{g}_o} = 1 \\ &U_{\underline{g}_a}^{\underline{g}_o} = \alpha, \text{ say} \end{aligned}\right\} \qquad 2.32$$

while

$$U_{\underline{g}_r}^{\underline{g}_o} = 0 \quad g_r \neq g_o \text{ or } \underline{g}_a.$$

There are essentially two cases to consider:

$$\left.\begin{aligned} &\text{(i)} \ \underline{g}_o'' = \underline{g}_a'' \\ &\text{(ii)} \ \underline{g}_o'' \neq \underline{g}_a'' \end{aligned}\right\} \qquad 2.33$$

Bragg peaks in the specular intensity

We deal with (i) first. This corresponds to a Bragg scattering from planes parallel to the crystal surface. The specularly transmitted beam, $(\underline{k}_o+\underline{g}_o)$, is Bragg reflected from the plane perpendicularly bisecting the reciprocal lattice vector $(\underline{g}_o-\underline{g}_a)$.

If we, again, consider the column of (Γ) denoted by $\underline{g}_o''$ we find, using 2.23 and 2.32, that:

$$\left.\begin{aligned} &\Gamma_{\underline{g}_r''\underline{g}_o''} = 0 \quad \underline{g}_r'' \neq \underline{g}_o'' \\ &\text{while} \\ &\Gamma_{\underline{g}_o''\underline{g}_o''} = \left(1 + \frac{k_o^{\perp}+g_o^{\perp}}{\sqrt{\frac{2mE}{\hbar^2} - (\underline{p}''+\underline{g}_o'')^2}}\right) + \alpha\left(1 + \frac{k_o^{\perp}+g_a^{\perp}}{\sqrt{\frac{2mE}{\hbar^2} - (\underline{p}''+\underline{g}_a'')^2}}\right) \end{aligned}\right\} \quad 2.34$$

Then 2.34 with 2.27 gives:

$$D(\underline{p}''+\underline{g}_s'') = 0, \quad \underline{g}_s'' \neq \underline{g}_o''; \quad D(\underline{p}''+\underline{g}_o'') = \frac{2A}{\left(1 + \frac{k_o^{\perp}+g_o^{\perp}}{p^{\perp}}\right) + \alpha\left(1 + \frac{k_o^{\perp}+g_a^{\perp}}{p^{\perp}}\right)} \quad 2.35$$

where we have used 2.25 and the fact that $\underline{g}_o'' = \underline{g}_a''$. Equation 2.35 with 2.21 now gives:-

$$\left.\begin{aligned} &\frac{A(\underline{p}''+\underline{g}_r'')}{A} = 0, \quad \underline{g}_r'' \neq \underline{g}_o'' \qquad \text{(i)} \\ &\text{while} \\ &\frac{A(\underline{p}''+\underline{g}_o'')}{A} = \frac{2(1+\alpha)}{\left(1 + \frac{k_p^{\perp}+g_o^{\perp}}{p^{\perp}}\right) + \alpha\left(1 + \frac{k_o^{\perp}+g_a^{\perp}}{p^{\perp}}\right)} - 1 \qquad \text{(ii)} \end{aligned}\right\} \quad 2.36$$

In our approximation α is only non-zero for $(\underline{k}_o+\underline{g}_o)$ lying close to the plane perpendicularly bisecting the vector $(\underline{g}_o-\underline{g}_a)$. Outside this range, we have $\alpha = 0$ and 2.36 goes over to 2.31. Over the small range for which we take α to be finite, p^+, $(k_o^+ + g_o^+)$ and $(k_o^+ + g_a^+)$ are essentially constant, so that the behaviour of 2.36(i) only depends significantly on α.

We determine α from the (2×2) equivalent of equation A2.52.

$$\begin{pmatrix} E_1-E & V_{\underline{g}} \\ V_{-\underline{g}} & E_2-E \end{pmatrix} \begin{pmatrix} 1 \\ \alpha \end{pmatrix} = 0 \qquad 2.37$$

where we have written $\underline{g}_o-\underline{g}_a = \underline{g}$ and we also have:

$$\left.\begin{aligned} E_1 &= \frac{\hbar^2}{2m}(\underline{k}_o+\underline{g}_o)^2 - V_o \\ E_2 &= \frac{\hbar^2}{2m}(\underline{k}_o+\underline{g}_a)^2 - V_o \end{aligned}\right\} \quad \text{for } k_o^+ < \frac{g}{2}, \text{ while for } k_o^+ > \frac{g}{2}: \qquad 2.38$$

$$\left.\begin{aligned} E_1 &= \frac{\hbar^2}{2m}(\underline{k}_o-\underline{g}_a)^2 - V_o \\ E_2 &= \frac{\hbar^2}{2m}(\underline{k}_o+\underline{g}_o)^2 - V_o \end{aligned}\right\}$$

In Appendix II, the energy bands associated with 2.37 were discussed in some detail. The free electron bands became perturbed in the manner shown in diagram 2.1. As the wave-vector of the specularly transmitted beam passes, in increasing energy, through the plane perpendicularly bisecting $(\underline{g}_o-\underline{g}_a)$, we pass through the band-structure in the manner indicated by the arrows.

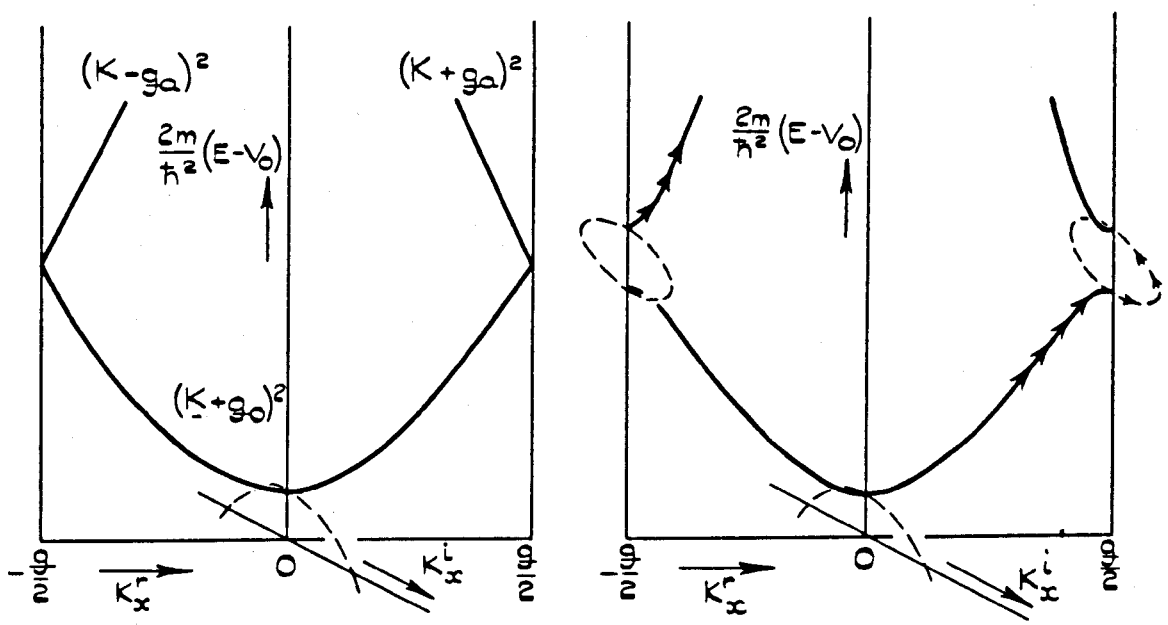

DIAGRAM 2·1

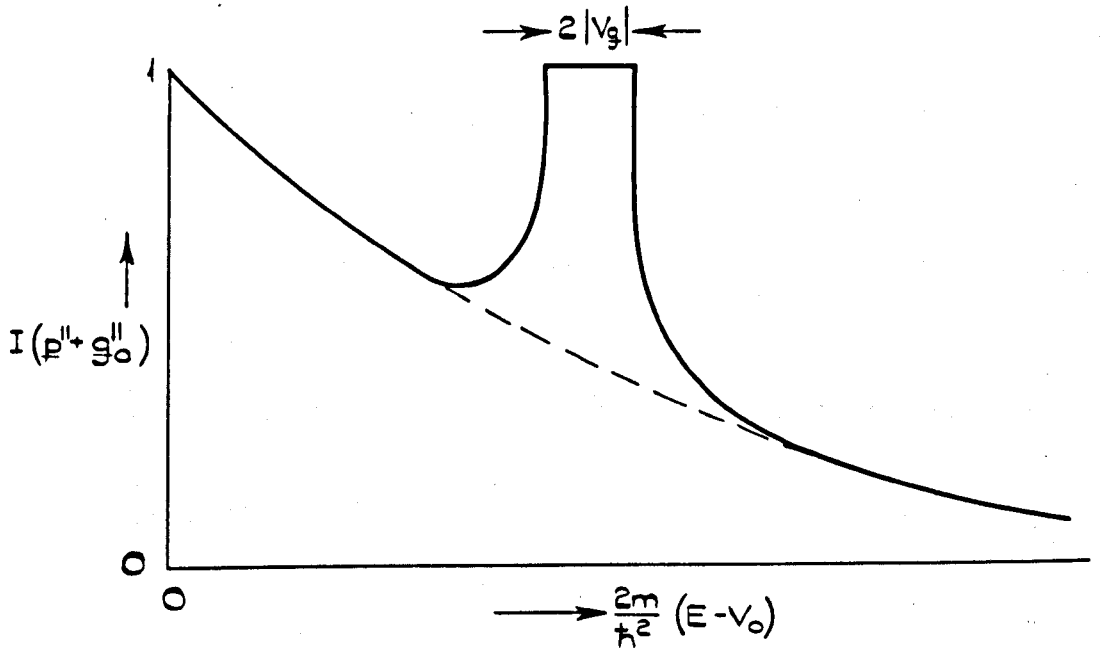

DIAGRAM 2·2

Equation 2.37 gives: $$\alpha = -\frac{V_g}{(E_2-E)} \qquad 2.39$$

while equation A2.54 gives:

$$E = \left(\frac{E_1+E_2}{2}\right) \pm \sqrt{\frac{E_1-E_2}{2} + |V_g|^2} \qquad 2.40$$

Substitution of 2.40 into 2.39 gives:

$$\xi = \frac{-1}{\xi \pm \sqrt{\xi^2+1}} \qquad 2.41$$

where

$$\xi = \left(\frac{E_1-E_2}{2V_g}\right) \qquad 2.42$$

We will take V_g to be an attractive potential, that is, positive; below the band gap in energy the negative sign in 2.41 is taken, while above it the positive sign.

As we go from the bottom of the band gap to lower energies we see that:

$$\left.\begin{array}{l} \xi \text{ goes monotonically from } 0 \to -\infty \\ \text{so that } \alpha \text{ goes from } \quad 1 \to 0 \end{array}\right\} \qquad 2.43$$

However, proceeding from the top of the band gap to higher energies:

$$\begin{array}{l} \xi \text{ goes monotonically from } 0 \to \infty \\ \text{so that } \alpha \text{ goes from } \quad -1 \to 0 \end{array} \qquad 2.44$$

If we are at energies within the gap we find;

$$\xi = i\,\frac{\underline{k}_i\cdot(\underline{g}_o-\underline{g}_a)}{\left(\frac{2m}{\hbar^2}V_g\right)} = i\,\frac{k_i\, g}{\left(\frac{2m}{\hbar^2}V_g\right)} = i\,\xi', \text{ say} \qquad 2.45$$

where k_i is the imaginary part of $\underline{k}_o$ and ξ' is real; hence:

$$\alpha = \frac{-1}{i\xi' \pm \sqrt{1-\xi'^2}} = \sqrt{1-\xi'^2} + i\xi' = e^{i\theta} \qquad 2.46$$

$$\text{where } \sin\theta = \frac{k_i g}{\left(\frac{2m}{\hbar^2} V_g\right)} \qquad 2.47$$

We consider the behaviour of $\frac{A(\underline{p}''+\underline{g}_o'')}{A}$ taking α to be the dominantly varying quantity in 2.36. We start at an energy well below the band gap and proceed up to the bottom of the gap. The value of α, from 2.41, goes smoothly from $0 \to 1$. At the top and bottom of the band gap $(k_o^{\pm}+g_o^{\pm}) = -(k_o^{\pm}+g_a^{\pm})$. Hence $\frac{A(\underline{p}''+\underline{g}_o'')}{A}$ goes smoothly from the value appropriate to the potential step to unity at the bottom of the gap. Throughout the gap, from 2.46, $\alpha = e^{i\theta}$; substitution into 2.36(ii) gives:

$$\frac{A(\underline{p}''+\underline{g}_o'')}{A} = \left[\frac{\cos\theta/2 - i\left\{\frac{(k_{or}^{\pm}+g_o^{\pm})}{p^{\pm}}\sin\theta/2 + \left[\frac{k_{oi}}{p^{\pm}}\right]\cos\theta/2\right\}}{\cos\theta/2 + i\left\{\frac{(k_{or}^{\pm}+g_o^{\pm})}{p^{\pm}}\sin\theta/2 + \left[\frac{k_{oi}}{p^{\pm}}\right]\cos\theta/2\right\}}\right] \qquad 2.48$$

where we have written $k_o^{\pm} = k_{or}^{\pm} + ik_{oi}$. As we increase the energy away from the gap we see, from 2.41, that α goes from $-1 \to 0$; 2.36 shows then that $\frac{A(\underline{p}''+\underline{g}_o'')}{A}$ goes from unity to the value appropriate to a potential step.

Thus the intensity $I(\underline{p}''+\underline{g}_o'')$, as $(\underline{k}_o+\underline{g}_o)$ approaches the plane perpendicularly bisecting $(\underline{g}_o-\underline{g}_a)$, from either side goes from the value associated with a potential step to unity on the plane. The vector $(\underline{k}_{or}+\underline{g}_o)$ remains on the plane for energies within the band gap when the intensity is the modulus of 2.48 squared. The latter is easily seen to be unity

since the numerator of 2.48 is the complex conjugate of the denominator. The result is sketched in diagram 2.2. Sommerfeld and Bethe (5), Morse (7) and more recently, Boudreaux and Heine (14) have obtained similarly shaped curves for Bragg reflections in the (0,0) beam.

Similarly shaped peaks will occur at energies: $n\frac{\hbar^2}{2m}\left(\frac{g}{2}\right)^2$, where n is an integer, and they correspond to Bragg peaks of order n. The effect of inelastic scattering is to remove flux from the elastically scattered beams to the background of the diffraction pattern; the more penetrating a particular beam is, the greater proportion of its flux will be inelastically scattered. From the energy bands we see that the centre of the flat-topped portion of the intensity plot corresponds to the least penetrating (high k_i) of the Bloch waves, while nearer the edges of the band gap the Bloch waves penetrate further ($k_i \rightarrow 0$). Thus the effect of inelastic scattering will be to round-off the flat-topped peaks obtained in this analysis.

We note also that we expect the widths of such peaks (equal to the band-gap) to decrease as they occur at higher and higher energies.

As we pass through a particular band gap the phase of the wave-function, $\theta/2$ (θ is given by 2.46), changes by $\pi/2$.

Bragg peaks in the non-specular intensities

We now consider the case 2.33(ii). The vector $(g_o - g_n)$ is not now perpendicular to the crystal surface, we take account of the surface periodicity thus introduced by also considering the beam with wave-vector

$(\underline{k}_b+\underline{g}_b)$, where:

$$(\underline{k}_b+\underline{g}_b)'' - (\underline{k}_o+\underline{g}_o)'' = -(\underline{g}_o-\underline{g}_a)'' \qquad 2.49$$

The lower half of diagram 2.3 shows the relative orientations of the wave-vectors. We adopt the convenient procedure, here and elswhere, of including in the same diagram the wave-vectors of plane waves both in the crystal and in the vacuum. However, we do separate them by the plane which is perpendicular to the direction of normal incidence.

Physically, the origin of $|\underline{k}_b+\underline{g}_b>$ may be thought of as the reflection of $|\underline{k}_o+\underline{g}_a>$ from the crystal surface.

The upper half of diagram 2.3 shows the free electron bands plotted at the value of $\underline{p}''$ on the k-space diagram. The points A and B on the energy bands correspond to the energy on the k-space diagram. Note that, for the time being, we assume $(k_o+g_a)^{\perp} > 0$.

We again take 2.32 to represent the coefficients in the Bloch wave expansion for that Bloch wave associated with the perturbation of $\exp i\,(\underline{k}_o+\underline{g}_o).\underline{r}$. We suppose initially that the plane-wave, $|\underline{k}_b+\underline{g}_b>$, is not near a Bragg condition; then we have:

$$U^{\underline{g}_b}_{\underline{g}_s} = 0, \quad \underline{g}_s \neq \underline{g}_b$$

2.50

while

$$U^{\underline{g}_b}_{\underline{g}_b} = 1$$

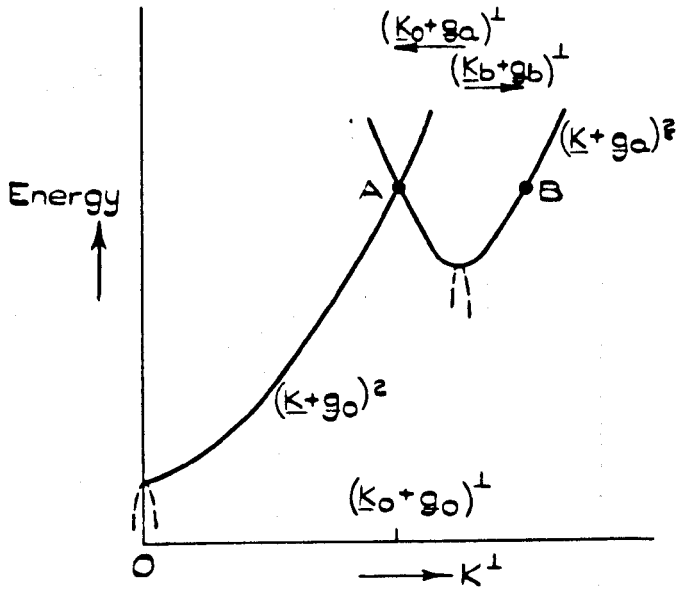
$(\underline{K}_0+\underline{g}_a)^\perp$
$(\underline{K}_b+\underline{g}_b)^\perp$
$(\underline{K}+\underline{g}_a)^2$
Energy
A
B
$(\underline{K}+\underline{g}_0)^2$
$(\underline{K}_0+\underline{g}_0)^\perp$
0
$K^\perp$

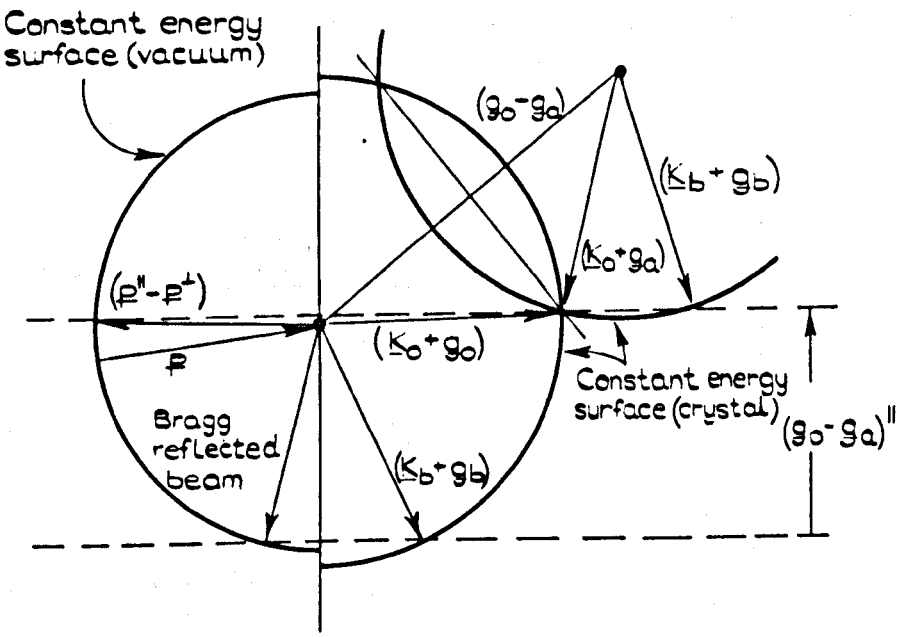
Constant energy surface (vacuum)
$(\underline{g}_0-\underline{g}_a)$
$(\underline{K}_b+\underline{g}_b)$
$(\underline{K}_0+\underline{g}_a)$
$(\underline{p}''-\underline{p}^\perp)$
$\underline{p}$
$(\underline{K}_0+\underline{g}_0)$
Constant energy surface (crystal)
Bragg reflected beam
$(\underline{K}_b+\underline{g}_b)$
$(g_0-g_a)''$

DIAGRAM 2.3.

We now consider the elements in the g_o'' column and the g_b'' column of (Γ). Equations 2.32 and 2.22 give:

$$\Gamma_{g_r''g_o''} = 0, \qquad g_r'' \neq g_o'' \text{ or } g_b'' \tag{2.51}$$

Note that 2.43 gives $g_a'' = g_b''$,

$$\left.\begin{aligned} &\text{while} \quad \Gamma_{g_o''g_o''} = \left[1 + \frac{k_o^{\pm}+g_o^{\pm}}{\sqrt{\frac{2mE}{\hbar^2} - (p''+g_o'')^2}}\right] \qquad \text{(i)} \\ &\text{and} \quad \Gamma_{g_b''g_o''} = \alpha\left[1 + \frac{k_o^{\pm}+g_a^{\pm}}{\sqrt{\frac{2mE}{\hbar^2} - (p''+g_b'')^2}}\right] \qquad \text{(ii)} \end{aligned}\right\} \tag{2.52}$$

we have used $g_a'' = g_b''$; it is not necessarily true that $g_a^{\pm} = g_b^{\pm}$. Equations 2.50 and 2.22 give for the elements in the g_b'' column:

$$\left.\begin{aligned} &\Gamma_{g_r''g_b''} = 0, \qquad g_r'' \neq g_b'' \\ &\Gamma_{g_b''g_b''} = \left[1 + \frac{(k_b^{\pm}+g_b^{\pm})}{\sqrt{\frac{2mE}{\hbar^2} - (p''+g_b'')^2}}\right] \end{aligned}\right\} \tag{2.53}$$

We substitute 2.51, 2.52 and 2.53 into det (Γ) and expand by the g_b'' column:

$$\det(\Gamma) = \Gamma_{g_b''g_b''} \det(\Gamma)_{g_b''g_b''}$$

we then expand det $(\Gamma)_{g_b''g_b''}$ by the column denoted by g_o'':

$$\det(\Gamma) = \Gamma_{g_b''g_b''}\,\Gamma_{g_o''g_o''} \det\left[(\Gamma)_{g_b''g_b''}\right]_{g_o''g_o''} \tag{2.54}$$

where $\det\left[(\Gamma)_{g_b''g_b''}\right]_{g_o''g_o''}$ means $\det(\Gamma)$ with the rows and columns denoted by g_o'' and g_b'' removed.

Suppose $g_r'' \neq g_o''$ or g_b'' and we expand $\det(\Gamma)_{g_o''g_r''}$ by the g_o'' column:

$$\det(\Gamma)_{g_o''g_r''} = \Gamma_{g_b''g_o''} \det\left[(\Gamma)_{g_o''g_r''}\right]_{g_b''g_o''}$$

Now the g_b'' column of $\det\left[(\Gamma)_{g_o''g_r''}\right]_{g_b''g_o''}$ has all its elements equal to zero. Hence:

$$\det(\Gamma)_{g_o''g_r''} = 0, \qquad g_r'' \neq g_o'' \text{ or } g_b'' \tag{2.55}$$

so that from 2.27

$$D(p''+g_r'') = 0, \qquad g_r'' \neq g_o'' \text{ or } g_b'' \tag{2.56}$$

We also have, expanding $\det(\Gamma)_{g_o''g_o''}$ by the g_o'' column

$$\det(\Gamma)_{g_o''g_o''} = \Gamma_{g_b''g_b''} \det\left[(\Gamma)_{g_o''g_o''}\right]_{g_b''g_b''} \tag{2.57}$$

and, expanding $\det(\Gamma)_{g_o''g_b''}$ by the g_o'' column

$$\det(\Gamma)_{g_o''g_b''} = \Gamma_{g_b''g_o''} \det\left[(\Gamma)_{g_o''g_o''}\right]_{g_b''g_o''} \tag{2.58}$$

It is clear that:

$$\det\left[(\Gamma)_{g_o''g_o''}\right]_{g_b''g_b''} = \det\left[(\Gamma)_{g_b''g_b''}\right]_{g_o''g_o''} = -\det\left[(\Gamma)_{g_o''g_o''}\right]_{g_b''g_o''} \tag{2.59}$$

because the modulus of each is just $\left|\det(\Gamma)\right|$ with the rows and columns denoted by g_o'' and g_b'' missing.

From 2.54, 2.57, 2.58 and 2.27 we obtain

$$\left.\begin{aligned} D(\underline{p}''+\underline{g}_o'') &= \frac{2A}{\Gamma_{\underline{g}_o''\underline{g}_o''}} \\ D(\underline{p}''+\underline{g}_b'') &= -\frac{2A\,\Gamma_{\underline{g}_b''\underline{g}_o''}}{\Gamma_{\underline{g}_b''\underline{g}_b''}\,\Gamma_{\underline{g}_o''\underline{g}_o''}} \end{aligned}\right\} \qquad 2.60$$

so that from 2.21:

$$\frac{A(\underline{p}''+\underline{g}_o'')}{A} = \frac{2}{\Gamma_{\underline{g}_o''\underline{g}_o''}} - 1 = \left|\frac{p^+ - \{k_o^+ + g_o^+\}}{p^+ + \{k_o^+ + g_o^+\}}\right| \qquad 2.61$$

where we have used 2.26 and 2.52(i). Equation 2.61 is the same as equation 2.31, so that the intensity of the specularly reflected spot, $I(\underline{p}''+\underline{g}_o'')$, behaves exactly as if the crystal were a potential step. We have, in addition of course, that the intensity, $I(\underline{p}''+\underline{g}_b'')$ is not zero, but from 2.60 and 2.21 is given by:

$$I(\underline{p}''+\underline{g}_b'') = \left|\frac{A(\underline{p}''+\underline{g}_b'')}{A}\right| = \left|\frac{2\left\{\alpha\Gamma_{\underline{g}_b''\underline{g}_b''} - \Gamma_{\underline{g}_b''\underline{g}_o''}\right\}}{\Gamma_{\underline{g}_o''\underline{g}_o''}\,\Gamma_{\underline{g}_b''\underline{g}_b''}}\right|^2$$

i.e.

$$I(\underline{p}''+\underline{g}_b'') = \left|\frac{2\alpha\left[\dfrac{(k_b+g_b)^+}{p_b^+} - \dfrac{(k_o+g_a)^+}{p_b^+}\right]}{\left[1+\dfrac{(k_o+g_o)^+}{p^+}\right]\left[1+\dfrac{(k_b+g_b)^+}{p^+}\right]}\right|^2 \qquad 2.62$$

where $p_b^+ = \sqrt{\dfrac{2mE}{\hbar^2} - (\underline{p}''+\underline{g}_b'')^2}$

Over the range for which $|\alpha|$ is finite, and for a fixed angle of incidence, all other quantities in 2.62 are essentially constant. Thus,

approximately, $I(\underline{p}''+\underline{g}_b'')$ is proportional to $|\alpha|^2$. Throughout the gap $|\alpha| \sim 1$, while $|\alpha|$ moves quickly to zero in our approximation as we move away from the gap.

If $|\underline{k}_b+\underline{g}_b\rangle$ is regarded as the result of $|\underline{k}_o+\underline{g}_a\rangle$ being reflected from the crystal surface, it is interesting to enquire what happens if we increase $(k_o+g_a)^+$ from its negative value (as in diagram 2.3) through zero to a positive value. First of all we notice that if $(k_o+g_a)^+$ tends to zero then so does the intensity of the Bragg peak. This follows from 2.62, if we note also the equality:

$$(\underline{k}_o+\underline{g}_a)^+ = -(\underline{k}_b+\underline{g}_b)^+ \qquad 2.63$$

If $(k_o+g_a)^+$ is allowed to become positive then the reciprocal lattice vector $-(\underline{g}_o+\underline{g}_a)$, as well as $(\underline{g}_o+\underline{g}_a)$, plays a role. The k-space diagram and energy bands are then sketched in diagram 2.4. In this diagram, the wave-vectors of the plane-waves in the vacuum are omitted. The points A and B on the energy bands correspond to the energy of the k-space diagram. The point B corresponds to a plane-wave propagating towards the surface so is excluded from consideration. The Bloch wave formed by $|\underline{k}_b+\underline{g}_b\rangle$ being reflected from $-(\underline{g}_o+\underline{g}_a)$ is formally equivalent to the Bloch wave containing the specularly transmitted beam. Thus only the latter is considered, it corresponds to the degeneracy denoted by A on the free electron bands. Of course, the degeneracy is split by the potential and in fact we have two Bloch waves with wave-vectors close to A. However, the plane wave components of these Bloch waves all carry flux away from the surface, thus we expect little reflection. A calculation in chapter II

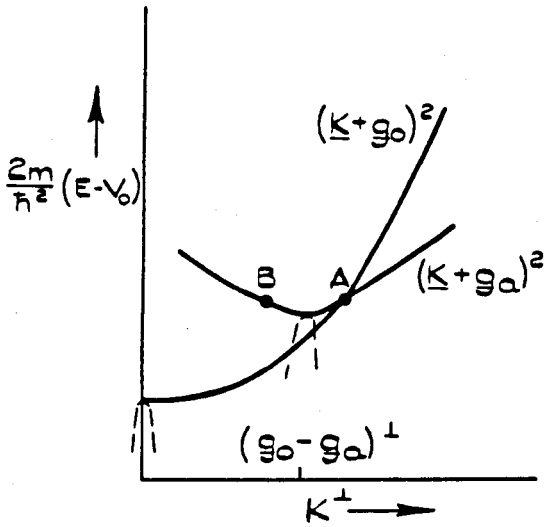
$\frac{2m}{\hbar^2}(E-V_0)$
$(\underline{K}+\underline{g}_0)^2$
$(\underline{K}+\underline{g}_a)^2$
B
A
$(\underline{g}_0-\underline{g}_a)^\perp$
$K^\perp$

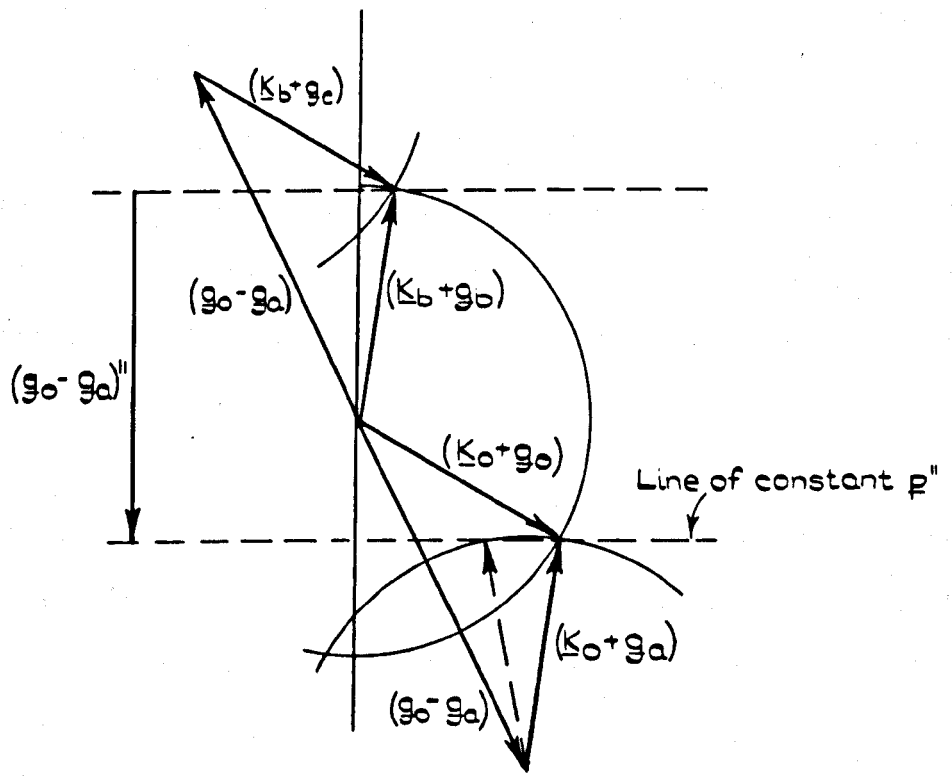
$(\underline{K}_b+\underline{g}_c)$
$(\underline{g}_0-\underline{g}_a)$
$(\underline{K}_b+\underline{g}_0)$
$(\underline{g}_0-\underline{g}_a)''$
$(\underline{K}_0+\underline{g}_0)$
Line of constant $\underline{p}''$
$(\underline{K}_0+\underline{g}_a)$
$(\underline{g}_0-\underline{g}_a)$

DIAGRAM 2.4

associated with a degeneracy such as A confirms this.

In support of our regarding $|\underline{k}_b+\underline{g}_b>$ as the result of internal reflection from the inner potential, we notice that its amplitude, $D(\underline{p}''+\underline{g}_b'')$ vanishes when the inner potential is put equal to zero. This follows from:

$$(k_o^+ + g_a^+) = -\sqrt{\frac{2mE}{\hbar^2} - (\underline{p}''+\underline{g}_b'')^2}$$

when $V_o = 0$, which makes $\Gamma_{\underline{g}_b''\underline{g}_o''}$ go to zero.

The foregoing demonstrates the origin of a Bragg peak in a spot other than (0,0). On the band-structure picture such a situation occurs at that type of band gap where the minima of one band does not occur at the same value of k^+_{real} as the maxima on the lower band. The loop of real energy with complex $\underline{k}$ is not now contained in a plane of k^+_{real} constant. The NFE bands and intensities for this situation are shown schematically in diagram 2.5.

The value of $I(\underline{p}''+\underline{g}_b'')$ on the flat portion of the intensity plot is given by 2.62 with $\alpha = 1$, which we have taken to be constant, that this is not quite true may explain why the peaks of Marcus and Jepsen (19) have flat tops which are sloping.

Secondary Bragg peaks in the specular intensity

It is possible that the intensity of the (0,0) spot may itself be enhanced in the situation just described if the wave, expi $(\underline{k}_b+\underline{g}_b)$, is near a Bragg condition exciting a wave, expi $(\underline{k}_b+\underline{g}_c)$, where $\underline{g}_c''=\underline{g}_o''$. In

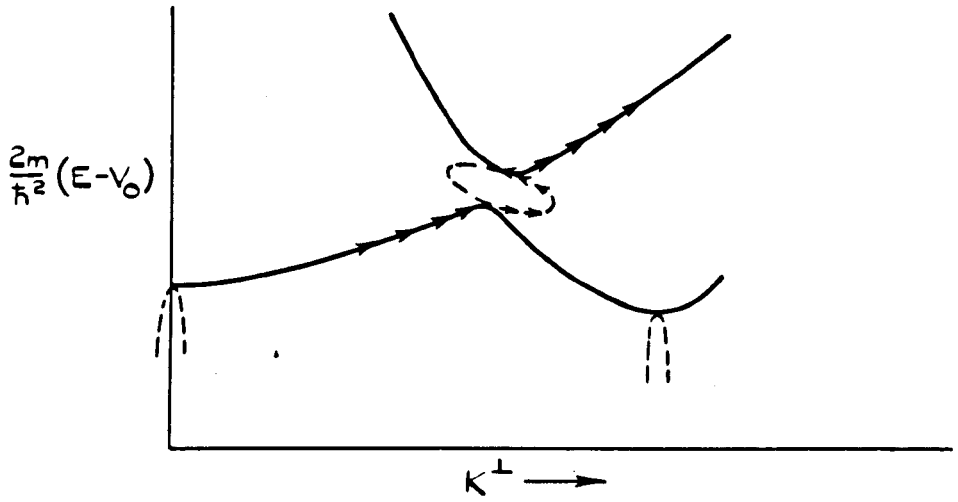
$\frac{2m}{\hbar^2}(E-V_0)$
$K^{\perp}$

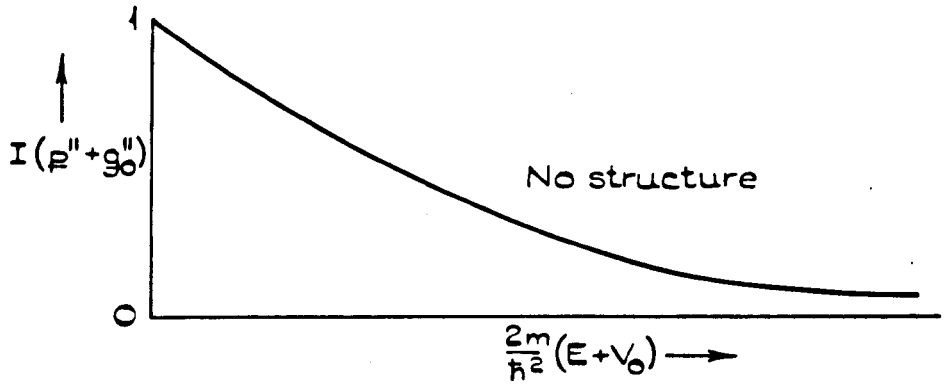
1
$I(p''+g_0'')$
0
No structure
$\frac{2m}{\hbar^2}(E+V_0)$

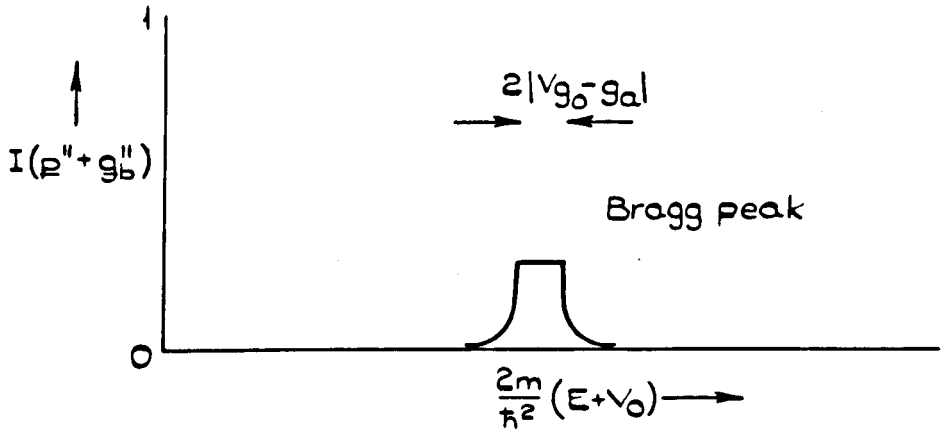
1
$I(p''+g_b'')$
0
$2|V_{g_0-g_a}|$
Bragg peak
$\frac{2m}{\hbar^2}(E+V_0)$

DIAGRAM 2.5

this case, 2.32 gives us the $U^{g_o}_{g_r}$, while:

$$\left.\begin{aligned} U^{g_b}_{g_r} &= 0 \qquad g_r \neq g_b \text{ or } g_o \\ U^{g_b}_{g_b} &= 1 \\ U^{g_b}_{g_c} &= \beta, \text{ say.} \end{aligned}\right\} \qquad 2.64$$

The elements in the g''_o column of (Γ) are still given by 2.31 and 2.52 but those in the g''_b $(=g''_c)$ columns are now given by:

$$\left.\begin{aligned} \Gamma_{g''_r g''_b} &= 0 \qquad g''_r \neq g''_o \text{ or } g''_b \\ \Gamma_{g''_b g''_b} &= \left[1 + \frac{k^+_b\, g^-_b}{\sqrt{\frac{2mE}{\hbar^2} - (p''+g''_b)^2}}\right] \\ \Gamma_{g''_o g''_b} &= \beta\left[1 + \frac{k^+_b + g^-_c}{\sqrt{\frac{2mE}{\hbar^2} - (p''+g''_o)^2}}\right] \end{aligned}\right\} \qquad 2.65$$

The values of $\det\,(\Gamma)_{g''_o g''_r}$ are given by 2.55, 2.57 and 2.58, but now $\det\,(\Gamma)$ is altered:

$$\det\,(\Gamma) = \Gamma_{g''_o g''_o} \det\,(\Gamma)_{g''_o g''_o} + \Gamma_{g''_b g''_o} \det\,(\Gamma)_{g''_o g''_o}$$

where we have expanded by the g''_o column, and now expanding the cofactors by their g''_b columns:

$$\det\,(\Gamma) = \Gamma_{g''_o g''_o}\Gamma_{g''_b g''_b} \det\left((\Gamma)_{g''_o g''_o}\right)_{g''_b g''_b} + \Gamma_{g''_b g''_o}\,\Gamma_{g''_o g''_b} \det\left((\Gamma)_{g''_b g''_o}\right)_{g''_o g''_b} \qquad 2.66$$

From 2.27, 2.55, 2.57, 2.58, 2.59 and 2.66 we have:

$$\left.\begin{aligned} D(\underline{p}''+\underline{g}_r'') &= 0 \qquad \underline{g}_r'' \neq \underline{g}_o'' \text{ or } \underline{g}_b'' \\ D(\underline{p}''+\underline{g}_o'') &= \frac{2A\,\Gamma_{\underline{g}_b''\underline{g}_b''}}{\Gamma_{\underline{g}_o''\underline{g}_o''}\,\Gamma_{\underline{g}_b''\underline{g}_b''} - \Gamma_{\underline{g}_b''\underline{g}_o''}\,\Gamma_{\underline{g}_o''\underline{g}_b''}} \\ D(\underline{p}''+\underline{g}_b'') &= \frac{-2A\,\Gamma_{\underline{g}_b''\underline{g}_o''}}{\Gamma_{\underline{g}_o''\underline{g}_o''}\,\Gamma_{\underline{g}_b''\underline{g}_b''} - \Gamma_{\underline{g}_b''\underline{g}_o''}\Gamma_{\underline{g}_o''\underline{g}_b''}} \end{aligned}\right\} \qquad 2.67$$

We immediately obtain the $\frac{A(\underline{p}''+\underline{g}_r'')}{A}$:-

$$\left.\begin{aligned} &\frac{A(\underline{p}''+\underline{g}_r'')}{A} = 0 \qquad \underline{g}_r'' \neq \underline{g}_o'' \text{ or } \underline{g}_b'' \qquad \text{(i)} \\ &\frac{A(\underline{p}''+\underline{g}_o'')}{A} = \left[\frac{D(\underline{p}''+\underline{g}_o'')}{A} - 1\right] + \beta\left[\frac{D(\underline{p}''+\underline{g}_b'')}{A}\right] \qquad \text{(ii)} \\ &\frac{A(\underline{p}''+\underline{g}_b'')}{A} = \left[\frac{D(\underline{p}''+\underline{g}_b'')}{A}\right] + \alpha\left[\frac{D(\underline{p}''+\underline{g}_o'')}{A}\right] \qquad \text{(iii)} \end{aligned}\right\} \qquad 2.68$$

where we have noted that $\underline{g}_o'' = \underline{g}_c''$ and $\underline{g}_a'' = \underline{g}_b''$. We substitute 2.52, 2.53 and 2.67 into 2.68(ii):

$$\frac{A(\underline{p}''+\underline{g}_o'')}{A} = \frac{2\left[\left[1 + \frac{k_b^{\pm}+g_b^{\pm}}{p_b^{\pm}}\right] - \alpha\beta\left[1 + \frac{k_o^{\pm}+g_a^{\pm}}{p_b^{+}}\right]\right]}{\left[\left[1 + \frac{k_o^{\pm}+g_o^{\pm}}{p^{\pm}}\right]\left[1 + \frac{k_b^{\pm}+g_b^{\pm}}{p_b^{\pm}}\right] - \alpha\beta\left[1 + \frac{k_o^{\pm}+g_a^{\pm}}{p_b^{\pm}}\right]\left[1 + \frac{k_b^{\pm}+g_c^{\pm}}{p^{+}}\right]\right]} - 1 \qquad 2.69$$

where

$$p_b^{\pm} = \sqrt{\frac{2mE}{\hbar^2} - (\underline{p}''+\underline{g}_b'')^2} \quad .$$

If $\beta = 0$ in 2.69 we have the expression appropriate to a potential step. The coupling of $|\underline{k}_b+\underline{g}_b>$ with $|\underline{k}_b+\underline{g}_c>$ has modified the intensity of the specularly reflected spot. The modification will be most marked when $|\underline{k}_b+\underline{g}_b>$ is exactly on a Bragg condition when $|\underline{k}_o+\underline{g}_o>$ is; that is, when β is large in 2.69.

This is exactly the case if there exists a reciprocal lattice vector, $(\underline{g}_b-\underline{g}_c)$, defined by:

$$(\underline{g}_b-\underline{g}_c) = (\underline{g}_o-\underline{g}_a)^{+} - (\underline{g}_o-\underline{g}_a)^{''} \qquad 2.70$$

Simple geometry then shows that, if,

$$(\underline{k}_o+\underline{g}_o)^{''} - (\underline{k}_b+\underline{g}_b)^{''} = (\underline{g}_o-\underline{g}_a)^{''}$$

then $|\underline{k}_b+\underline{g}_b>$ will be exactly on a Bragg condition with $(\underline{g}_b-\underline{g}_c)$ when $|\underline{k}_o+\underline{g}_o>$ is on a similar condition with $(\underline{g}_o-\underline{g}_a)$. In diagram 2.6 we sketch the case when the plane containing the reciprocal lattice vectors $(\underline{g}_o-\underline{g}_a)$ is coincident with the plane of incidence, we stress that this is not essential, all we really require is 2.70. We assume, for the time being, that $(k_o+g_a)^{\perp} < 0$. On the energy bands, the degeneracies, A and B, are at the energy of the k-space diagram. If 2.70 is satisfied, we have:

$$(k_o+g_o)^{\perp} = -(k_b+g_c)^{\perp} \text{ and } (k_b+g_b)^{\perp} = -(k_o+g_a)^{\perp} \qquad 2.71$$

so that 2.69 becomes:

$$\frac{A(\underline{p}''+\underline{g}_o'')}{A} = \frac{2}{(1+Y)}\left[1-\alpha\beta\left\{\frac{1-Z}{1+Z}\right\}\right]\left[1-\alpha\beta\left\{\frac{1-Z}{1+Z}\right\}\left\{\frac{1-Y}{1+Y}\right\}\right]^{-1} - 1 \qquad 2.72$$

where $Y = \dfrac{k_o^{\perp}+g_o^{\perp}}{p^{\perp}}$ and $Z = \dfrac{k_b^{\perp}+g_b^{\perp}}{p_b^{\perp}}$. Both Y and Z are positive. Also

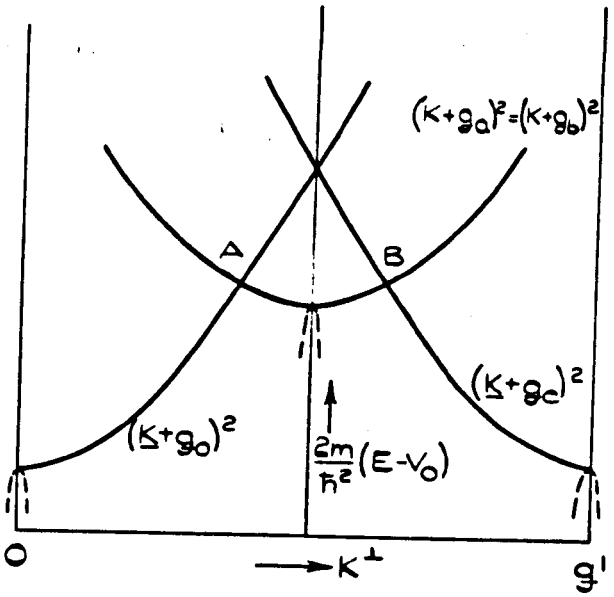
$(K+g_a)^2=(K+g_b)^2$
A
B
$(K+g_c)^2$
$(K+g_o)^2$
$\frac{2m}{\hbar^2}(E-V_o)$
O
$K^\perp$
g'

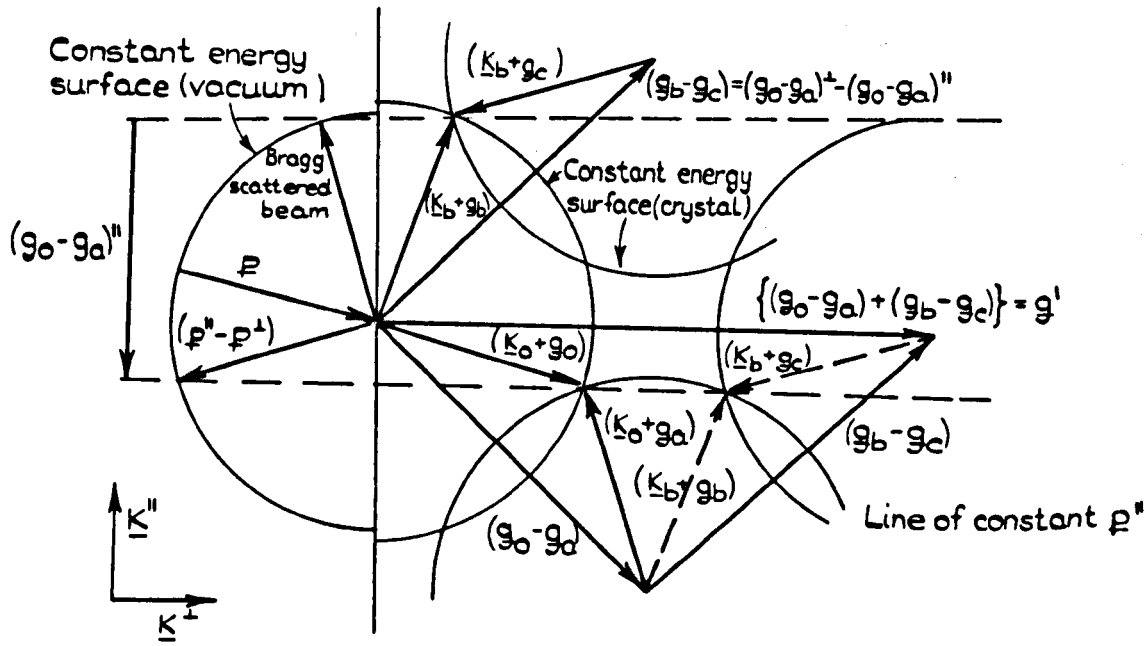
Constant energy surface (vacuum)
(K_b+g_c)
$(g_b-g_c)=(g_o-g_a)^\perp-(g_o-g_a)''$
Bragg scattered beam
(K_b+g_b)
Constant energy surface(crystal)
$(g_o-g_a)''$
p
$\{(g_o-g_a)+(g_b-g_c)\}=g'$
$(p''-p^\perp)$
(K_o+g_o)
(K_b+g_c)
(K_o+g_a)
(g_b-g_c)
(K_b+g_b)
Line of constant p''
(g_o-g_a)
K''
$K^\perp$

DIAGRAM 2.6

$|\alpha\beta| \leq 1$, so that $\alpha\beta\left\{\frac{1-Z}{1+Z}\right\}\left\{\frac{1-Y}{1+Y}\right\}$ is less than unity and we can expand $\left[1-\alpha\beta\left\{\frac{1-Z}{1+Z}\right\}\left\{\frac{1-Y}{1+Y}\right\}\right]^{-1}$ by the binomial theorem. Equation 2.72 becomes:

$$\frac{A(\underline{p}''+\underline{g}_o'')}{A} = \left[\left\{\frac{p^+-(k_o^+ + g_o^+)}{p^+ + (k_o^+ + g_o^+)}\right\}\right] + \frac{2}{(1+Y)}\left[\alpha\beta\left\{\frac{1-Z}{1+Z}\right\} + \left\{1+\alpha\beta\left\{\frac{1-Z}{1+Z}\right\}\right\}\sum_{n=1}^{\infty}\left\{\alpha\beta\left\{\frac{1-Y}{1+Y}\right\}\left\{\frac{1-Z}{1+Z}\right\}\right\}^n\right] \qquad 2.73$$

The first term on the RHS of 2.73 is the value appropriate for a potential step. The rest of the expression is entirely due to the coupling between $|\underline{k}_b+\underline{g}_b>$ and $|\underline{k}_b+\underline{g}_c>$ which vanishes if we put $\beta = 0$. A resulting increase in the intensity of the (0,0) spot when another spot is being Bragg excited has been termed a secondary Bragg peak by McRae(13).

We also make the distinction that the present physical explanation of secondary Bragg peaks is not the same as that derived by Boudreaux and Heine (14). Their discussion does not consider internal reflections from the inner potential, so that their description is on the basis of a single Bloch function in the crystal. Consequently, they do not obtain secondary Bragg peaks using zero order wave functions. This is also true for our analysis if we prevent the internal reflections by putting the inner potential equal to zero, then:

$$p^+ = (k_o^+ + g_o^+) \text{ and } p_b^+ = (k_b^+ + g_b^+)$$

whence, in 2.73

$$Y = Z = 1$$

so that the secondary Bragg peak vanishes. Thus, taking the inner potential to be zero, secondary Bragg peaks can only arise through first order corrections to the Bloch states.

For a finite inner potential, such corrections are also necessary if 2.70 does not apply. However, 2.70 is valid in a large number of cases, for example, it is always true for every reciprocal lattice vector in cubic systems for a (100) crystal surface. Moreover, since we predict secondary Bragg peaks taking the Bloch states to only zero order, they are likely to be much more intense than the peaks predicted by the mechanism of Broudeaux and Heine. The physics is also very clear as can be seen by referring to diagram 2.6. The specularly transmitted beam $|\underline{k}_o+\underline{g}_o>$ is on a Bragg condition producing $|\underline{k}_o+\underline{g}_a>$, this can be regarded as being reflected from the crystal surface to produce $|\underline{k}_b+\underline{g}_b>$ which in turn excites $|\underline{k}_b+\underline{g}_c>$. Now $|\underline{k}_b+\underline{g}_c>$ is propagating in just the right direction to enhance the (0,0) reflected intensity.

Again, it is reasonable, physically, to expect the secondary Bragg peak in $I(\underline{p}''+\underline{g}_o'')$ and the Bragg peak in $I(\underline{p}''+\underline{g}_b'')$ to disappear when $(k_o+g_a)^{\perp} > 0$. However, the situation is more complicated when $(k_o+g_a)^{\perp}$ is close to zero. This is because the reciprocal lattice vector $\{(\underline{g}_b-\underline{g}_c) + (\underline{g}_o-\underline{g}_a)\}$ exists. This vector is of the type producing Bragg peaks in the (0,0) beam. When $(k_o+g_a)^{\perp}$ is zero, then we are exactly on such a Bragg condition at the same time as being on the secondary Bragg condition already described. However, for the time being, we show that indeed, the reflected intensities do disappear when $(k_o+g_a)^{\perp}$ is sufficiently positive that we can ignore the presence of the reciprocal lattice vector $\{(\underline{g}_o-\underline{g}_a) + (\underline{g}_b-\underline{g}_c)\}$. This situation is sketched in diagram 2.7, where the wave-vectors of the plane waves in the vacuum have been omitted.

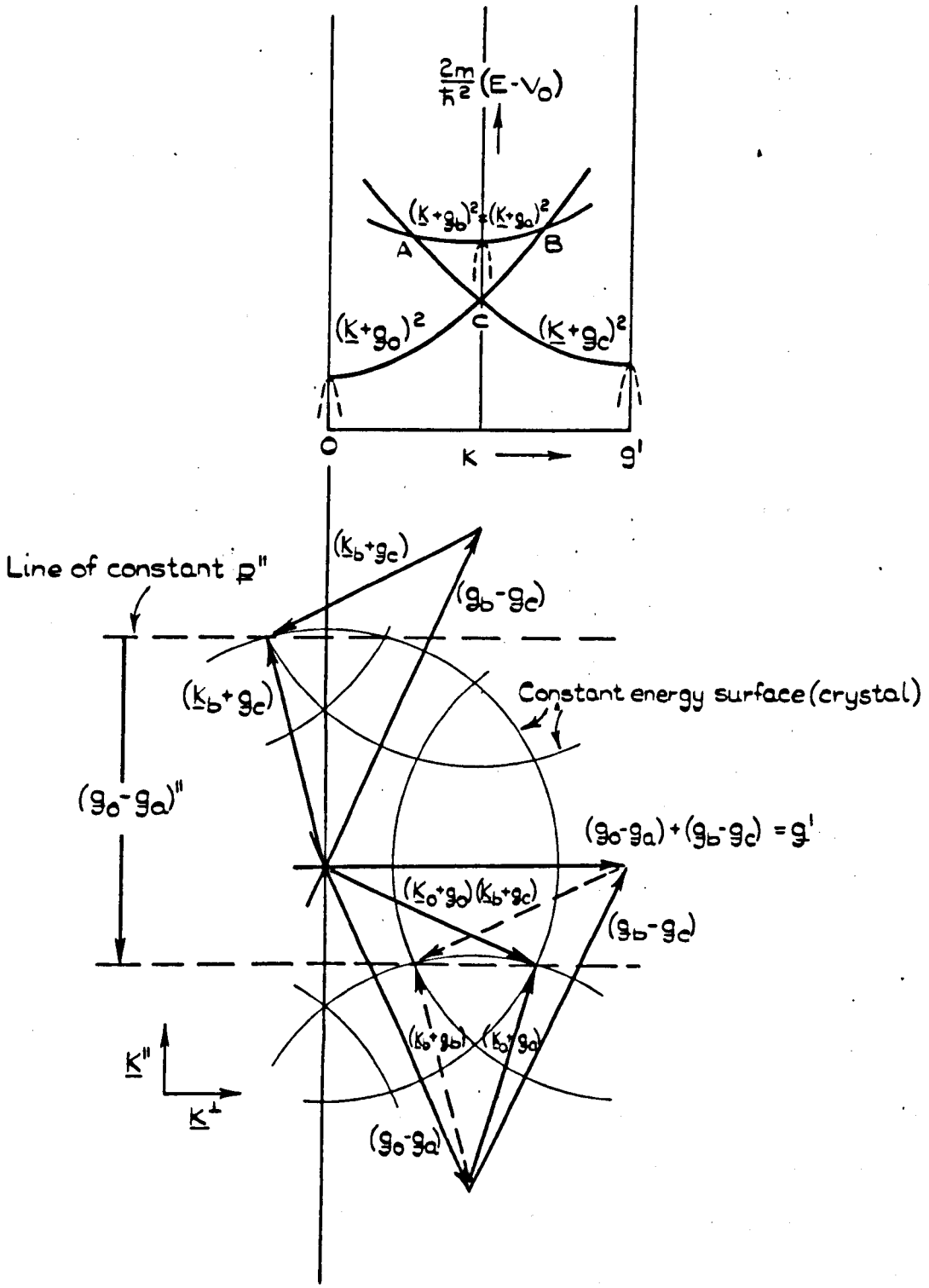
$\frac{2m}{\hbar^2}(E-V_0)$
$(\underline{K}+g_b)^2$ $(\underline{K}+g_a)^2$
A
B
C
$(\underline{K}+g_0)^2$
$(\underline{K}+g_c)^2$
0
K
g'
Line of constant p"
$(\underline{K}_b+g_c)$
(g_b-g_c)
$(\underline{K}_b+g_c)$
Constant energy surface (crystal)
$(g_0-g_a)''$
$(g_0-g_a)+(g_b-g_c)=g'$
$(\underline{K}_0+g_0)(\underline{K}_b+g_c)$
(g_b-g_c)
$(\underline{K}_b+g_b)$ $(\underline{K}_b+g_a)$
$\underline{K}''$
$\underline{K}^\perp$
(g_0-g_a)

DIAGRAM 2.7

The points A and B on the energy bands correspond to the energy of the k-space diagram. The point marked C corresponds to the energy at which a Bragg peak due to g' is expected for this value of $\underline{p}''$. The free electron bands (at A) show that the Bloch wave, whose components are $\exp i(\underline{k}_b+\underline{g}_b).\underline{r}$ and $\exp i(\underline{k}_b+\underline{g}_c).\underline{r}$, propagates flux towards the surface ($\nabla_{\underline{k}} E < 0$ for both the free electron bands) and so must be excluded, at the outset, from the set of matching functions. We are then left with the situation encountered in connection with diagram 2.5. Thus the reflected intensity is weak when $(k_o+g_a)^{\perp}$ is positive.

We disregard the case when $(k_o+g_a)^{\perp} = 0$ until we come, in the next chapter, to a calculation appropriate for such a situation.

The foregoing, with $(k_o+g_a)^{\perp} < 0$, demonstrates the origin of a secondary Bragg peak in the specularly reflectivity which is accompanied by a Bragg peak in the $I(\underline{p}''+\underline{g}_b'')$ intensity. The NFE energy bands and intensities are shown schematically in diagram 2.8. As far as the energy bands are concerned, the only difference between the present situation and that of diagram 2.5, is that now $E(k^{\perp}) = E(-k^{\perp})$.

Comparison with experiment

The mechanism we have proposed for secondary Bragg peaks is likely to be the dominant one. Firstly, this is because such peaks are predicted to zero order in the wavefunctions. Secondly, because the mechanism involves the minimum amount of multiple scattering in the crystal. Such peaks produced by higher order processes in multiple scattering are likely to be damped out to a much greater degree by the inelastic scattering

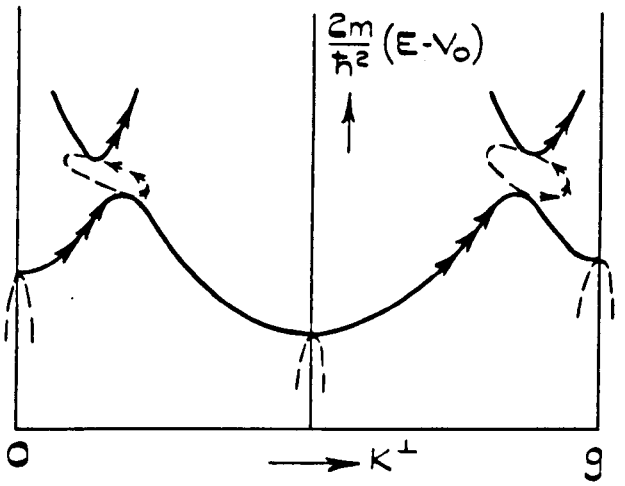
$\frac{2m}{\hbar^2}(E-V_0)$
0
$K^{\perp}$
g

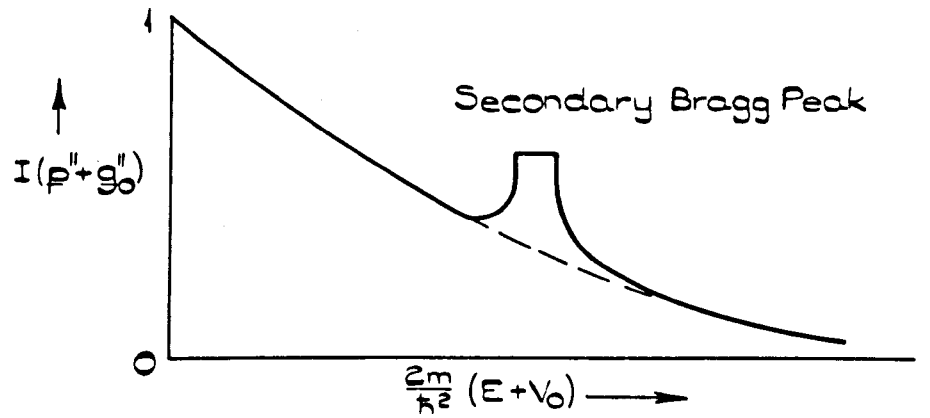
$I(p''+g_0'')$
Secondary Bragg Peak
0
$\frac{2m}{\hbar^2}(E+V_0)$

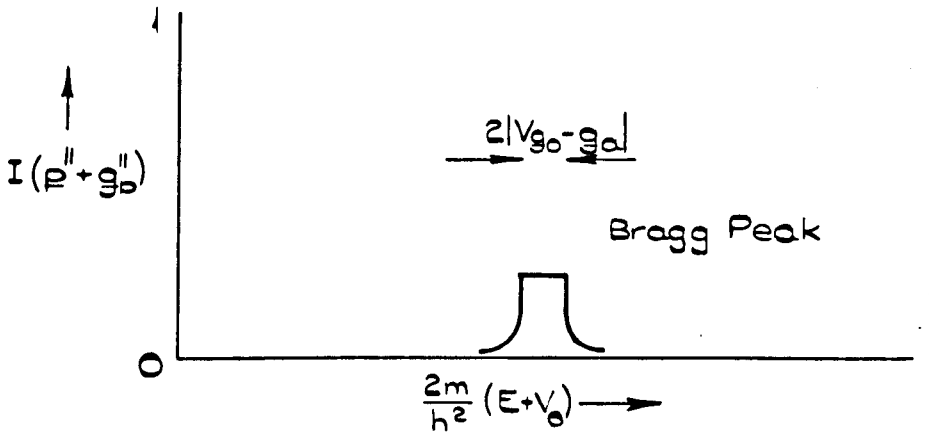
$I(p''+g_0'')$
$2|V_{g_0}-g_a|$
Bragg Peak
0
$\frac{2m}{\hbar^2}(E+V_0)$

DIAGRAM 2.8

processes. We can test this hypothesis by evaluating what peak should occur for a given structure and compare this with experiment. We choose the (111) face of the face-centred cubic structure. We evaluate the peaks for normal incidence and compare the results with those obtained by Taylor (28) at an angle of incidence of 4° on the (111) face of copper.

For this surface, not all the reciprocal lattice points of the b.c.c. reciprocal lattice play a role in the production of peaks in the (0,0) intensity. We consider the lattice as a stacking of hexagonal planes, in the familiar sequence ABCABC ... , as shown in diagram 2.9, which are perpendicular to the direction of normal incidence. If 2a is the length of the cube edge in the direct lattice then the reciprocal lattice points within a given layer are $2\sqrt{2}\left(\frac{\pi}{a}\right)$ apart. Reciprocal lattice vectors within a layer, $g_{\ell m}$, have:

$$g_{\ell m}^2 = \left(\frac{\pi}{a}\right)^2 (2\ell^2 + 6m^2) \qquad 2.74$$

where the integers ℓ and m are both even or both odd. Identical layers are spaced at intervals of $\sqrt{3}\left(\frac{\pi}{a}\right)$. It is clear from the diagram that if we choose the origin of k-space to be in an A-plane, say, then pairs of reciprocal lattice points satisfying 2.70 can only occur on the A-planes. Reciprocal lattice points on the B and C planes, within the frame-work of this discussion, will not contribute to the (0,0) intensity. Thus the reciprocal lattice vectors of interest, $g_{\ell mn}$, have:

$$g_{\ell mn}^2 = g_{\ell m}^2 + g_n^2 \qquad 2.75$$

where $g_{\ell m}^2$ is given by 2.74 and:

Body-centred cubic reciprocal lattice points viewed normally for a (111) face. The points in layer A are denoted by ● , in layer B by Δ and in layer C by X.

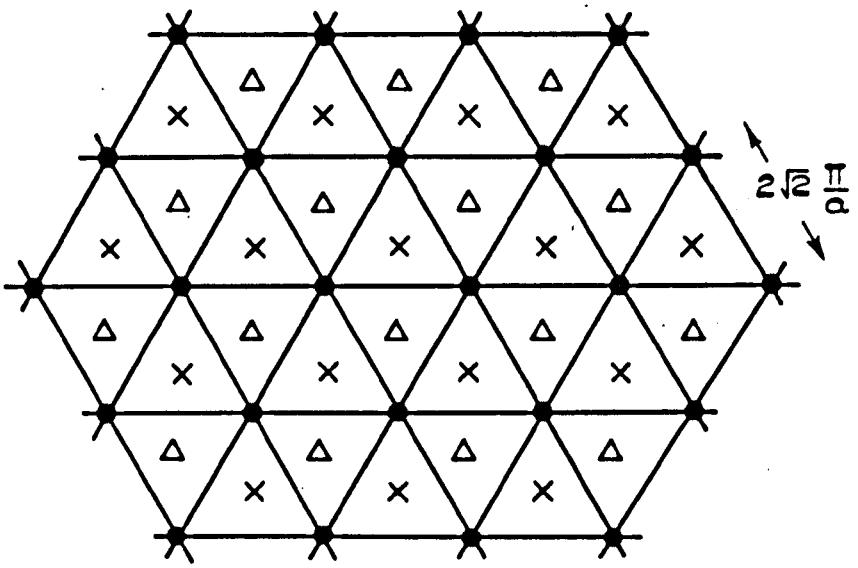

DIAGRAM 2.9

n	1	2	3	4	5	6	7	8
$2l^2+6m^2$	0	0,8	0,8,24	0,8,24,32	0,8,24,32	0.8.24,32	0,8	0
γ	1	2,$2\frac{1}{3}$	3,$3\frac{8}{9}$,$5\frac{2}{3}$	4,$4\frac{2}{3}$,6,$6\frac{2}{3}$	5,$5\frac{8}{15}$,$6\frac{3}{5}$,$7\frac{2}{15}$	6,$6\frac{4}{9}$,$7\frac{1}{3}$,$7\frac{7}{9}$	7,$7\frac{8}{21}$	8

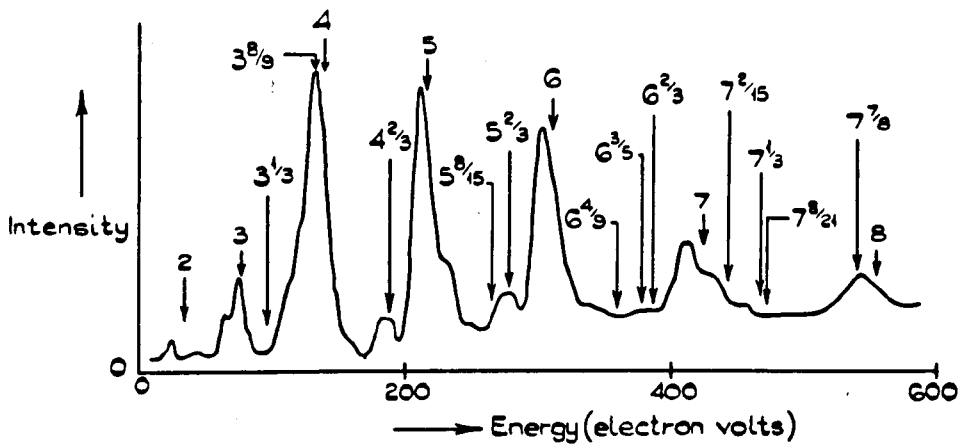

Taylor's results for the specular intensity obtained for Cu (111) at 4° incidence. Superimposed are the positions of the secondary Bragg peaks expected to be most intense. These positions have not been corrected for the inner potential.

DIAGRAM 2.10

$$g_n = n\sqrt{3}\,\frac{\pi}{a}\,. \qquad 2.76$$

The Bragg condition is:

$$2\underline{k}\cdot\underline{g}_{\ell mn} = g^2_{\ell mn} \qquad 2.77$$

which for the vectors 2.75 gives intensity peaks in the (0,0) beam. We ignore the inner potential correction so that $\underline{k}$ is the wave-vector of the incident beam. For normal incidence 2.77 becomes:

$$2k = \frac{g^2_{\ell mn}}{g_n} \qquad 2.78$$

Conventionally, when we refer to Bragg peaks of order n for the (111) face of a face-centred cubic direct lattice and at normal incidence, we have:

$$2k = n\sqrt{3}\left(\frac{\pi}{a}\right) \qquad 2.79$$

Hence, 2.78 refers to Bragg peaks of order γ, where:

$$\gamma = \frac{g^2_{\ell mn}}{g_{n\frac{\pi}{a}\sqrt{3}}} = n\left(1 + \frac{2\ell^2+6m^2}{3n^2}\right) \qquad 2.80$$

where we have used 2.74 and 2.76. We notice also that the restriction:

$$0 < k^+ \leq (\underline{k}-\underline{g}_{\ell mn})^+ \qquad 2.81$$

reduces in this case to:

$$n > 0 \text{ with } (2\ell^2+6m^2) \leq 3n^2 \qquad 2.82$$

We see that γ is not necessarily an integer, and following convention, we refer to 'fractional order' peaks.

In diagram 2.10 we tabulate values of γ up to eight using 2.80 and paying due regard to 2.81. These are superimposed on Taylor's results in the same diagram. There appears to be a fair degree of correlation. That the peaks of orders $3^{1}/3$ and $7^{7}/9$ are missing is no denial of our hypothesis since we make no prediction as to the intensities of such peaks. At higher energies where the flux is shared amongst many beams we expect the secondary peaks to have particularly low intensity. A better test of the hypothesis would be to seek secondary Bragg peaks which have an order which is not predicted on the present basis. We remember that the predicted peak positions have not been corrected for the inner potential which should be most noticeable at the lower energies. Despite this there appear to be weak peaks at about $2^{1}/3$ and $2^{2}/3$. On the whole, however, the correlation is encouraging. We note especially that the number of secondary Bragg peaks seen is of the same order as the number predicted by the present process. It would therefore appear that the mechanism of Heine and Boudreaux predicts far too many peaks.

Our discussion has been mainly restricted to the cases where, at most, two Bloch waves have been excited in the crystal. In principle there is no difficulty in dealing with a large number of such waves where one imagines secondary Bragg peaks can occur in a much more complicated manner. From a simple-minded point of view it would appear that such processes (where electrons suffer many more collisions before being ejected) are less likely in general to produce large peaks because of the inelastic scattering.

(iii) The specularly transmitted beam being coupled to beams lying in the crystal surface

The calculations of McRae (13) show that the (0,0) intensity undergoes a maximum followed by a minimum at energies where possible diffracted beams lie in the crystal surface. We look now at this possibility in our formulation of the problem.

Boudreaux and Heine (14) have already shown how the specularly reflected beam can suffer such a resonance, however, in practice, their particular example should not be observed. At around the energy of interest their wavefunction in the crystal consisted of two Bloch waves. The first comprised, essentially, of plane-wave components lying in, or nearly in, the surface. The second propagated flux into the crystal. Now, because they chose the situation of normal incidence, the first Bloch wave formed a standing wave in the crystal surface at the energy when its plane-wave components lay in the surface. They also ignored the inner potential correction which, at this critical energy, ensured that the boundary conditions required that the amplitude of the second propagating Bloch wave became zero. Thus, physically, it is clear why a peak in reflectivity was obtained. There was no propagating wave, at this energy, to remove flux from the crystal surface except the specularly reflected wave. This thus acquired the same intensity as the incident wave. In practice, as they point out, the zero in the amplitude of the propagating Bloch wave is likely to be so effectively removed by the inner potential that no peak will be observed. This is also indicated in a calculation in Chapter III.

In Chapter III we show how the specular intensity can be large when we strongly excite beams lying in the crystal surface. This is achieved with reasonable values for the inner potential and even if the wavefunctions are evaluated to zero-order. However, the situation then described is really our secondary Bragg peak mechanism operating through intermediate beams lying in the crystal surface, and not a surface resonance.

For our present purposes we just point out that a surface resonance need not be observed just because the specularly transmitted wave is strongly coupled to beams lying in the surface. We can see this by looking at the results of the last section associated with diagram 2.3. We see from 2.61 that the specularly reflected intensity is always that associated with a potential step. Thus, even if $|\underline{k}_o+\underline{g}_a>$ propagates in the surface, no special structure is seen in the (0,0) intensity.

We delay further discussion of the so-called surface resonance effect until we have performed some relevant calculations in Chapter III.

(iv) In conclusion

We have discussed only a few effects one might observe with multiple scattering. Indeed, the simplicity of the situations described will only be encountered at the lowest energies. There is a whole hierarchy of multiple scattering situations which grow in complexity as the energy increases. We do expect, however, that the Bragg peaks, which are so

intense, will dominate the intensity structure at all energies. It might be that at higher energies, where many beams are excited, the fine structure due to the secondary Bragg peaks and surface resonances will be less intense. The reason being that the intensity has to be shared between so many beams.

In the next chapter we amplify and add to the results of this chapter. The results of both chapters are then summarised, for future use, in the concluding section of Chapter III. Throughout these two chapters we only take the wavefunctions to zero-order. The predictions made should thus, at least, describe the gross effects seen in the intensity plots at the lowest energies. At higher energies, calculations, using the formalism of section B of this chapter, would seem more appropriate than a qualitative discussion.

We have assumed the inner potential to be independent of energy. A simple model, predicting the behaviour of the inner potential as a function of energy due to the polarizing effects of the incident electrons is described in Appendix V.

CHAPTER III

Calculations of LEED intensities at normal incidence on a (100) face of the NaCl crystal structure

In this chapter we use the methods of Chapter II and Appendix II to carry out some detailed numerical calculations of LEED intensities. In particular, we treat the case of normal incidence on a (100) face of the f.c.c. structure which has two oppositely charged ions per unit cell. The calculations may, therefore, be indicative of observations on the alkali halides in LEED experiments; the real purpose, however, is to confirm and add to the qualitative results of Chapter II.

The results of the calculations can only be expected to give qualitatively feasible results. This is because we use the model described at the beginning of Chapter II, which carries with it various approximations, and we also determine the wavefunctions in the crystal only to zero-order in the perturbation. While the NFE approximation would clearly not be appropriate for calculating the energy bands and wavefunctions for the valence electrons, it seems a reasonable first approach for the energies of interest.

First, we find the free electron bands appropriate for normal incidence. Then, from Chapter II, we know that the crystal behaves like a potential step scatterer when the free electron energy band associated with the specularly transmitted beam is not (or not nearly) degenerate

with any other. The energies of interest, near which the intensities will show special structure, are then those energies where the free electron energy band of the specularly transmitted beam is degenerate with other bands. These points of degeneracy are treated in turn as we increase the energy up to a value which corresponds to ~ 60 eV for lithium fluoride.

A. Free Electron Bands

(i) Notation and units

The direct lattice of interest is the f.c.c. lattice with a translation group consisting of a positive ion separated by half the cube diagonal from a negative ion. We define the unit vectors, $\underline{i}$, $\underline{j}$ and $\underline{k}$ to lie along the x, y and z cartesian directions. The direct lattice cube has edges of length 2a which are parallel to $\underline{i}$, $\underline{j}$ and $\underline{k}$.

The primitive basis vectors of the direct lattice are then:

$$\left.\begin{aligned} \underline{a}_1 &= a(\underline{j}+\underline{k}) \\ \underline{a}_2 &= a(\underline{k}+\underline{i}) \\ \underline{a}_3 &= a(\underline{i}+\underline{j}) \end{aligned}\right\} \qquad 3.1$$

so that the positively charged ions are found at $\underline{r}_{\ell mn}$, where ℓ, m and n are integers:

$$\underline{r}_{\ell mn} = \ell\underline{a}_1 + m\underline{a}_2 + n\underline{a}_3 = a\left[\underline{i}(m+n) + \underline{j}(\ell+n) + \underline{k}(\ell+m)\right] \qquad 3.2$$

while the negatively charged ions are found at $\underline{r}'_{\ell mn}$:

$$\underline{r}'_{\ell mn} = \underline{r}_{\ell mn} + a(\underline{i}+\underline{j}+\underline{k}). \qquad 3.3$$

We define the primitive basis vectors of the reciprocal lattice in the usual way:

$$\underline{b}_1 = \frac{2\pi\ \underline{a}_2 \wedge \underline{a}_3}{\underline{a}_1 \cdot (\underline{a}_2 \wedge \underline{a}_3)} \quad \text{etc.}$$

so that

$$\left.\begin{aligned} \underline{b}_1 &= \frac{\pi}{a}(-\underline{i}+\underline{j}+\underline{k}) \\ \underline{b}_2 &= \frac{\pi}{a}(\underline{i}-\underline{j}+\underline{k}) \\ \underline{b}_3 &= \frac{\pi}{a}(\underline{i}+\underline{j}-\underline{k}) \end{aligned}\right\} \qquad 3.4$$

A general reciprocal lattice vector is then given by:

$$\underline{G}_{rst} = \frac{\pi}{a}\left(\underline{i}(-r+s+t) + \underline{j}(r-s+t) + \underline{k}(r+s-t)\right) \qquad 3.5$$

where r, s and t are integers.

The free electron bands are given by the paraboloids:

$$E_{rst} = \frac{\hbar^2}{2m}(\underline{k}+\underline{G}_{rst})^2 \qquad 3.6$$

where $\underline{k}$ lies within the first Brillouin zone. We choose to use dimensionless units where k and G_{rst} are measured in units of $\frac{\pi}{a}$ and the energy in units of $\frac{\hbar^2}{2m}\left(\frac{\pi}{a}\right)^2$, then we write 3.6 as:

$$E_{rst} = (\underline{k} + \underline{i}\{-r+s+t\} + \underline{j}\{r-s+t\} + \underline{k}\{r+s-t\})^2 \qquad 3.7$$

For future reference we note the following: for lithium fluoride, $a = 2.01$ Å so that:

$$\left[\frac{\hbar^2}{2m}\left(\frac{\pi}{a}\right)^2\right]_{LiF} = 9.31 \text{ eV} \qquad 3.8$$

while for sodium fluoride, a ≈ 2.31 Å, so that:

$$\left[\frac{\hbar^2}{2m}\left(\frac{\pi}{a}\right)\right]_{NaF} = 7.05 \text{ eV} \qquad 3.9$$

3.9

In the case of a (100) face, the band structure has a period of $\frac{2\pi}{a}$ in k^+. The band-structure of interest, for a fixed $\underline{p}''$, is then restricted to:

$$-\frac{\pi}{a} < k^+ < \frac{\pi}{a}$$

(ii) Evaluation of the energy bands over the energy range of interest

We first find the maximum value of $|G_{rst}|$ in order that we can tabulate values of (r,s,t) such that E_{rst} covers a convenient range. If we are interested in electron energies in the vacuum up to about 50 eV, say, and take an inner potential of 10 eV then:

$$E_{rst} \leq 60 \text{ eV}$$

or, in particular, for lithium fluoride, using 3.8

$$E_{rst} \leq \frac{60}{9.3} \sim 6.5 \text{ units of } \frac{\hbar^2}{2m}\left(\frac{\pi}{a}\right)^2 \qquad 3.10$$

Then 3.7 gives with 3.10:

$$(\underline{k}+\underline{G}_{rst})^2_{max} \sim 6.5 \qquad 3.11$$

where $|\underline{k}+\underline{g}|$ is measured in units of $\frac{\pi}{a}$. Now

$$\left|\underline{k}\right|_{max} = 1$$

for normal incidence, so that:

$$\left|\underline{G}_{rst}\right|_{max} \sim \sqrt{6.5} + 1 \sim 3.6$$

Now

$$G_{rst}^2 = (-r+s+t)^2 + (r-s+t)^2 + (r+s-t)^2 \qquad 3.12$$

so that we will require all (r,s,t) such that

$$12 \geq (-r+s+t)^2 + (r-s+t)^2 + (r+s-t)^2 \qquad 3.13$$

These are tabulated in diagram 3.1.

For normal incidence we write $\underline{k} = \underline{i}k$ in 3.7 to obtain:

$$E_{rst} = k^2 + 2k(-r+s+t) + G_{rst}^2 \qquad 3.14$$

E_{rst} is clearly real for k real and 3.14 are tabulated in diagram 3.1. Now k may be complex provided E_{rst} is real. Writing $k = k_r+ik_i$ 3.14 becomes:

$$E_{rst} = (k_r^2-k_i^2+2k_r(-r+s+t)+G_{rst}^2) + i(2k_ik_i+2k_i(-r+s+t)) \qquad 3.15$$

so that for lines of real energy:

$$k_i(k_r+(-r+s+t)) = 0$$

If $k_i \neq 0$ we can then have lines of real energy for

$$k_r = -(-r+s+t) \qquad 3.16$$

Then

$$E_{rst} = -k_i^2 - (-r+s+t)^2 + G_{rst}^2 \qquad 3.17$$

3.17 are also tabulated in diagram 3.1. The free electron bands are then plotted in diagram 3.2.

G^2_{rst}	r s t	E_{rst} K real	E_{rst} K complex
0	0 0 0	K^2 *	$-K_i^2$ ($K_r = 0$)
3	0 0 1 0 1 0 1 0 0 1 1 1	K^2+2K+3	$-K_i^2+2$ ($K_r = -1$)
	1 0 0 0 0 -1 0 -1 0 -1 -1 -1	K^2-2K+3	$-K_i^2+2$ ($K_r = 1$)
4	1 0 1 1 1 0 -1 -1 0 -1 0 -1	K^2+4	$-K_i^2+4$ ($K_r = 0$)
	0 1 1	K^2+4K+4*	—
	0 -1 -1	K^2-4K+4	—
8	2 1 1 -2 -1 -1 0 -1 1 0 1 -1	K^2+8	$-K_i^2+8$ ($K_r = 0$)
	1 1 2 1 2 1 -1 0 1 -1 1 0	K^2+4K+8	—
	-1 -1 -2 -1 -2 -1 1 0 -1 1 -1 0	K^2-4K+8	—
11	0 1 2 0 2 1 1 2 2 -1 1 1	$K^2+6K+11$	—
	0 -1 -2 0 -2 -1 -1 -2 -2 1 -1 -1	$K^2-6K+11$	—
	1 0 2 1 2 0 -2 0 -1 -2 -1 0 2 1 2 2 2 1 -1 1 -1 -1 -1 1	$K^2+2K+11$	$-K_i^2+10$ ($K_r = -1$)
	2 0 1 2 1 0 -1 0 -2 -1 -2 0 -2 -1 -2 -2 -2 -1 1 -1 1 1 1 -1	$K^2-2K+11$	$-K_i^2+10$ ($K_r = 1$)
12	0 0 2 0 2 0 -2 0 0 2 2 2	$K^2+4K+12$	—
	2 0 0 0 0 -2 0 -2 0 -2 -2 -2	$K^2-4K+11$	—

* The portions of these bands with $\nabla_{\underline{k}} E > 0$ correspond to the specularly transmitted beam.

DIAGRAM 3.1.

FREE ELECTRON BANDS ALONG ΓΔX OF b.c.c. RECIRROCAL LATTICE

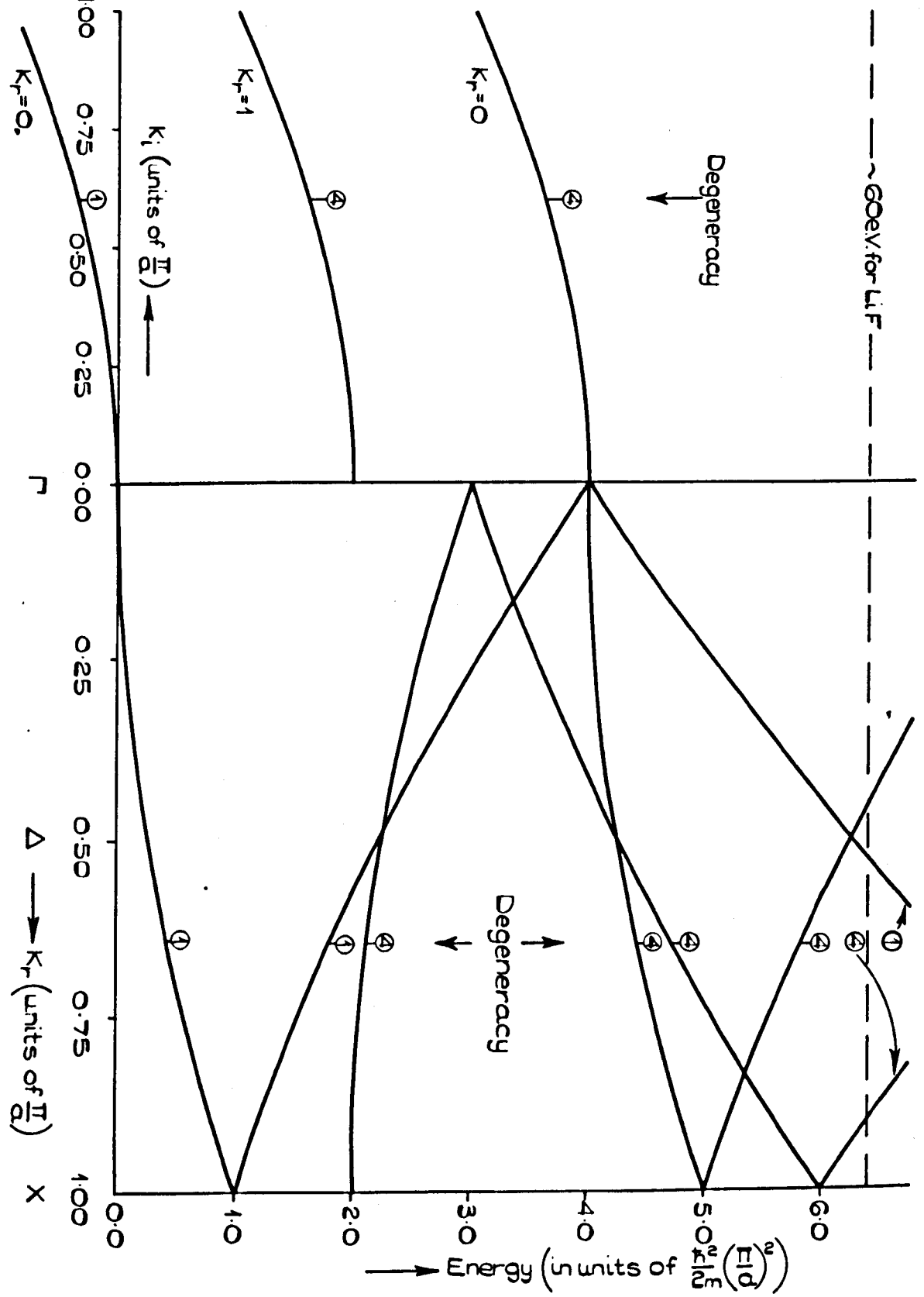

DIAGRAM 3.2

B. Calculation of the Energy Bands to First Order in the Perturbation, the Wavefunctions to Zero-order and the Resulting Reflection Coefficients

(i) Preliminary remarks

We now look in detail at points in the free electron energy bands where the specularly transmitted wave is degenerate with others. Using the equations in diagram 3.1 we easily evaluate the positions of these degeneracies. Within the energy range of interest, they occur at the following values of (k^+,E):

$$(1,1)\ ;\quad (-\tfrac{1}{2},\ 2^{1}/4)\ ;\quad (-\tfrac{1}{6},\ 3^{13}/36)\ ;\quad (0,4)\ ;\quad (\tfrac{1}{2},\ 6^{1}/4). \qquad 3.18$$

Provided (k^+,E) is not close to any of 3.18, then, in our approximation, the crystal scatters like a potential step.

Diagram 3.3 is the result of a computation for the reflection coefficient of a potential step as a function of E/V_o. For this we have used A1.23 with $\theta = 0$. The reflection coefficient is seen to fall off rapidly with E/V_o. When $E = V_o$, less than three per cent of the flux is back-scattered.

The form of the potential we will use in the perturbation is given by A4.20. As we have already indicated, we only expect qualitatively correct results and so A and $\left(\frac{q^+}{q^-}\right)$ are chosen to facilitate computation. Throughout $\left(\frac{q^+}{q^-}\right)$ is taken to be 0.5.

REFLECTION COEFFICIENT OF A POTENTIAL STEP AS A FUNCTION OF (E/V_0) AT NORMAL INCIDENCE.

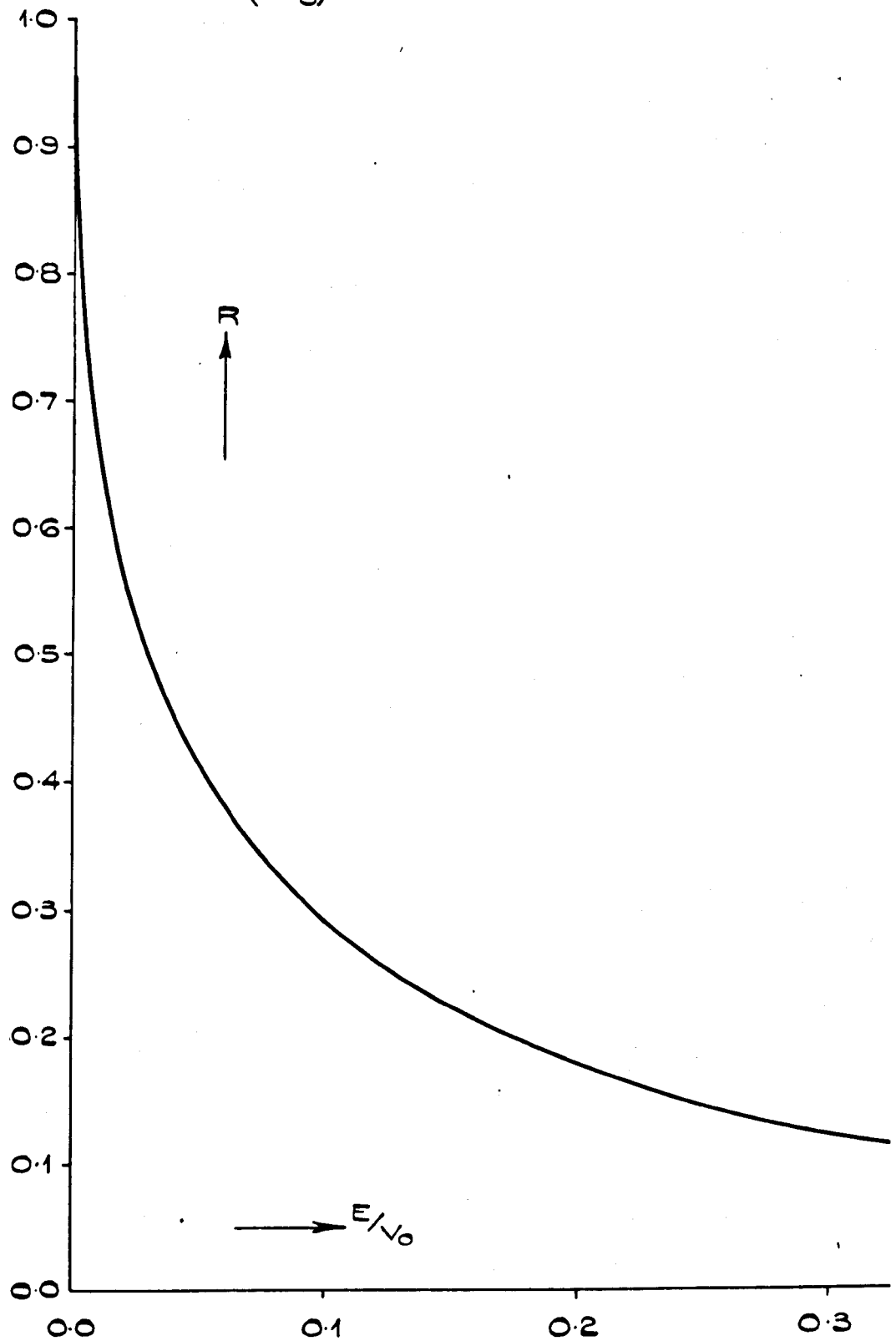

DIAGRAM 3.3.

In Appendix II we see that, in order to find the zero-order wave-functions and the first order corrections to the energy bands, we must diagonalise the matrix of the perturbation in the representation of plane waves having the same $\underline{k}$, and having approximately the same energy. The space is invariant under the group of $\underline{k}$ and so can be divided into irreducible subspaces. The perturbation matrix will then be in block diagonal form and the relatively low dimension blocks can, easily and independently, be diagonalised.

Before going on to look in detail at the situations near 3.18, we need to label the diffracted electron beams. From 2.18, we see that the intensities of the back-scattered beams are labelled by $(\underline{p}''+\underline{g}_r'')$. In the present situation we have $\underline{p}''=0$, so that the intensities will be labelled by:

$$\underline{g}_{nm}'' = n\underline{b}_1'' + m\underline{b}_2'' \qquad 3.19$$

where $\underline{b}_1$ and $\underline{b}_2$ are defined by 3.4. For conciseness, $I(\underline{g}_{nm}'')$ will be written R_{nm}. Incidentally, 3.19 (with regard to section C(a) of Chapter II) shows that the diffraction pattern will be a square array of spots which makes an angle of $\frac{\pi}{4}$ with the cube axes in the surface of the direct lattice. Experiments, of course, confirm this, e.g. McRae and Caldwell (9).

(ii) Calculations

We will now consider the situations presented by 3.18 in turn. For each we evaluate the energy bands and the R_{nm}, we also discuss the physical origin of the structure obtained in the calculated intensities. The section headings refer to the locality, (k^{+},E), of the situation being discussed. Throughout, the energy is measured from the zero of the energy bands.

(a) (1,1)

The situation in k-space, is sketched in diagram 3.4. The degeneracy corresponds to the specularly transmitted wave expi kx, being on a Bragg condition associated with the reciprocal lattice vector $\underline{G}_{011}$. In diagram 3.4, the wave-vector of the specularly transmitted beam is labelled a, while b denotes the wave-vector of the Bragg excited beam, expi(k-2)x.

Using the method of Appendix II, the energy bands are given by:

$$E = (k^2-2k+2) \pm \sqrt{(2k-2)^2 + V_{011}^2} \qquad 3.20$$

in the locality of the two-fold degeneracy. The energy bands are clearly real for k real. If we write:

$$k = 1 + ik_i \qquad 3.21$$

then 3.20 becomes:

$$E = (1-k_i^2) \pm \sqrt{(V_{011}-2k_i)(V_{011}+2k_i)} \qquad 3.22$$

K-SPACE DIAGRAMS

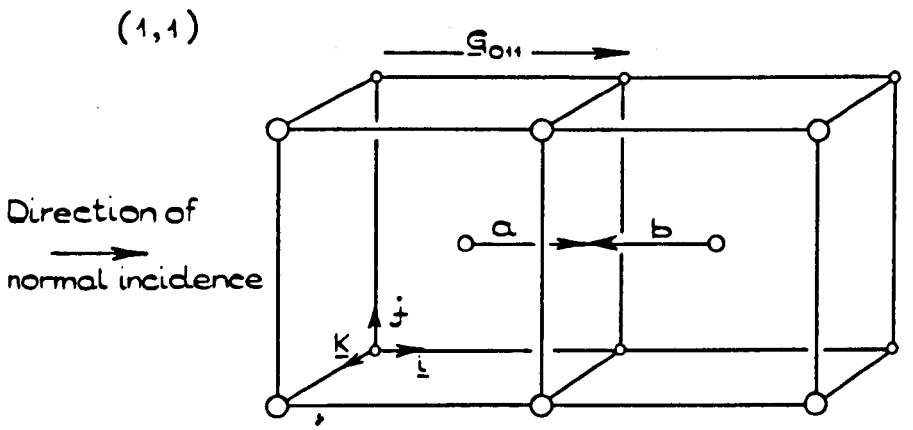

DIAGRAM 3.4

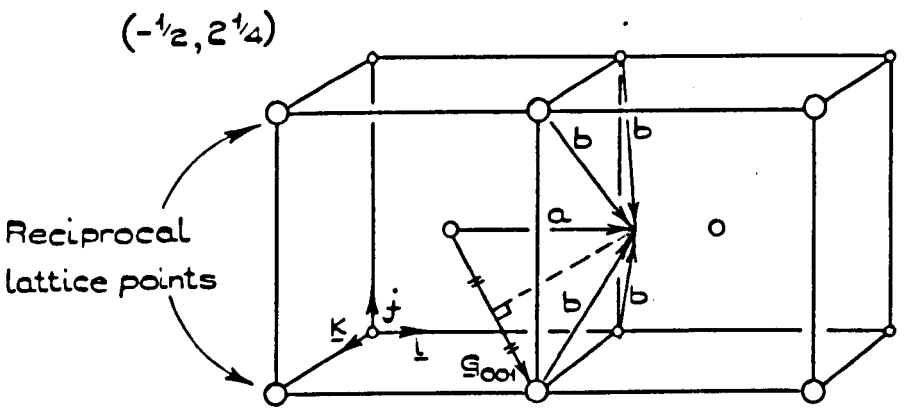

DIAGRAM 3.5

which is real for:

$$|k_i| \leq \frac{V_{011}}{2}$$

The points, $k_i = \pm \frac{V_{011}}{2}$, are branch points at which the energy is real. The energy bands for real k, 3.20, and complex k, 3.21, have been computed and are shown in diagram 3.6. The value of A, in the potential A4.20, has been taken as one. For our purposes, it is only of incidental interest that this corresponds to a band gap of ~ 2.3 eV for lithium fluoride.

We now come to a determination of the reflectivity. The wavefunction near the degeneracy, in our approximation, is:

$$\psi_i = B(e^{ikx} + \alpha e^{i(k-2)x}) \qquad 3.23$$

where

$$\alpha = -\frac{(k^2-E)}{V_{011}} \qquad 3.24$$

It is easy to show, in the manner described in Chapter II, that 3.23 is the only contribution to the matched wavefunction in the crystal. In the vacuum, the wavefunction is:

$$\psi_o = Ae^{ipx} + A_o e^{-ipx} \qquad 3.25$$

where the first term is the incident wave and the second is the specularly reflected wave.

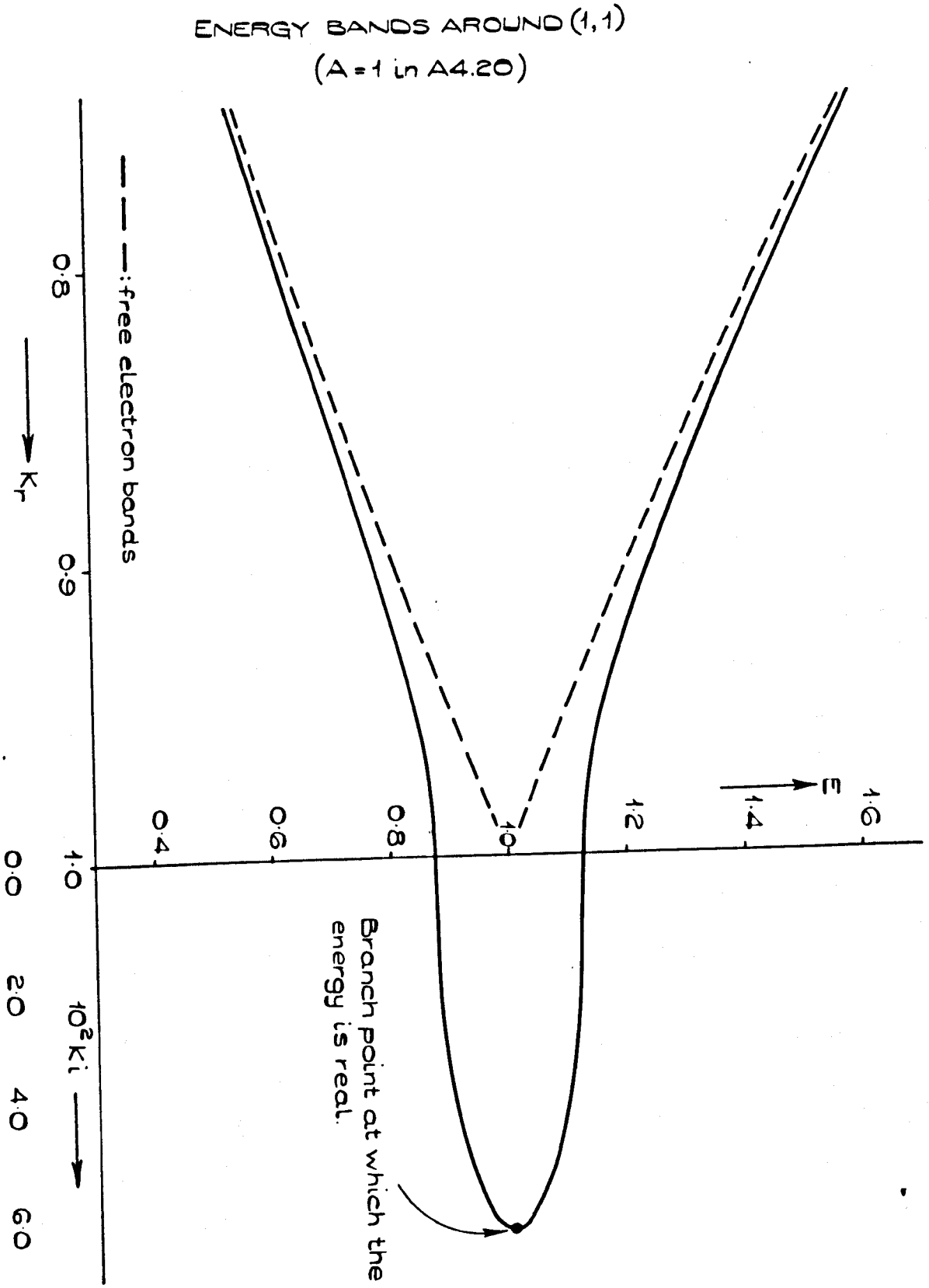
ENERGY BANDS AROUND (1,1)
(A = 1 in A4.20)
— — —: free electron bands
k_r
0·8
0·9
1·0
0·0
2·0
4·0
6·0
$10^2 k_i$
0·4
0·6
0·8
1·0
1·2
1·4
1·6
E
Branch point at which the energy is real.

DIAGRAM 3.6

The boundary conditions, 2.3 and 2.4, give:

$$R_{oo} = \left|\frac{A_o}{A}\right|^2 = \left|\frac{(p-k) + \alpha(p-k+2)}{(p+k) + \alpha(p+k-2)}\right|^2 \qquad 3.26$$

The specular intensity can now, with the use of 3.20, 3.24 and:

$$p = \sqrt{E-V_o} = \sqrt{\text{Incident Energy}} \qquad 3.27$$

be evaluated as a function of energy. This is shown in diagram 3.7 Several values of the inner potential, V_o, have been used.

For a zero inner potential, the shape of the Bragg peak is more or less symmetical about its centre. The immediate effects of a non-zero inner potential are to take R_{oo} to one for zero incident energy and to decrease the value at energies just above the peak. In fact R_{oo} becomes zero at an energy higher than that at the peak. This happens at the energy where:

$$\left(\frac{p-k}{g}\right) = \left(\frac{\alpha}{1+\alpha}\right) \qquad 3.28$$

It is easy to show that the zero only lies close to the peak if:

$$\left(\frac{E_B}{V_o}\right) \ll 1 \qquad 3.29$$

where E_B is the incident energy at which the Bragg peak is observed. The occurrence of the zero might be regarded as tenuous in the light of our approximations.

SPECULARLY REFLECTED INTENSITY AS A FUNCTION OF ENERGY

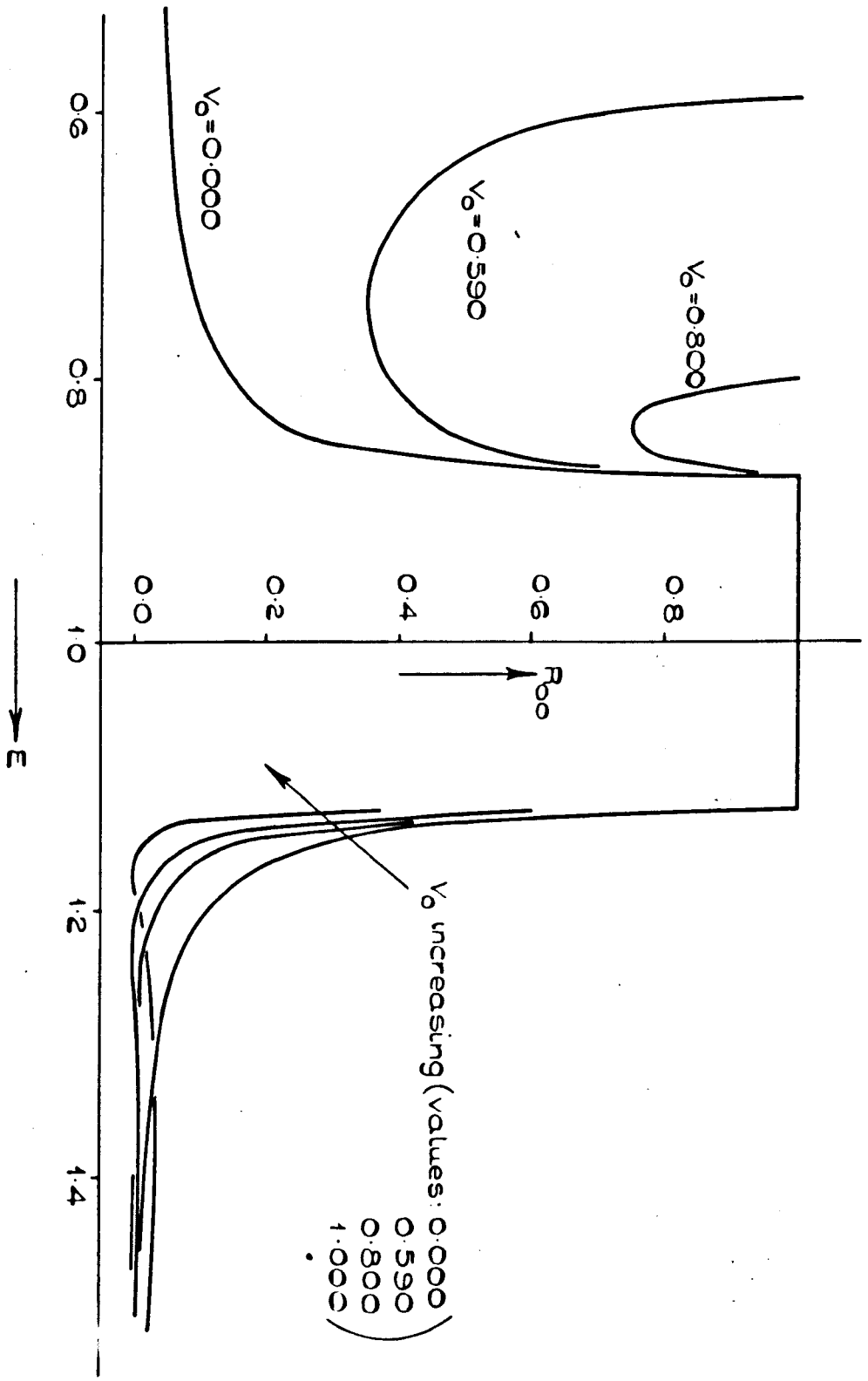

DIAGRAM 3.7

However, the peak in the R_{oo} should in no way be regarded as tenuous. The reason for its occurrence is easily appreciated. As we increase the incident energy from below the band gap the specularly transmitted beam moves closer to the Bragg condition so that the beam with wave-vector b (diagram 3.4) is more strongly excited. The flux in the latter is directed immediately into the specularly reflected beam whose intensity is thus enhanced. At energies within the band gap the only wave that can be excited in the crystal is localised at x = 0 and can carry no flux, thus all the incident flux is reflected. As we move to higher energies away from the Bragg condition the intensity of the beam with wave-vector b decreases. In all, the qualitative behaviour follows that outlined in Chapter II.

(b) $(-\frac{1}{2}, 2^{1/4})$

The situation in k-space is sketched in diagram 3.5. The five-fold degeneracy corresponds to the specularly transmitted wave, with wave-vector labelled a, being simultaneously on Bragg conditions for each of the reciprocal lattice vectors:

$$\underline{G}_{100}, \underline{G}_{111}, \underline{G}_{010} \text{ and } \underline{G}_{001}.$$

Thus four additional waves, with wave-vectors labelled b, are excited.

The wavefunctions near $(-\frac{1}{2}, 2^{1/4})$ will be linear combinations of the five plane waves:

$$\left.\begin{aligned}
\phi_1 &= \gamma\ \mathrm{expi}(k+2)x \\
\phi_2 &= \gamma\ \mathrm{expi}[(k+1)x+y+z] \\
\phi_3 &= \gamma\ \mathrm{expi}[(k+1)x-y-z] \\
\phi_4 &= \gamma\ \mathrm{expi}[(k+1)x+y-z] \\
\phi_5 &= \gamma\ \mathrm{expi}[(k+1)x-y+z]
\end{aligned}\right\} \qquad 3.30$$

where γ is a normalisation constant. The perturbation matrix near $(-\frac{1}{2}, 2^{1/4})$, following Appendix II, is shown in diagram 3.8. Since the wave-vector lies on a symmetry axis of the Brillouin zone, group theory suggests a change of basis from ϕ, 3.30, to ϕ':

$$\phi' = s\ \phi \qquad 3.31$$

and where s is given in diagram 3.8. The wavefunctions ϕ_3', ϕ_4' and ϕ_5' transform irreducibly under symmetry rotations about the normal to the crystal face, but they clearly do not transform according to the unit representation. Thus, for normal incidence, these wavefunctions cannot enter into the total, matched wavefunction. We shall desregard them, and their associated energy bands, from now on. The energy bands of interest are then given by $E^{\pm}$ (diagram 3.8). which ensure that $\det A' = 0$. These energy bands have been computed for $A = {}^{1}/_{10}$ in A4.20. The result is shown in diagram 3.9. The energy is real for real k only. This is because no extrema for real k occur in the energy near $(-\frac{1}{2}, 2^{1/4})$.

We proceed now to investigate the reflectivity. The wavefunctions associated with the two bands shown in diagram 3.9 are:

PERTURBATION MATRIX NEAR $(-1/2, 2\,1/4)$

$$\det A = \begin{vmatrix} \Delta E_1 & V_{-100} & V_{111} & V_{010} & V_{001} \\ V_{100} & \Delta E_2 & V_{211} & V_{110} & V_{101} \\ V_{-1-1-1} & V_{-2-1-1} & \Delta E_2 & V_{-10-1} & V_{-1-10} \\ V_{0-10} & V_{-1-10} & V_{101} & \Delta E_2 & V_{0-11} \\ V_{00-1} & V_{-10-1} & V_{110} & V_{01-1} & \Delta E_2 \end{vmatrix} = \begin{vmatrix} \Delta E_1 & -b & -b & -b & -b \\ -b & \Delta E_2 & b/8 & b/4 & b/4 \\ -b & b/8 & \Delta E_2 & b/4 & b/4 \\ -b & b/4 & b/4 & \Delta E_2 & b/8 \\ -b & b/4 & b/4 & b/8 & \Delta E_2 \end{vmatrix} = 0$$

where $\Delta E_1 = (K+2)^2 - E = E_1 - E$; $\Delta E_2 = (K^2+2K+3) - E = E_2 - E$

and $b = -V_{100}$

$$S = \begin{vmatrix} 1 & 0 & 0 & 0 & 0 \\ 0 & 1/2 & 1/2 & 1/2 & 1/2 \\ 0 & 1/2 & 1/2 & -1/2 & -1/2 \\ 0 & 1/2 & -1/2 & 0 & 0 \\ 0 & 0 & 0 & 1/2 & -1/2 \end{vmatrix}$$

$$SAS^{-1} = \begin{vmatrix} \Delta E_1 & -2b & 0 & 0 & 0 \\ -2b & (\Delta E_2 + 5/8 b) & 0 & 0 & 0 \\ 0 & 0 & (\Delta E_2 - 3/8 b) & 0 & 0 \\ 0 & 0 & 0 & (\Delta E_2 - b/8) & 0 \\ 0 & 0 & 0 & 0 & (\Delta E_2 - b/8) \end{vmatrix} ; \det A' = \begin{vmatrix} \Delta E_1 & -2b \\ -2b & (\Delta E_2 + 5/8 b) \end{vmatrix} = 0$$

$$E^{\pm} = 1/2 \left[\{E_1 + E_2 + 5/8 b\} \pm \sqrt{(E_1 - E_2)^2 + 5/4 b (E_2 - E_1) + 16\,25/54\, b^2} \right]$$

DIAGRAM 3.8

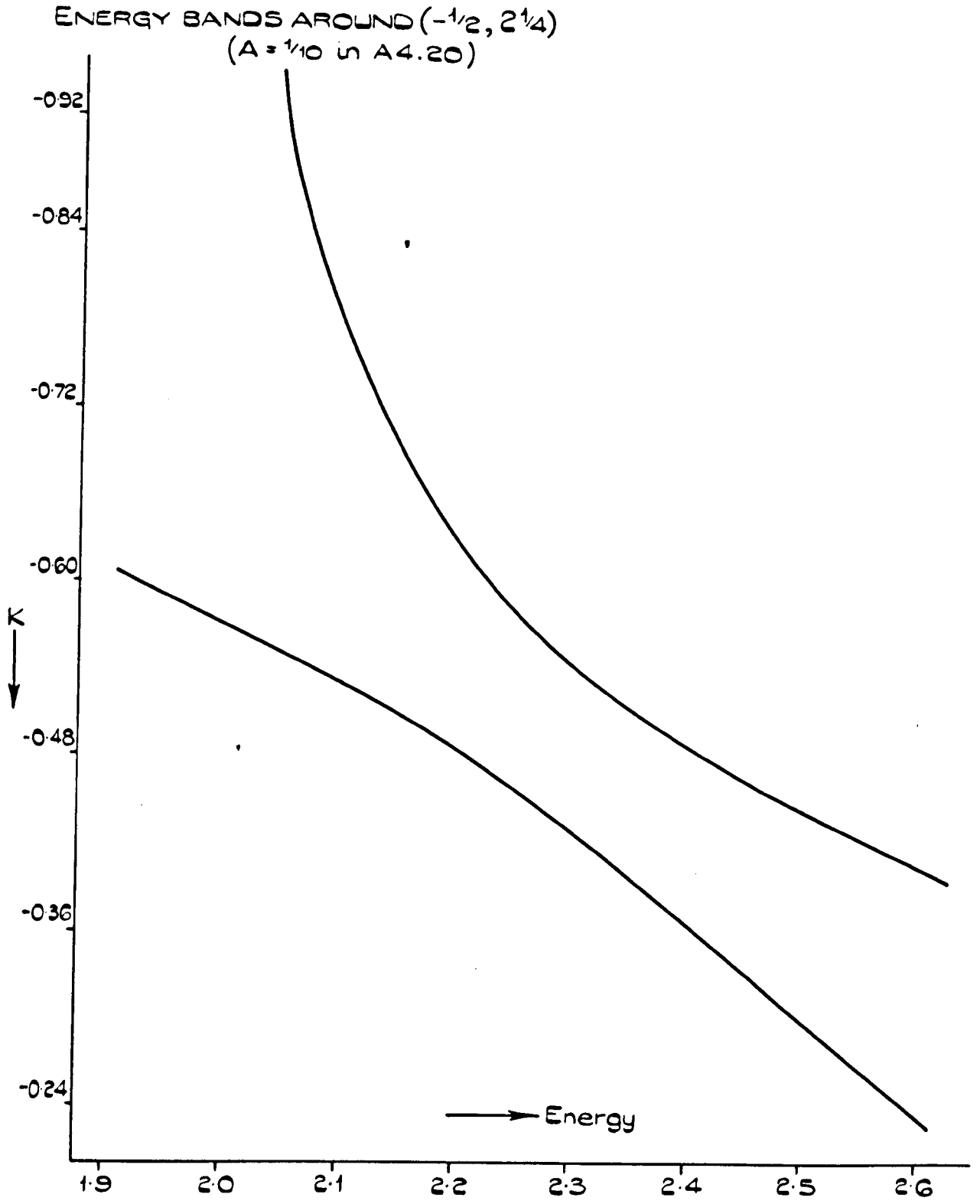
ENERGY BANDS AROUND (-½, 2¼)
(A = 1/10 in A4.20)
-0·92
-0·84
-0·72
-0·60
-0·48
-0·36
-0·24
K
Energy
1·9
2·0
2·1
2·2
2·3
2·4
2·5
2·6

DIAGRAM 3.9

$$\psi^{\pm}(k) = \phi_1'(k) + a^{\pm}\phi_2'(k) \qquad 3.32$$

where

$$a^{\pm} = \frac{E_1 - E^{\pm}}{2b} \qquad 3.33$$

The positive sign in the superscript of 3.33 refers to the upper energy band and the negative sign to the lower. It is easy to show, in the manner of Chapter II, that the wavefunction in the crystal consists only of a linear combination of 3.32:

$$\psi_i = B_1\ \psi^{+}(k_1) + b_2\psi^{-}(k_2) \qquad 3.34$$

In the vacuum we have:

$$\psi_o = Ae^{ipx} + A_o e^{-ipx} + A_1 e^{-i\Gamma x}\{e^{i(y+z)} + e^{-i(y+z)} + e^{i(y-z)} + e^{i(z-y)}\} \qquad 3.35$$

where

$$\left.\begin{aligned} p &= \sqrt{E - V_o}' \\ \text{and} \quad \Gamma &= \sqrt{E - (V_o+2)}' \end{aligned}\right\} \qquad 3.36$$

On matching the wavefunctions, 3.32 and 3.35, at the crystal boundary, we find that:

$$R_{oo} = \left|\frac{A_o}{A}\right|^2 = \left|\frac{a^{-}(k_2+1+\Gamma)(p-k_1-2) - a^{+}(k_1+1+\Gamma)(p+k_2+2)}{a^{-}(k_2+1+\Gamma)(p+k_1+2) - a^{+}(k_1+1+\Gamma)(p-k_2-2)}\right|^2 \qquad 3.37$$

and

$$R_{10} = \left|\frac{A_1}{A}\right|^2 = \left|\frac{a^{+}a^{-}(k_1-k_2)(1+\frac{A_o}{A})}{2(a^{+}\{k_1+1+\Gamma\} - a^{-}\{k_2+1+\Gamma\})}\right|^2 \qquad 3.38$$

Of course, $R_{10} = R_{01} = R_{0-1} = R_{-10}$. From the equations we have obtained it is now possible to evaluate R_{oo} and R_{10} as functions of energy. The results are shown in diagram 3.14for two values of the inner potential.

Reference to the intensity scale in diagram 3.14 shows that the reflectivity is very small. This confirms an idea expressed in Chapter II. The physical interpretation is that the specularly transmitted wave (with wave-vector denoted by a in diagram 3.4) excites four other waves (with wave-vectors b), which have no component of flux directed back towards the crystal surface. Thus, in this simple picture, no enhancement of R_{oo} and R_{10} should be expected. In fact R_{oo} and R_{10} increase slowly as the energy decreases. The slight increase in R_{oo} is partially the result of scattering from the inner potential, but (and this applies to R_{10} as well) is also caused by a surface resonance phenomenon of the type described by Heine and Boudreaux (14) at the energy ~ 2, which is discussed later. The surface resonance is far less effective for a finite inner potential, so that R_{01} is an order of magnitude smaller at E ~ 2.1 when the inner potential is increased from zero to one. Of course, the presence of the inner potential enhances the specular reflectivity.

(c) $(-\frac{1}{6}, 3^{13}/36)$

In k-space (diagram 3.15) the degeneracy at $(-\frac{1}{6}, 3^{13}/36)$ corresponds to the specularly transmitted beam, with wave-vector a, being on Bragg

conditions associated with the reciprocal lattice vectors $\underline{G}_{012}$, $\underline{G}_{021}$, $\underline{G}_{-111}$ and $\underline{G}_{122}$ and thus four additional beams, with wave-vectors b, are excited. At the same energy but with $k = +\frac{1}{6}$ the set of four {10} transmitted waves, with wave-vectors d, are each on a Bragg condition ($\underline{G}_{0-1-2}$, $\underline{G}_{0-2-1}$, $\underline{G}_{1-1-1}$ and $\underline{G}_{-1-2-2}$) all exciting the beam with wave-vector c.

We now find the energy bands around $(+\frac{1}{6}, 3^{13/36})$. Those at around $(-\frac{1}{6}, 3^{13/36})$ follow immediately because of the time reversal symmetry: $E(\underline{k}) = E(-\underline{k})$. The five degenerate plane waves at $(\frac{1}{6}, 3^{13/36})$ are:

$$\left.\begin{aligned}
\phi_1 &= \gamma \exp i(k-2)x \\
\phi_2 &= \gamma \exp i(\{k+1\}x+y-z) \\
\phi_3 &= \gamma \exp i(\{k+1\}x-y+z) \\
\phi_4 &= \gamma \exp i(\{k+1\}x-y-z) \\
\phi_5 &= \gamma \exp i(\{k+1\}x+y+z)
\end{aligned}\right\} \qquad 3.39$$

The perturbation matrix near $(\frac{1}{6}, 3^{13/36})$ is given in diagram 3.13 Again, only two energy bands are of interest. The transformation matrix S, is the same as that shown in diagram 3.8. The energy bands, $E^{\pm}$, are shown in diagram 3.10 for real k. In addition we have a loop of real energy around which the wave-vector is complex. The loop lies between the two values of the real part of the wave-vector given by:

$$k_r = \frac{1}{6}\left[1 - (b+2c) \pm \sqrt{(b+2c)^2 - 4a^2}\right] \qquad 3.40$$

the imaginary part of the wave-vector is given by:

ENERGY BANDS AROUND $(1/6, 3\,13/36)$ AS A FUNCTION OF THE REAL WAVEVECTOR

(A = 0·1 in A4.20)

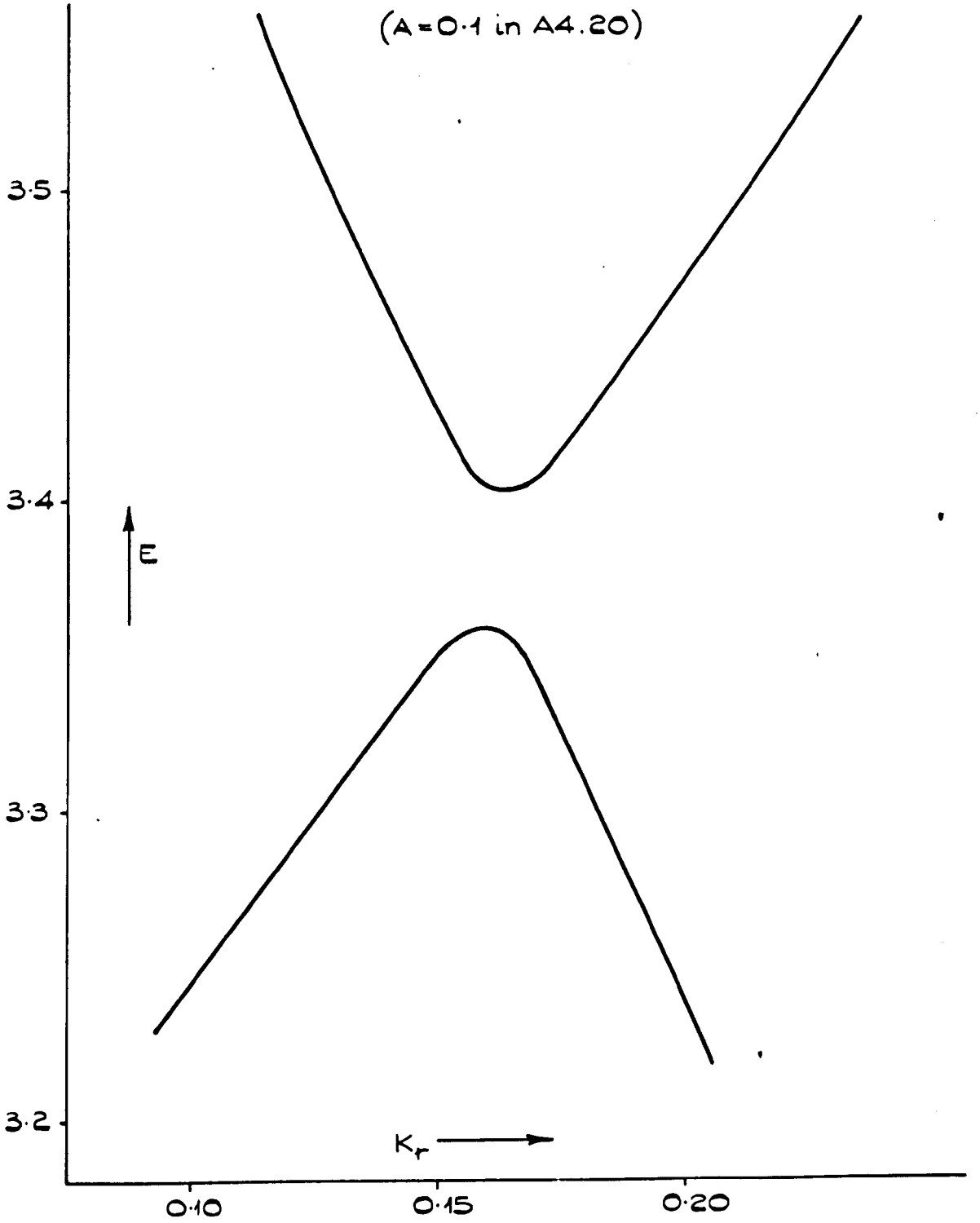

DIAGRAM 3.10

$$k_i^2 = \frac{\frac{1}{4}[72k_r-12+12(b+2c)]^2 - [4k_r-2]^2[36k_r^2+1+12(b+2c)(6k_r-1)+16a^2]}{[4k_r-2]^4 - 36[4k_r-2]^2} \qquad 3.41$$

The relationship between k_r and k_i is shown in diagram 3.11. The same diagram illustrates the relationship between k_r and the energy when $k_i \neq 0$. We see that the loop of real energy goes around a branch point where the energy is complex which is in accordance with the general theory of Heine (8).

We now come to an evaluation of the intensities of the diffraction spots. At energies around $3^{13}/_{36}$, the energy bands look schematically, like those sketched in diagram 2.8. It can then be shown, in the manner of Chapter II, that the only waves contributing to the total matched wavefunction at this energy are those coming from these two paths of real energy. The wavefunction in the crystal is then written:

$$\psi_i = B_1[\exp i(k_a-2)x+a(k_a)\phi_2'(k_a)] + B_2[\exp i(k_a+2)x+a(k_b)\phi_2'(k_b)] \qquad 3.42$$

where $k_a \sim \frac{1}{6}$ and $k_b \sim -\frac{1}{6}$. The $\phi_2'(k)$ are given by:

$$\phi_2'(k) = \frac{\gamma}{2}\left(\exp i(y+z)+\exp i(y-z)+\exp i(z-y)+\exp i(-y-z)\right)\exp i(k+1)x \qquad 3.43$$

and the a(k) by:

$$\left.\begin{aligned} a^{\pm}(k_a) &= \frac{E^{\pm}(k_a) - (k_a^2-4k_a+4)}{2a} \\ a^{\pm}(k_b) &= \frac{E^{\pm}(k_b) - (k_b^2+4k_b+4)}{2a} \end{aligned}\right\} \qquad 3.44$$

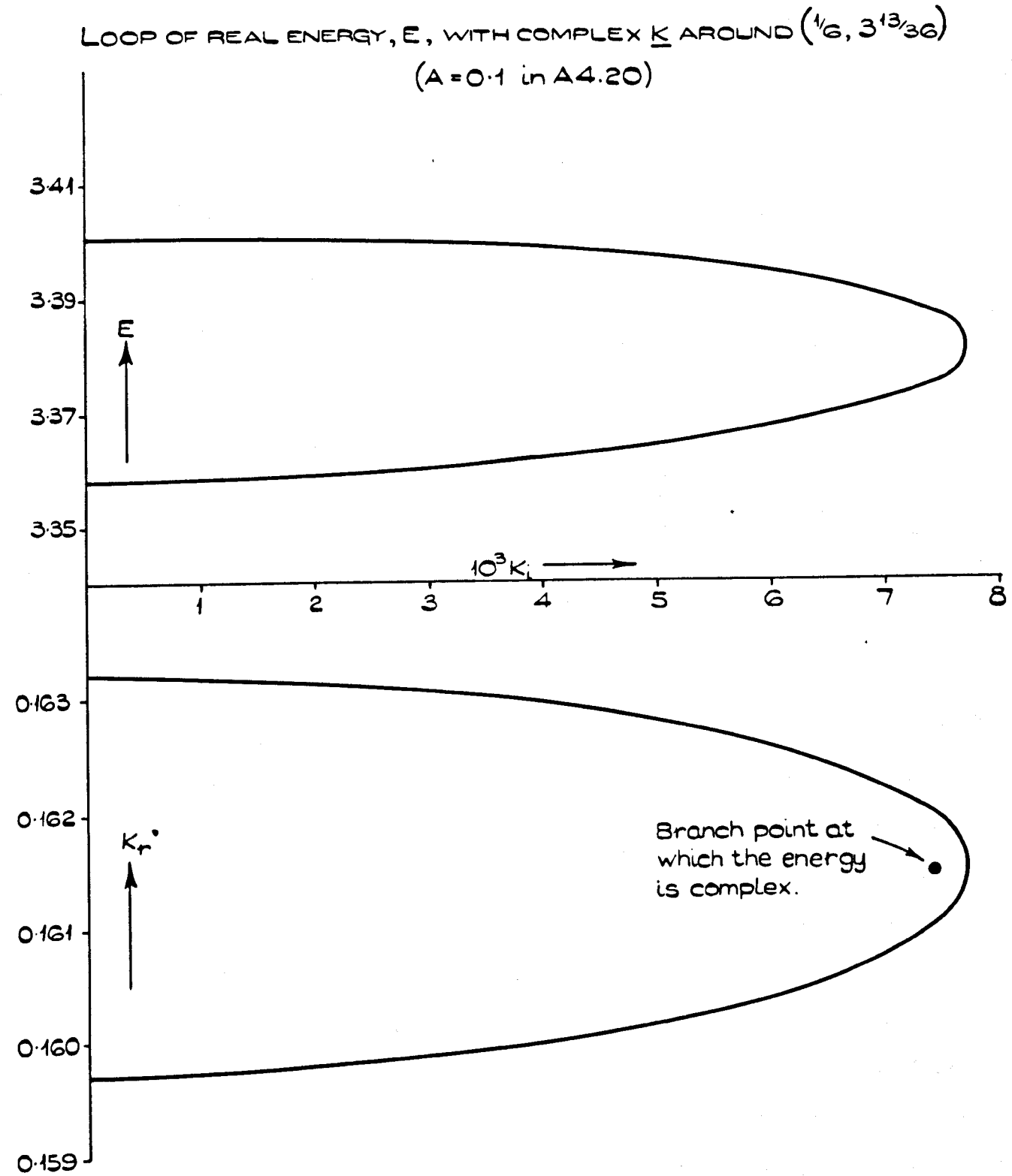
LOOP OF REAL ENERGY, E, WITH COMPLEX K AROUND (1/6, 3 13/36)
(A = 0·1 in A4.20)
3·41
3·39
E
3·37
3·35
10³ Kᵢ
1
2
3
4
5
6
7
8
0·163
0·162
Kᵣ
0·161
0·160
0·159
Branch point at which the energy is complex.

DIAGRAM 3.11

In 3.44 the appropriate superscript is taken depending on whether the energy lies in the upper, or the lower branch of the energy bands. The wavefunction in the vacuum is given by 3.35. The boundary conditions, 2.3 and 2.4, then give:

$$R_{oo} = \left|\frac{A_o}{A}\right|^2 = \left|\frac{a(k_a)(\Gamma+k_a+1)(p-k_b-2) - a(k_b)(\Gamma+k_b-1)(p+k_a-2)}{a(k_a)(\Gamma+k_a+1)(p+k_b+2) - a(k_b)(\Gamma+k_b-1)(p-k_a+2)}\right|^2 \qquad 3.45$$

while

$$R_{10} = \left|\frac{A_1}{A}\right|^2 = \left|\frac{a(k_a)a(k_b)(1+\frac{A_o}{A})(\{k_a+1\} - \{k_b-1\})}{2(a(k_a)(\Gamma+k_a+1) - a(k_b)(\Gamma+k_b-1))}\right|^2 \qquad 3.46$$

Of course, $R_{10} = R_{-10} = R_{01} = R_{0-1}$. The results of computing 3.45 and 3.46 are shown in diagram 3.12 . Three different values of the inner potential have been used.

The physical origin of the reflectivity peaks has been described in Chapter II. The situation is one in which a Bragg peak in R_{10} is accompanied by a secondary Bragg peak in R_{oo}. We see that the peak heights for both R_{oo} and R_{10} increase as V_o is increased. This is possible because the set of (10) intensities propagate at angles closer to the surface as V_o is increased. We can appreciate this by arguments involving flux conservation. At energies corresponding to the peak maxima, all the incident flux is reflected out of the crystal. This is because the wavefunction in the crystal is localised near the surface. No net flux can propagate in directions normal to the incident direction because each plane wave component $|\underline{k}^+ + \underline{k}''>$, is attended by another plane-wave component $|\underline{k}^+ - \underline{k}''>$, which has an equal amplitude. Thus, the normally

R_{00} AND R_{10} AS FUNCTIONS OF E AROUND $3^{13}/_{36}$.

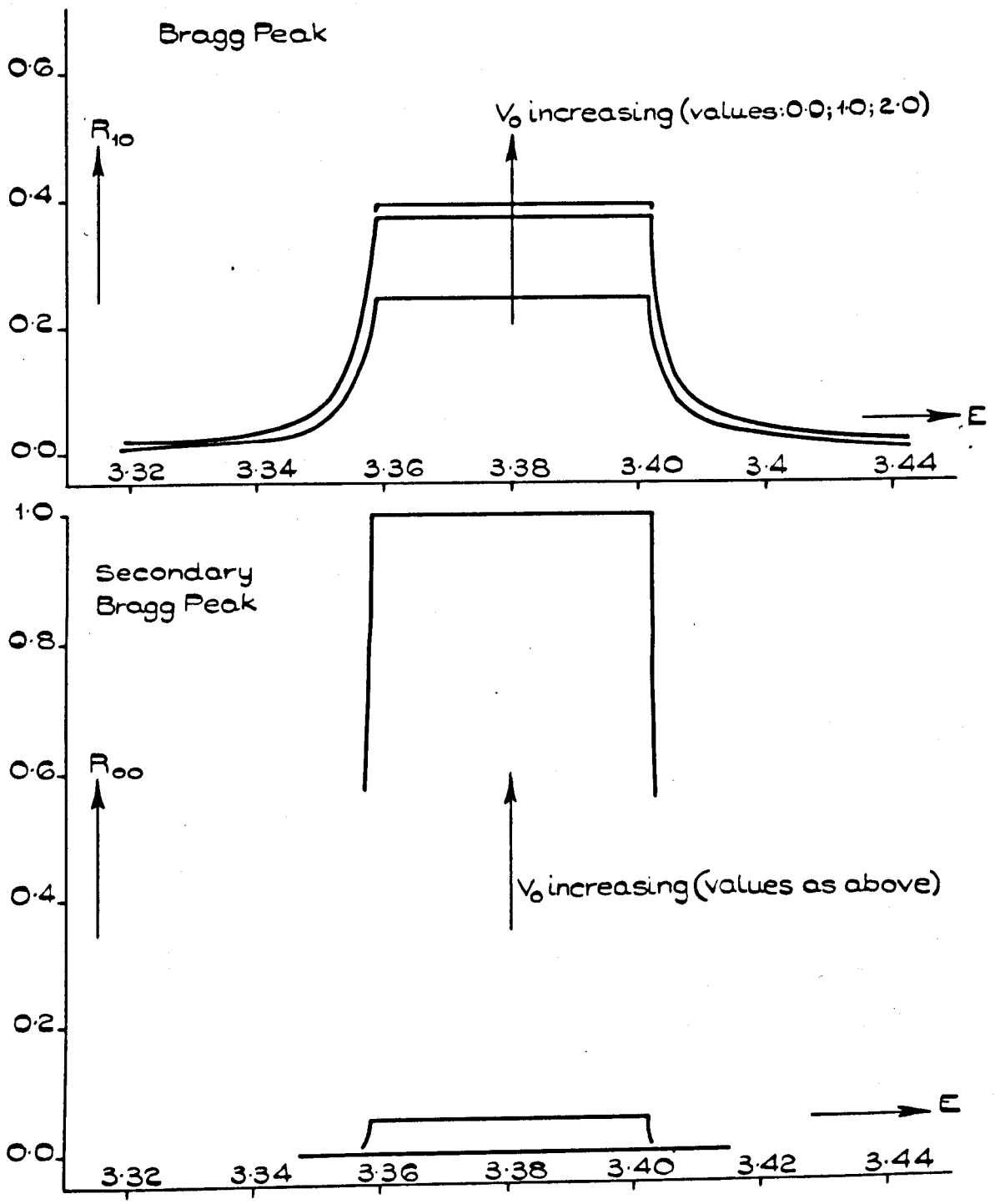

DIAGRAM 3.12

PERTURBATION MATRIX NEAR $(1/6, 3^{12}/36)$

$$\det A = \begin{vmatrix} \Delta E_1 & V_{0\text{-}1\text{-}2} & V_{0\text{-}2\text{-}1} & V_{1\text{-}1\text{-}1} & V_{-1\text{-}2\text{-}2} \\ V_{012} & \Delta E_2 & V_{0\text{-}11} & V_{101} & V_{-1\text{-}10} \\ V_{021} & V_{01\text{-}1} & \Delta E_2 & V_{110} & V_{-10\text{-}1} \\ V_{-111} & V_{-10\text{-}1} & V_{-1\text{-}10} & \Delta E_2 & V_{2\text{-}1\text{-}1} \\ V_{122} & V_{110} & V_{101} & V_{211} & \Delta E_2 \end{vmatrix} = \begin{vmatrix} \Delta E_1 & a & a & a & a \\ a & \Delta E_2 & b & c & c \\ a & b & \Delta E_2 & c & c \\ a & c & c & \Delta E_2 & b \\ a & c & c & b & \Delta E_2 \end{vmatrix} = 0$$

where $\Delta E_1 = (k-2)^2 - E = E_1 - E$; $\Delta E_2 = (k^2+2k+3) - E = E_2 - E$

and $a = V_{012}$, $b = V_{211}$ and $c = V_{110}$

$$SAS^{-1} = \begin{vmatrix} \Delta E_1 & 2a & 0 & 0 & 0 \\ 2a & (\Delta E_2+b+2c) & 0 & 0 & 0 \\ 0 & 0 & (\Delta E_2+b-2c) & 0 & 0 \\ 0 & 0 & 0 & (\Delta E_2-b) & 0 \\ 0 & 0 & 0 & 0 & (\Delta E_2-b) \end{vmatrix} ; \det A' = \begin{vmatrix} \Delta E_1 & 2a \\ 2a & (\Delta E_2+b+2c) \end{vmatrix} = 0$$

$$E^{\pm} = \tfrac{1}{2}\left[\{E_1+E_2+b+2c\} \pm \sqrt{(E_1-E_2)^2 + 2(b+2c)(E_2-E_1) + 16a^2}\right]$$

DIAGRAM 3.13

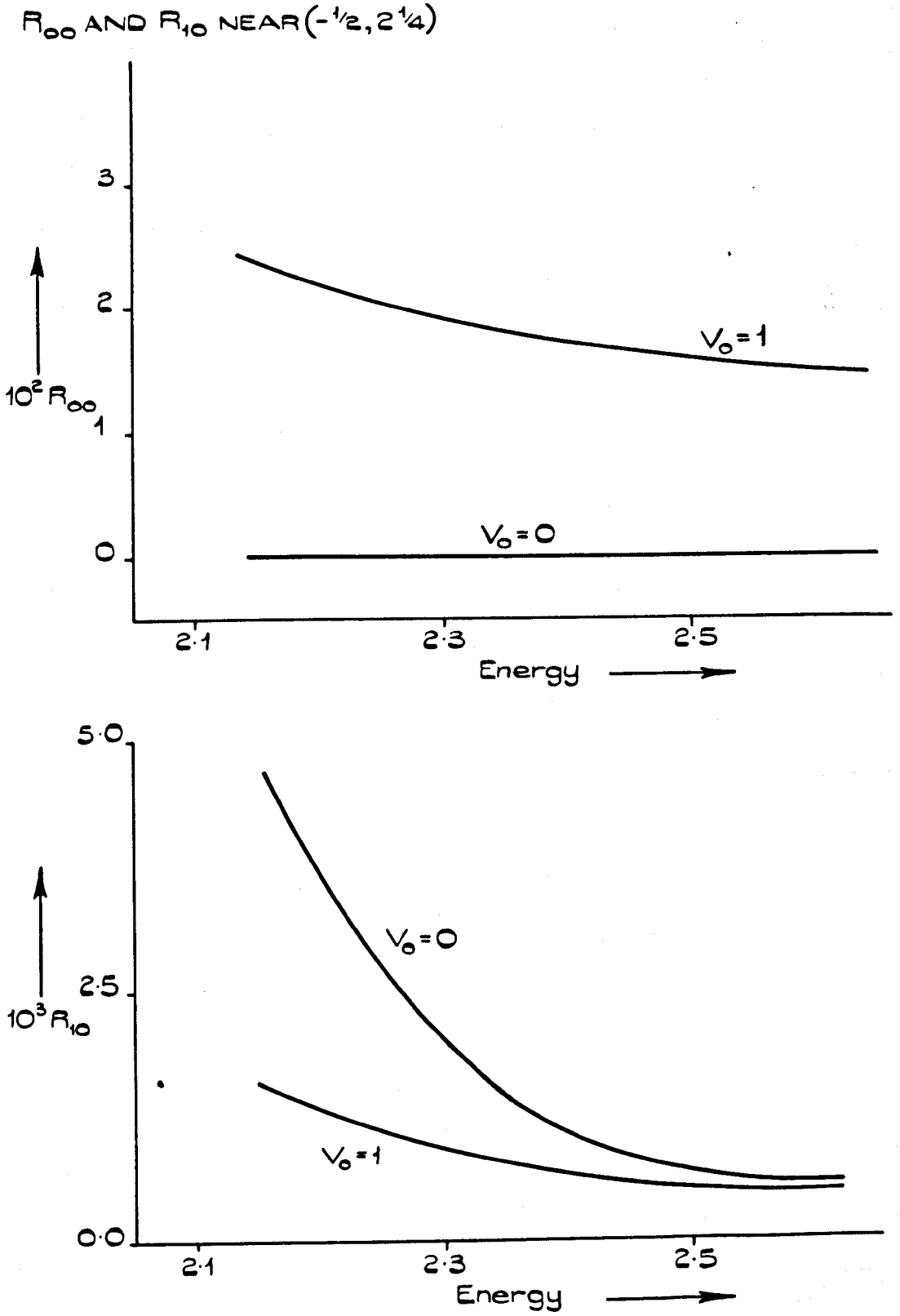
R_{00} AND R_{10} NEAR $(-1/2, 2\,1/4)$
3
2
1
0
$10^2 R_{00}$
$V_0 = 1$
$V_0 = 0$
2·1
2·3
2·5
Energy
5·0
2·5
0·0
$10^3 R_{10}$
$V_0 = 0$
$V_0 = 1$
2·1
2·3
2·5
Energy

DIAGRAM 3.14

incident flux has to be the same as the normally reflected flux. If θ denotes the angle between the propagation directions of the (0,0) and the set of (1,0) intensities, flux conservation requires that:

$$1 = R_{oo} + 4R_{10} \cos \theta \qquad 3.47$$

Of course, the last equation holds only if Γ, 3.36, is real, i.e. if $V_o \leq (E-2)$. Now:

$$\cos \theta = \frac{\Gamma}{p} \qquad 3.48$$

so that, using 3.36, 3.46 becomes:

$$1 = R_{oo} + 4R_{10}\sqrt{1 - \frac{2}{E-V_o}} \qquad 3.49$$

The curves in diagram 3.12 which correspond to Γ being real (i.e. V_o $V_o = 0$ and 1), are found to satisfy 3.49. Of course, if Γ is complex the specularly reflected intensity must equal the incident intensity. Thus R_{oo}, for $V_o = 2$, shows a peak height of one. We also note, in confirmation of our qualitative remarks in Chapter II, that a zero inner potential makes the secondary Bragg peak in R_{oo} vanish.

(d) (0,4)

Diagram 3.16 shows the situation in $\underline{k}$-space. The specularly transmitted beam (with wave-vector a) is simultaneously on Bragg conditions for the reciprocal lattice vectors $\underline{G}_{-110}$, $\underline{G}_{-101}$, $\underline{G}_{121}$, G_{112} and $\underline{G}_{022}$. Thus, kinematically, four other beams are excited. Those with wave-vector b would apparently form a standing wave in the surface,

K-SPACE DIAGRAMS

$(\pm 1/6, 3\,13/36)$

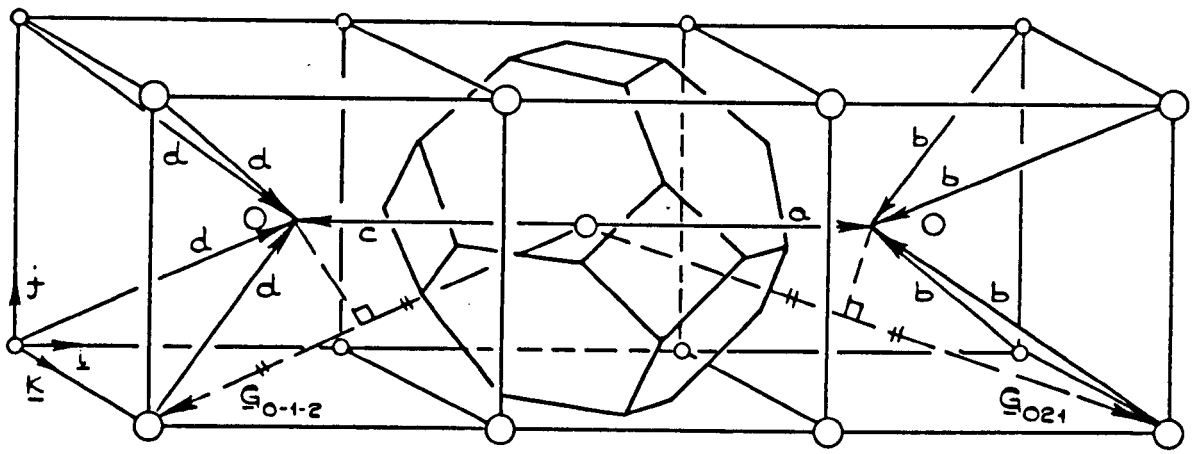

DIAGRAM 3.15

(0, 4)

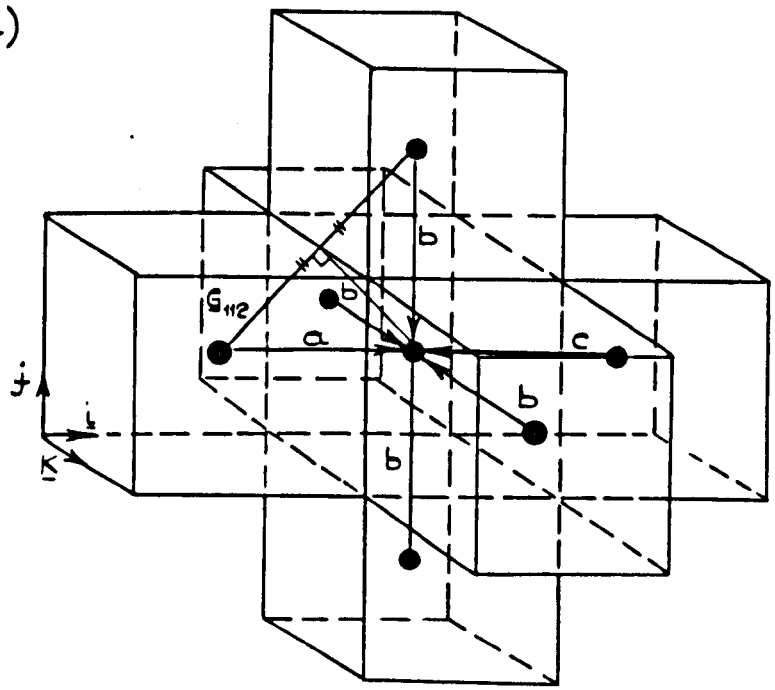

For clarity, only the body-centred points are shown.

DIAGRAM 3.16

while that with wave-vector c should provide flux in the (0,0) intensity. In the section dealing with secondary Bragg peaks in the specular reflectivity in Chapter II, we put off discussion of this situation. That is, where our particular secondary Bragg peak mechanism tries to operate through intermediate beams lying in the crystal surface and where, necessarily, the condition for a Bragg peak in the (0,0) intensity is also satisfied.

We find the energy-bands first. The six quasi-degenerate plane-waves near(0,4) are:

$$\left.\begin{aligned}
\phi_1 &= \gamma\ \mathrm{expi}(k+2)x \\
\phi_2 &= \gamma\ \mathrm{expi}(kx+2y) \\
\phi_3 &= \gamma\ \mathrm{expi}(kx+2z) \\
\phi_4 &= \gamma\ \mathrm{expi}(kx-2z) \\
\phi_5 &= \gamma\ \mathrm{expi}(kx-2y) \\
\phi_6 &= \gamma\ \mathrm{expi}(k-2)x
\end{aligned}\right\} \qquad 3.50$$

Then the perturbation matrix is that given in diagram 3.17 . This is brought into block-diagonal form by the change of basis:

$$\phi' = S'\phi$$

where S' is given in diagram 3.17. Again, for symmetry reasons we can disregard certain of the energy bands, these are associated with the wavefunctions ϕ_3', ϕ_4' and ϕ_5'. The remaining three energy bands are found by solving the cubic equation in ΔE_2, which is shown in diagram 3.17. This has been done using the standard methods and the resulting bands

PERTURBATION MATRIX NEAR (0,4)

$$\det A = \begin{vmatrix} \Delta E_1 & V_{-110} & V_{-101} & V_{121} & V_{112} & V_{022} \\ V_{1-10} & \Delta E_2 & V_{01-1} & V_{-2-1-1} & V_{-20-2} & V_{-1-1-2} \\ V_{10-1} & V_{0-11} & \Delta E_2 & V_{-2-20} & V_{-2-1-1} & V_{-1-2-1} \\ V_{-1-2-1} & V_{211} & V_{220} & \Delta E_2 & V_{01-1} & V_{10-1} \\ V_{-1-1-2} & V_{202} & V_{211} & V_{0-11} & \Delta E_2 & V_{1-10} \\ V_{0-2-2} & V_{112} & V_{121} & V_{-101} & V_{-110} & \Delta E_3 \end{vmatrix} = \begin{vmatrix} \Delta E_1 & b & b & b & b & b/2 \\ b & \Delta E_2 & b & b & b/2 & b \\ b & b & \Delta E_2 & b/2 & b & b \\ b & b & b/2 & \Delta E_2 & b & b \\ b & b/2 & b & b & \Delta E_2 & b \\ b/2 & b & b & b & b & \Delta E_3 \end{vmatrix} = 0$$

where $\Delta E_1 = (K^2+4K+4) - E$; $\Delta E_2 = (K^2+4) - E$; $\Delta E_3 = (K^2-4K+4) - E$,

and $b = V_{112}$. Also note that $\Delta E_1 + \Delta E_3 = 2\Delta E_2$

$$S' = \begin{vmatrix} 1/\sqrt{6} & 1/\sqrt{6} & 1/\sqrt{6} & 1/\sqrt{6} & 1/\sqrt{6} & 1/\sqrt{6} \\ 1/\sqrt{3} & -1/2\sqrt{3} & -1/2\sqrt{3} & -1/2\sqrt{3} & -1/2\sqrt{3} & 1/\sqrt{3} \\ 0 & 1/2 & -1/2 & -1/2 & -1/2 & 0 \\ 0 & 0 & -1/\sqrt{2} & -1/\sqrt{2} & 0 & 0 \\ 0 & 1/\sqrt{2} & 0 & 0 & -1/\sqrt{2} & 0 \\ 1/\sqrt{2} & 0 & 0 & 0 & 0 & -1/\sqrt{2} \end{vmatrix} ; S'AS'^{-1} = \begin{vmatrix} (\Delta E_2 + 4\frac{1}{2}b) & 0 & 0 & 0 & 0 & \frac{8K}{\sqrt{12}} \\ 0 & (\Delta E_2 - \frac{3}{2}b) & 0 & 0 & 0 & \frac{8K}{\sqrt{6}} \\ 0 & 0 & (\Delta E_2 - \frac{3}{2}b) & 0 & 0 & 0 \\ 0 & 0 & 0 & (\Delta E_2 - b/2) & 0 & 0 \\ 0 & 0 & 0 & 0 & (\Delta E_2 - b/2) & 0 \\ \frac{8K}{\sqrt{12}} & \frac{8K}{\sqrt{6}} & 0 & 0 & 0 & (\Delta E_2 - b/2) \end{vmatrix},$$

$$\Delta E_2^3 + \Delta E_2^2 \cdot \tfrac{5}{2} b - \Delta E_2 \left(16K^2 + \tfrac{33}{4} b^2\right) + \left(\tfrac{27}{8} b^3 - 40bK^2\right) = 0$$

DIAGRAM 3.17

are shown in diagram 3.18. We see that the energy is real for k being real or purely imaginary. The lines of real energy for imaginary k consist of a loop and lines going to $E = -\infty$.

We proceed now to evaluate the reflectivity. At a fixed energy the total wavefunction in the crystal only consists of the functions associated with the two paths of real energy in diagram 3.18. If we denote the wave-vector of the path containing the loop by k_1, and the wave-vector of the other path by k_2, the total wave-function in the crystal is written:

$$\begin{aligned}\psi_i = {} & B_1\left(a_1^1\ \phi_1'(k_1) + a_2^1\ \phi_2'(k_1) + a_3^1\ \phi_6'(k_1)\right) \\ & + B_2\left(a_1^2\ \phi_1'(k_2) + a_2^2\ \phi_2'(k_2) + a_3^2\ \phi_6'(k_2)\right)\end{aligned} \qquad 3.51$$

where

$$\frac{a_1^n}{a_3^n} = -\frac{8k_n}{\sqrt{12}\ (\Delta E_2 + 4^{1/2}b)}$$

and

$$\frac{a_2^n}{a_3^n} = -\frac{8k_n}{\sqrt{6}\ (\Delta E_2 - 3/2b)}$$

In the vacuum the wavefunction is:

$$\psi_o = Ae^{ipx} + A_o e^{-px} + A\ e^{-i\Gamma x}\left\{e^{2iy} + e^{-2iy} + e^{2iz} + e^{-2iz}\right\} \qquad 3.52$$

where

$$p = \sqrt{E - V_o} \quad \text{and} \quad \Gamma = \sqrt{E - (V_o + 4)} \qquad 3.53$$

The boundary conditions, 2.3 and 2.4, then give:

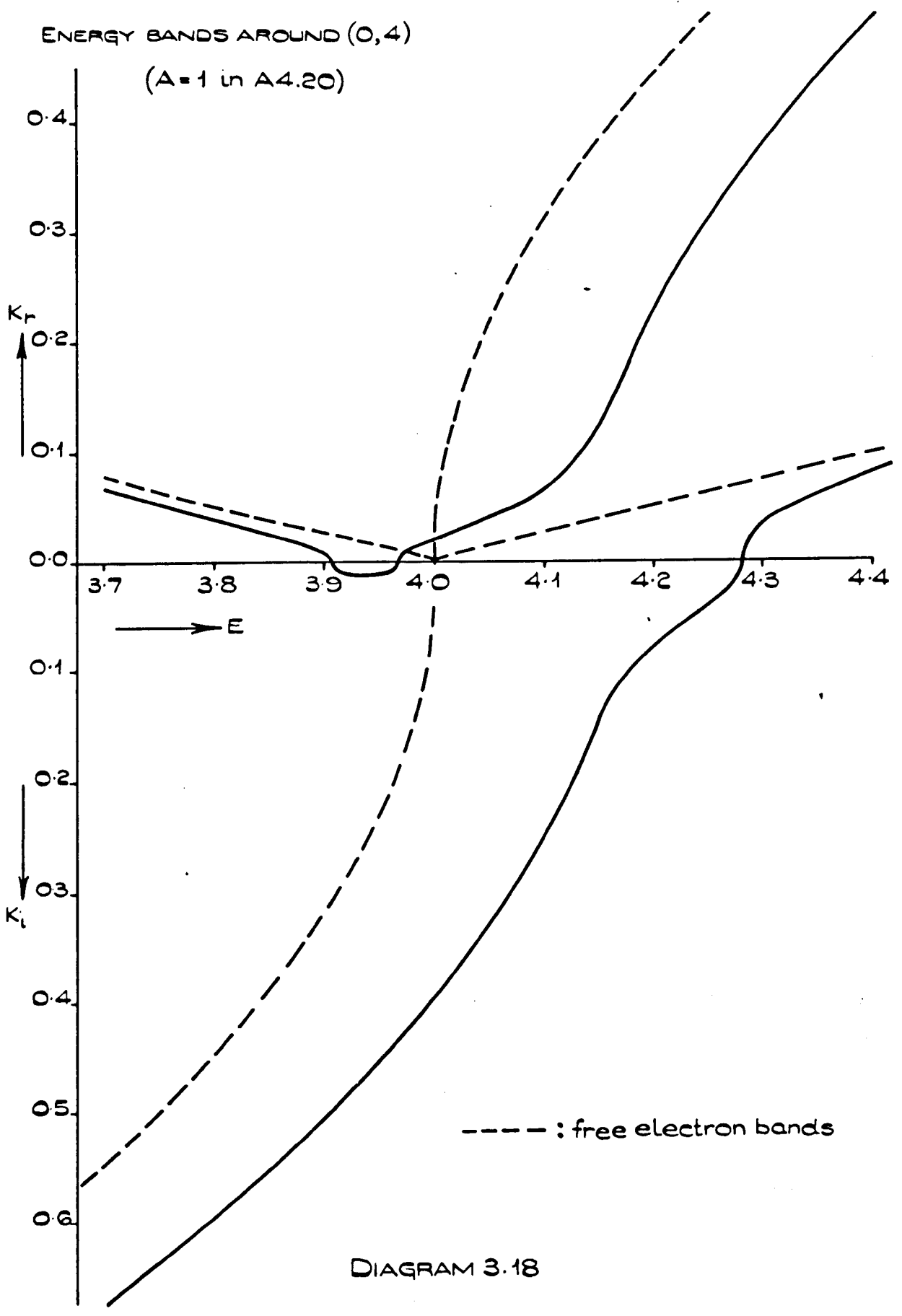
ENERGY BANDS AROUND (0,4)
(A = 1 in A4.20)
0·4
0·3
Kr
0·2
0·1
0·0
3·7
3·8
3·9
4·0
4·1
4·2
4·3
4·4
E
0·1
0·2
0·3
Ki
0·4
0·5
0·6
---- : free electron bands

DIAGRAM 3.18

$$R_{oo} = \left|\frac{A_o}{A}\right|^2 = \left|\frac{\alpha_1(k_1+\Gamma)\{(p-k_2)\alpha_2-1\}-\alpha_2\beta(k_2+\Gamma)\{(p-k_1)\alpha_1-1\}}{\alpha_1(k_1+\Gamma)\{(p+k_2)\alpha_2-1\}-\alpha_2\beta(k_2+\Gamma)\{(p+k_1)\alpha_2+1\}}\right|^2 \qquad 3.54$$

and

$$R_{11} = \left|\frac{A_1}{A}\right|^2 = \left|\tfrac{1}{2}(1+\frac{A_o}{A})\left[\frac{k_1-k_2}{(k_1+\Gamma)_2-(k_2+\Gamma)\gamma_1}\right]\right|^2 \qquad 3.55$$

where

$$\alpha_n = \left(\frac{a_1^n+\sqrt{2}\,a_2^n}{2\sqrt{3}\,a_3^n}\right), \quad \beta = \left(\frac{\sqrt{2}\,a_1^n-a_2^n}{\sqrt{2}\,a_1^n-a_1^n}\right) \text{ and } \quad \gamma_n = \left(\frac{\sqrt{2}\,a_1^n+2a_2^n}{\sqrt{2}\,a_1^n-a_2^n}\right) \qquad 3.56$$

The intensities R_{oo} and R_{11} are shown in diagram 3.19, for various values of the inner potential.

We now discuss the forms of R_{oo} and R_{11}. At energies intersecting the loop of real energy no flux can be transmitted through the crystal because there are no propagating waves in it. The set of (1,1) reflected waves are localised in the surface (Γ is imaginary) and so cannot carry any flux normally away from the crystal. Thus throughout this band gap the specular intensity is one.

As we increase the energy to $(4+4\frac{1}{2}b)$, we see a peak in both R_{oo} and R_{11}. At this energy we have $k_2 = 0$. If we now choose the inner potential to be $4\frac{1}{2}b$ then, from 3.53, $\Gamma = 0$ also. Then from 3.54, it immediately follows that $R_{oo} = 1$, and from 3.55 that $R_{11} = 1$. The physics of the situation is as follows. In the crystal at this energy there is a propagating Bloch wave (with amplitude B_1) and a standing wave (B_2). Now the boundary conditions, 2.3 and 2.4, give:

R_{oo} AND R_{11} AS FUNCTIONS OF ENERGY ~4

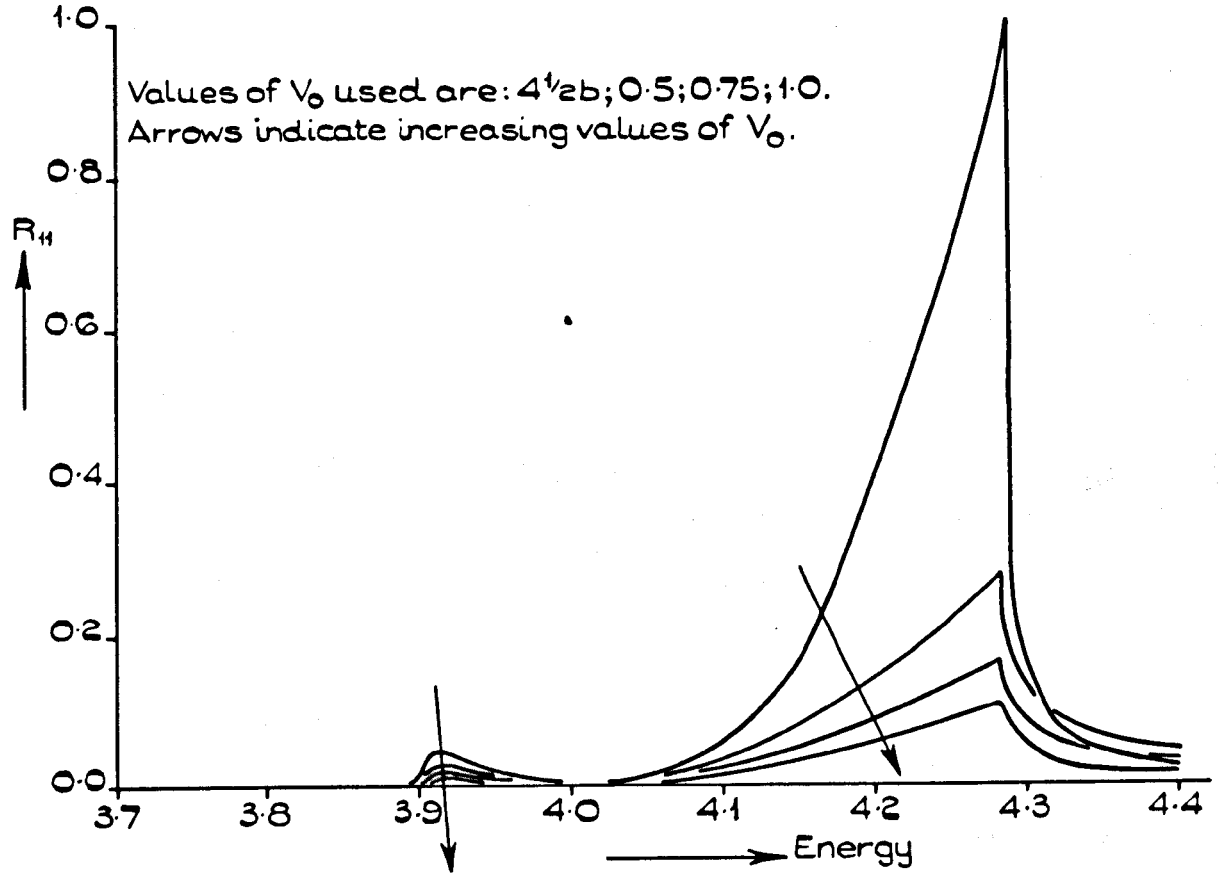

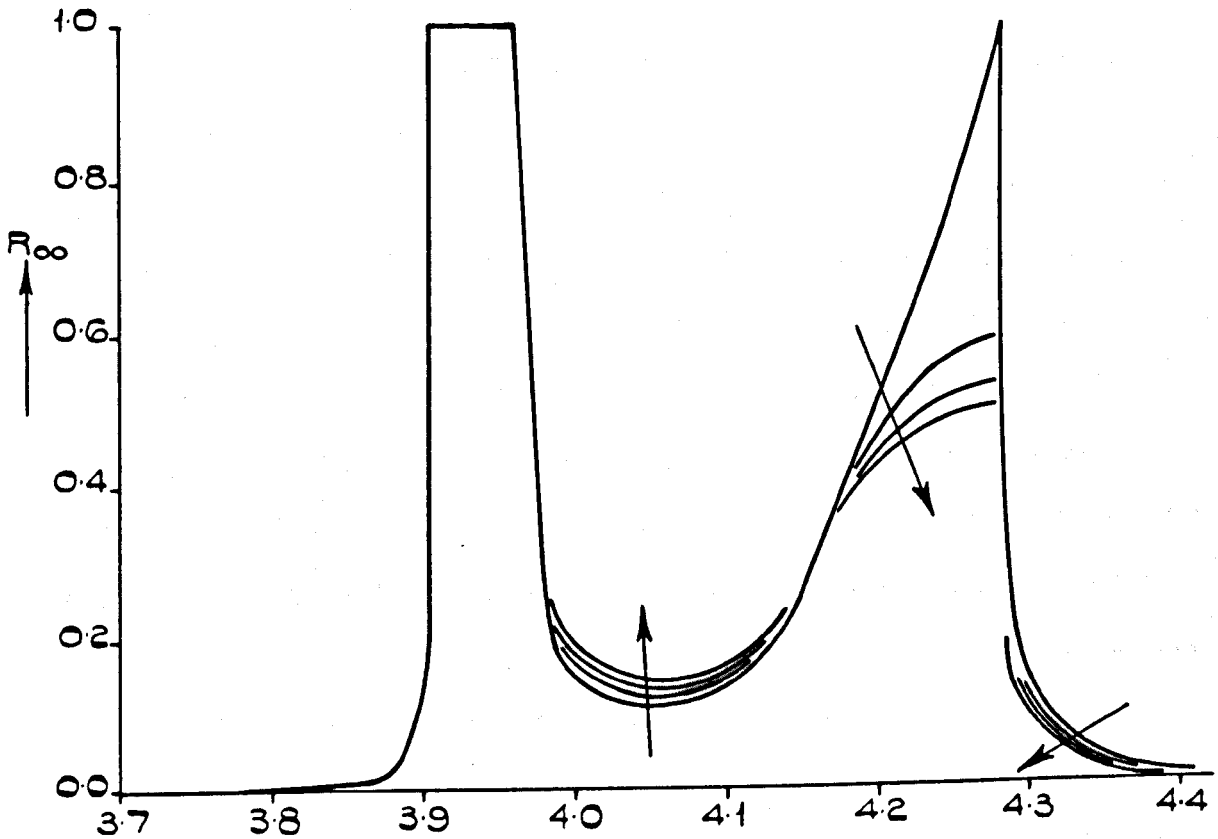

DIAGRAM 3.19

$$\frac{B_1}{B_2} = -\beta\left(\frac{k_2+\Gamma}{k_1+\Gamma}\right) = 0 \qquad 3.57$$

since $\Gamma = k = 0$. Thus we only match on to a standing wave in the crystal so that all the incident flux is reflected. The set of (1,1) reflected waves lie in the surface and so cannot remove flux normally away from the crystal. Thus R_{oo} has to be one. For different values of the inner potential we do not have the zero, 3.57. Thus the propagating Bloch function is able to carry flux into the crystal, and the reflectivity drops as is shown in diagram 3.19.

Because we are strongly exciting beams in the crystal surface at the energy $(4+4^{1}/_{26})$, it might appear that we are dealing with a surface resonance phenomenon. This is not the case. The resonance peak mechanism as described by McRae (13) operates for a single atomic layer whereas in the present case the surface waves are produced by Bragg scattering associated with reciprocal lattice vectors of the bulk crystal. Of course, if we had only the surface layer of atoms of our crystal, the energy $(4+4\frac{1}{2}b)$ would coincide with the surface resonance of McRae (13). The surface waves would then come into discussion as first order corrections to the specularly transmitted beam. This coincidence for the cubic crystals may account for the claims of McRae and Caldwell (16) to have observed the resonance phenomena. Of course, the work of Duke and Tucker (4) now shows that the mechanism of McRae (13) for the resonance peak, is inhibited by the damping of the elastic wave field by the inelastic scattering processes.

We proceed now with our calculations. The situation at $(\frac{1}{2}, 6^{1}/4)$, in the free electron bands, is algebraically and physically the same as the situation at $(-\frac{1}{6}, 3^{13}/36)$. There is little point in doing an additional calculation. Instead we evaluate the intensities at (-1,2) where, by taking the largest first order corrections to the wavefunctions, the surface resonance mechanism described by Boudreaux and Heine (14) should operate.

(e) (-1,2)

At this energy, it is easily shown that the total matched wavefunction in the crystal consists of only two Bloch functions provided they are approximated as follows. The first Bloch function comes from the energy bands at - (-0.6,2) and the second from the energy band at - (-1,2). By choosing the appropriate value of β in A2.35, it is possible to use the zero order wavefunctions already found at - $(-\frac{1}{2},2)$, whereas in the same approximation we must add first order corrections to the wavefunctions at - (-1,2). These first order corrections come from the energy bands at - (-1,1).

The first task is then to find the wave-functions and energy bands at - (-1,2). There are four degenerate plane-waves at (-1,2):

$$\left.\begin{aligned}
\phi_1 &= \gamma\ \mathrm{expi}(\{k+1\}x+y-z) \\
\phi_2 &= \gamma\ \mathrm{expi}(\{k+1\}x-y+z) \\
\phi_3 &= \gamma\ \mathrm{expi}(\{k+1\}x-y-z) \\
\phi_4 &= \gamma\ \mathrm{expi}(\{k+1\}x+y+z)
\end{aligned}\right\} \qquad 3.58$$

The zero-order wavefunctions are found by diagonalising the perturbation matrix in the representation 3.58. This is done in diagram 3.20 where we change the basis from ϕ, 3.58, to ϕ'' according to S". For symmetry reasons only one of the resulting enery bands is of interest:

$$E = (k^2+2k+3) + (b+2c) \qquad 3.59$$

The associated zero-order wavefunction with the first order corrections is:

$$\psi(k) = \gamma\left[\phi_1''+\alpha_1\ e^{ikx}+\alpha_2\ e^{i(k+2)x}\right] \qquad 3.60$$

where ϕ_1'' is the zero-order wavefunction:

$$\phi_1'' = \frac{1}{2}\left(e^{i(y+z)}+e^{i(y-z)}+e^{i(z-y)}+e^{i(-z-y)}\right)e^{i(k+1)x} \qquad 3.61$$

The coefficient α_1 and α_2 are given by:

$$\alpha_1 = \frac{\langle k|\ V(\underline{r})\ |\phi_1''\rangle}{(E-k^2)} \qquad 3.62$$

$$\alpha_2 = \frac{\langle k+2|\ V(\underline{r})\ |\phi_1''\rangle}{\left(E-(k^2+4k+4)\right)} \qquad 3.63$$

PERTURBATION MATRIX NEAR (-1, 2)

$$\det A = \begin{vmatrix} \Delta E_2 & V_{0-11} & V_{101} & V_{-1-10} \\ V_{01-1} & \Delta E_2 & V_{110} & V_{-10-1} \\ V_{-10-1} & V_{-1-10} & \Delta E_2 & V_{-2-1-1} \\ V_{110} & V_{101} & V_{211} & \Delta E_2 \end{vmatrix} = \begin{vmatrix} \Delta E_2 & b & c & c \\ b & \Delta E_2 & c & c \\ c & c & \Delta E_2 & b \\ c & c & b & \Delta E_2 \end{vmatrix} = 0$$

where $V_{211} = b$, $V_{101} = c$ and $\Delta E_2 = (K^2 + 2K + 3) - E$

$$S'' = \begin{vmatrix} \frac{1}{2} & \frac{1}{2} & \frac{1}{2} & \frac{1}{2} \\ \frac{1}{2} & \frac{1}{2} & -\frac{1}{2} & -\frac{1}{2} \\ \frac{1}{2} & -\frac{1}{2} & 0 & 0 \\ 0 & 0 & \frac{1}{2} & -\frac{1}{2} \end{vmatrix} ; S''AS''^{-1} \begin{vmatrix} (\Delta E_2+b+2c) & 0 & 0 & 0 \\ 0 & (\Delta E_2+b-2c) & 0 & 0 \\ 0 & 0 & (\Delta E_2-b) & 0 \\ 0 & 0 & 0 & (\Delta E_2-b) \end{vmatrix}$$

K-space diagram

(-1, 2)

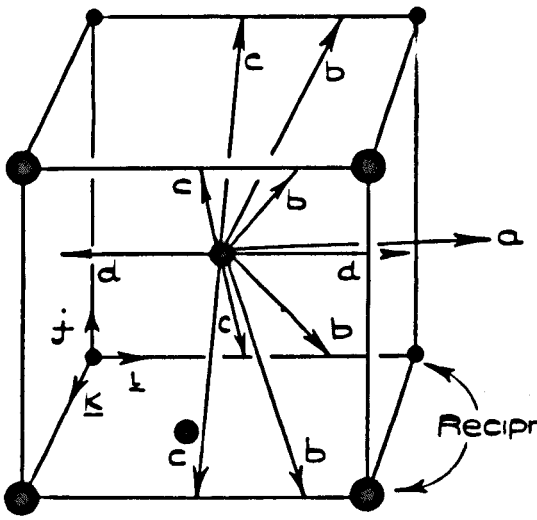

DIAGRAM 3.20.

The total wavefunction in the crystal is then:

$$\psi_i = B_1\ \psi(k_1) + B_2\ \psi^-(k_2) \qquad 3.64$$

where $\psi(k)$ is given by 3.60 and $\psi^-(k)$ by 3.32. In the vacuum the wavefunction is given by 3.35. We also note from 3.59 that:

$$(k_1+1) = \sqrt{E - (2+b+2c)} \qquad 3.65$$

We now determine the intensities R_{oo} and R_{10}. The boundary conditions, 2.3 and 2.4, give:

$$\frac{B_2}{B_1} = -\frac{1}{a^-}\left[\frac{\Gamma+k_1+1}{\Gamma+k_2+1}\right] \qquad 3.66$$

$$R_{oo}\quad \left|\frac{A_o}{A}\right|^2 = \left|\frac{\frac{B_1}{B_1}(p-k_2-2) + (p-k_1)(\alpha_1+\alpha_2) - 2\alpha_2}{\frac{B_2}{B_1}(p+k_2+2) + (p+k_1)(\alpha_1+\alpha_2) + 2\alpha_2}\right|^2 \qquad 3.67$$

$$R_{10} = \left|\frac{A_1}{A}\right|^2 = \left|\frac{pa^-(k_2-k_1)}{a^-(\Gamma+k+1)(\{p+k_1\}\{\alpha_1+\alpha_2\}+2\alpha_2) - (\Gamma+k_1+1)(p+k_2+2)}\right|^2 \qquad 3.68$$

where, of course, a^- is given by 3.33. In diagram 3.21 we plot R_{oo} and R_{10} as functions of the energy for two values of the inner potential.

Before discussing the forms of R_{oo} and R_{10}, we show the situation in k-space at the energy (2+b+2c). This is indicated in diagram 3.20. The wave-vector of the specularly transmitted beam is labelled s, while those of the other plane waves making up the Bloch function at k = - 0.6 are denoted by b. The Bloch function at k = -1 consists of the set of

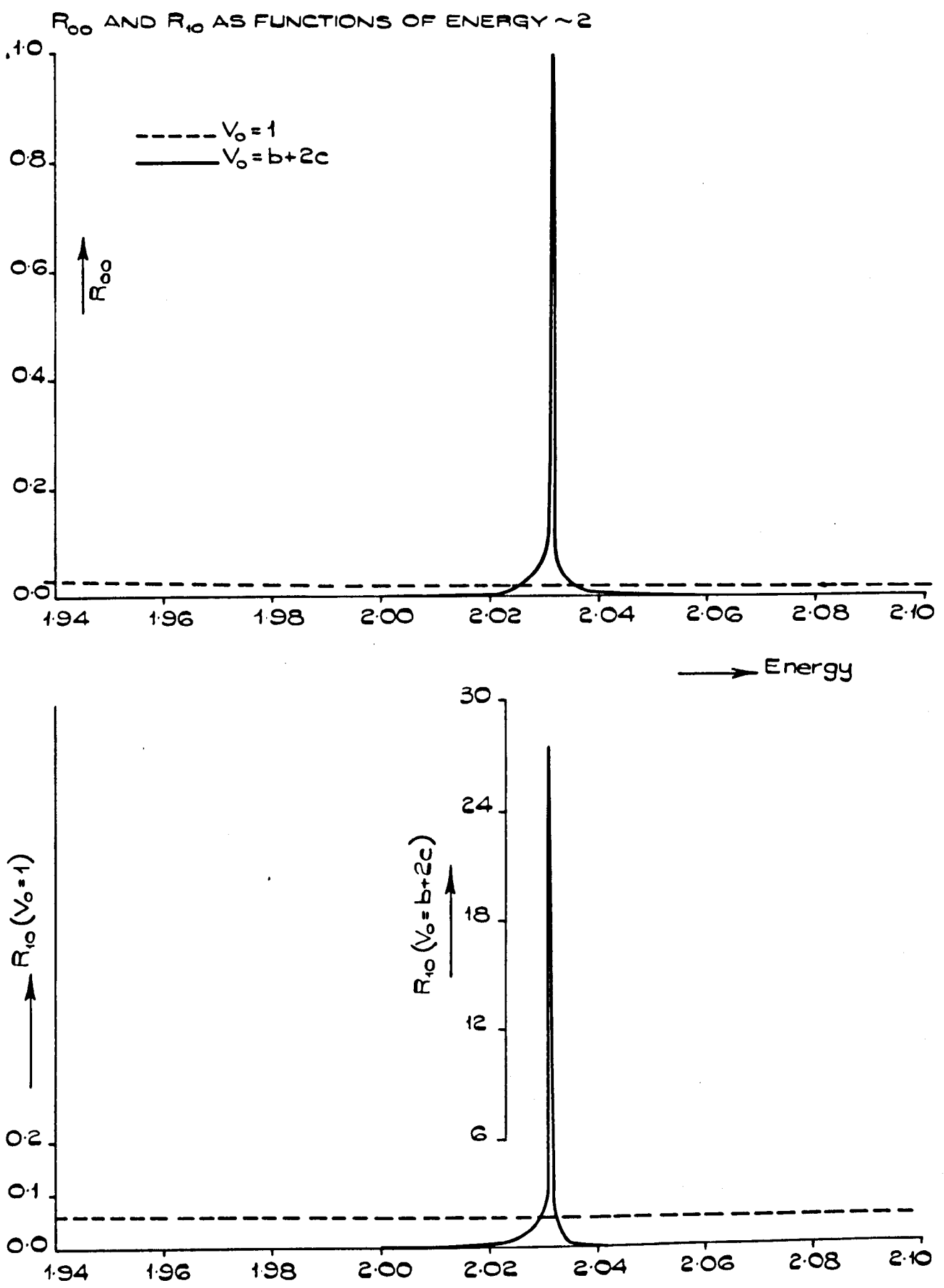
R_{00} AND R_{10} AS FUNCTIONS OF ENERGY ~2
1·0
0·8
0·6
0·4
0·2
0·0
$V_0 = 1$
$V_0 = b+2c$
R_{00}
1·94
1·96
1·98
2·00
2·02
2·04
2·06
2·08
2·10
Energy
30
24
18
12
6
R_{10} ($V_0 = b+2c$)
R_{10} ($V_0 = 1$)
0·2
0·1
0·0

DIAGRAM 3.2 1

(1,0) transmitted beams with wave-vectors c, plus the first order corrections with wave-vectors denoted by d.

At the outset we note that at the energy (2+b+2c) we have:

$$\alpha_1 = -\alpha_2 \text{ and } (k_1+1) = 0 \qquad 3.69$$

which follow from 3.62, 3.63 and 3.65. Now the first of 3.69 ensures that the Bloch function at k = -1 forms a standing wave at this energy. The reflectivity is then controlled by the amplitude of the other Bloch wave, B_2. If the inner potential is (b+2c), then from 3.36, $\Gamma = 0$. This, with 3.69, makes B_2, 3.66, equal to zero. We thus expect total reflection at this energy and for this value of the inner potential. Indeed, this is the surface resonance peak found by Boudreaux and Heine (14) and 3.67 gives $R_{oo} = 1$. In diagram 3.21 we see that R_{10} is very large at this energy where the set of (1,0) reflected waves would be lifted out of the crystal surface for a slight increase in the energy. Equation 2.68, with 3.69 and $\Gamma = 0$, gives:

$$R_{10} = \left|\frac{p}{2\alpha_2}\right|^2 \qquad 3.70$$

which is large by virtue of α_2 being small.

The zero in the amplitude, B_2, will not occur for any other value of the inner potential. As a consequence the resonance peak will be weaker. In fact the peaks in R_{oo} and R_{10} are seen to vanish entirely in our calculation for an inner potential of one (this value corresponds to about 8 or 9 eV as can be seen from 3.8 and 3.9). This, at least for our model,

confirms the assertion of Boudreaux and Heine (14) that the peak would probably not be observed in practice.

C. Summary

It is convenient now to summarise the results of Chapters II and III concerning the qualitative behaviour of the reflected intensities. Our results have been derived on the basis of taking the wavefunctions to zero-order in the crystal. This necessarily makes the intensities of all but a small number of the diffraction spots become zero. Of course, in practice, this is not the case. The other spots derive their intensities from higher order corrections to the wavefunctions. We assume that these intensities are much smaller than those which are directly involved in the mechanism under discussion.

The summary of those results we shall need to refer to later is:

(a) If the specularly transmitted beam does not lie on or nearly on a Bragg condition, then the crystal scatters as though it were a potential step. The step height has the magnitude of the inner potential. 3.71

(b) If the specularly transmitted beam is on or nearly on a Bragg condition associated with a reciprocal lattice vector perpendicular to the crystal surface (we loosely but conveniently refer to the 'crystal surface' in reciprocal space meaning a plane perpendicular to $\underline{p}^{+}$), then a Bragg peak is seen in the specularly reflected beam. 3.72

(c) If the specularly transmitted beam is on or nearly on a Bragg condition associated with a reciprocal lattice vector, $\underline{g}$, not perpendicular to the crystal surface, then we expect an appreciable Bragg peak in a non-specular intensity only if:

$$0 < k^{\perp} < g^{\perp} ,$$

where k is the wave-vector of the specularly transmitted beam. The specular intensity is then as if the crystal were a potential step scatterer. We suspect that the mechanism of Boudreaux and Heine (14), for secondary Bragg peaks in the specular reflectivity, which should apply in this situation, will produce peaks of weak intensity compared with those expected for the conditions in (d). 3.73

(d) If, apart from the reciprocal lattice vector of (c), there exists a reciprocal lattice vector $\underline{g}'$, where

$$\underline{g}' = \underline{g}^{\perp} - \underline{g}''$$

then we may also see an appreciable secondary Bragg peak in the specular reflectivity provided: 3.74

$$0 < k^{\perp} \leq g^{\perp}$$

We note that the mechanism of Boudreaux and Heine (14) is not appropriate if we have a non-zero inner potential and $\underline{g}'$ exists.

(e) We do not expect to see surface resonance peaks in practice. 3.75

We shall specifically use the results 3.72 to 3.75 in the next chapter.

CHAPTER IV

A Simple Theory for Predicting the Positions of Peaks in the Specular Reflectivity

In this chapter we develop a simple graphical method for predicting peak positions, as a function of energy and angle of incidence, in the specular reflectivity. The resulting formalism is then used in an attempt to interpret experimental data obtained by McRae and Caldwell for LiF (9) and NaF (16).

The formalism will specifically use the results 3.71 to 3.75. Because of 3.71, we only expect to obtain appreciable reflectivity when the specularly transmitted beam is on a Bragg condition. The essential method of this chapter is to plot out, as a function of energy, the angles of incidence at which such Bragg conditions are satisfied, in the free-electron limit. This enables us to predict the positions of Bragg and secondary Bragg peaks in the specular reflectivity. The latter are only expected to give appreciable intensity if 3.74 applies.

The method, of course, is very similar in basis to that developed by Marcus/Jona and Jepsen (20). However, their method predicts far too much structure in the specular intensity. This arises out of their assumption concerning the occurrence of secondary Bragg peaks. They point out that the calculations of Marcus and Jepsen (19) indicate that

the secondary Bragg peaks for the specularly reflected beam, can be regarded as the result of strong interaction with another beam containing a Bragg peak at the same energy. They then assume that a secondary Bragg peak is seen in the specular intensity whenever a non-specular Bragg peak is excited. From our analysis leading up to 3.73 and 3.74, and in particular our discussion of Taylor's results in Chapter II, we see that this is not generally the case. Our formalism takes specific account of 3.73 and 3.74.

Throughout our assumption will be that the degeneracies in the free electron bands correspond closely in energy and wave-vector to the band gaps for the actual energy bands.

We now present the formalism.

A. Formalism

We denote the wave-vector of the specularly transmitted beam by $\underline{t}$:

$$\underline{t} = t_1\underline{i}+t_2\underline{j}+t_3\underline{k} \qquad 4.1$$

where $\underline{i}$, $\underline{j}$ and $\underline{k}$ are unit vectors forming a right-handed set. The vector $\underline{i}$ is directed normally into the crystal whereas $\underline{j}$ and $\underline{k}$ are contained in the surface plane. We similarly define the reciprocal lattice vectors:

$$\underline{G}^{rst} = G_1^{rst}\,\underline{i} + G_2^{rst}\,\underline{j} + G_3^{rst}\,\underline{k} \qquad 4.2$$

We only expect appreciable intensity in the specularly reflected beam when the specularly transmitted wave is on a Bragg condition:

$$\underline{t}-\underline{k} = \underline{G}_{rst} \qquad 4.3$$

where

$$t^2 = k^2 \qquad 4.4$$

The vector $\underline{k}$ is the wave-vector of the Bragg reflected beam travelling back towards the crystal surface. Equation 4.4 expresses the idea that all the electron beams in the crystal, excited by the specularly transmitted beam, have the same energy, which we can take to be the case in our 'free electron' approximation.

Equations 4.3 and 4.4 have to be supplemented by:

$$G_1^{rst} \geq t > 0 \qquad 4.5$$

in order that $\underline{k}$ is indeed directed back towards the crystal surface.

From 4.3 and 4.4 we have:

$$\frac{(\underline{G}^{rst})^2}{2} - \underline{t}.\underline{G}^{rst} = 0 \qquad 4.6$$

If we fix the plane of incidence by:

$$t_3 = \beta t_2 \qquad 4.7$$

where β is constant, equation 4.6 becomes:

$$t_1 = \frac{(\underline{G}^{rst})^2}{2G_1^{rst}} - t_2\left(\frac{G_2^{rst}+\beta\, G_3^{rst}}{G_1^{rst}}\right) \qquad 4.8$$

We now denote the incident wave-vector by $\underline{p}$, and the angle of incidence by θ so that:

$$p \sin\theta = (t_2^2+t_3^2)^{\frac{1}{2}} = t_2(1+\beta^2)^{\frac{1}{2}} \qquad 4.9$$

where we have used 4.7. Thus:

$$t_2 = \frac{p \sin\theta}{(1+\beta^2)^{\frac{1}{2}}} \qquad 4.10$$

Now we also have:

$$t_1^2 = t^2 - p^2 \sin^2\theta \qquad 4.11$$

but the energy of the incident beam determines the energy of the specularly transmitted beam, so that:

$$t^2 = p^2 + \eta \qquad 4.12$$

where

$$\eta = \frac{2m}{\hbar^2} V_o \qquad 4.13$$

and V_o is the inner potential; combining 4.11 and 4.12:

$$t_1 = \sqrt{p^2 \cos^2\theta + \eta} \ . \qquad 4.14$$

Using 4.14 and 4.10 we eliminate t_1 and t_2 from 4.8:

$$p^2+\eta + \frac{(G^{rst})^4}{4(G_1^{rst})^2} + p^2\sin^2\theta\left[1 + \left\{\frac{G_2^{rst}+\beta G_3^{rst}}{G_1^{rst}\sqrt{1+\beta^2}}\right\}^2\right] - p\sin\theta\left[\frac{(G_2^{rst}+\beta G_3^{rst})G^{rst^2}}{G_1^{rst^2}\sqrt{1+\beta^2}}\right]$$

$$4.15$$

Multiplying 4.15 by $\frac{\hbar^2}{2m}$ we obtain:

$$E+V_o = \frac{\hbar^2}{2m}\left[p^2\sin^2\theta\left\{1+\left[\frac{G_2^{rst}+\beta G_3^{rst}}{G_1^{rst}\sqrt{1+\beta^2}}\right]\right\}^2 - p\,\sin\theta\left\{\frac{(G_2^{rst}+\beta G_3^{rst})G^{rst^2}}{G_1^{rst^2}\sqrt{1+\beta^2}}\right\} + \frac{G^{rst^4}}{4G_1^{rst^2}}\right]$$

4.16

Equation 4.16 is essentially our final result. For a fixed angle of incidence, θ and β, the values of energy given by 4.16 for all $\underline{G}^{rst}$ denote the positions of intensity peaks in the specular reflectivity. If $G_2^{rst} = G_3^{rst} = 0$ we have a Bragg peak otherwise a secondary Bragg peak. Of course, equation 4.5 must always hold.

The extreme ease of plotting $(E+V_o)$ versus p sin θ using 4.16, as against $(E+V_o)$ versus θ (which involves a lot more computation) suggests that we do the former. Of course, we then have to superimpose curves of constant angle of incidence to obtain the same information, but this presents no difficulty. There is anyway some advantage in presenting the constant angle of incidence curves on separate graphical axis (in our case E versus p sin θ) if they are drawn on tracing paper. Then, if the empirical results are transferred to the tracing paper we can superimpose these curves upon the $(E+V_o)$ versus p sin θ curves causing the E axis of the former to coincide with the $(E+V_o)$ axis of the latter. Then merely by sliding the graphs over one another, always ensuring that these axes coincide, we have a very convenient way of allowing V_o to vary with energy. We can thus determine the value of V_o which gives the best fit between experimental and theoretical results, also the same basic curves of $(E+V_o)$ versus p sin θ can be used for all crystals having the same lattice structure but different inner potentials.

There is a slight disadvantage in plotting $(E+V_o)$ versus p sin θ, as against $(E+V_o)$ versus θ, at high angles of incidence. This is because the factor of sin θ causes a loss of resolution in the theoretical results as θ tends to $\frac{\pi}{2}$. At the angles of incidence with which we shall be concerned, in interpreting the results of McRae and Caldwell, this will cause no difficulty.

Of course, the constant angle of incidence curves plotted on the axes E versus p sin θ (i.e. p") axes are given by:

$$E = \left(\frac{\hbar^2}{2m \sin^2\theta}\right) p''^2, \ \theta \text{ fixed} \qquad 4.17$$

Also, there is an advantage in the additional information afforded by knowing the value of p", as well as $(E+V_o)$ and θ, at which we expect a peak in the specular reflectivity. It allows us, very quickly, to locate the position of the wave-vector of the specularly transmitted beam in k-space at intersecting points in the specular reflectivity.

We need to reformulate 4.5 on the basis of finding the equivalent limits on p sin θ for the curves given by 4.16. Provided G_1^{rst} and t_1 are positive we can rewrite 4.5:

$$G_1^{rst\,2} \geq t_1^2 = p^2\cos^2\theta + \eta \qquad 4.18$$

where we have also used 4.14. Rearranging 4.18:

$$(E+V_o) \leq \frac{\hbar^2}{2m}\left(G_1^{rst} + p^2\sin^2\theta\right) \qquad 4.19$$

Taking $(E+V_o)$ from 4.16, 4.19 becomes:

$$p^2\sin^2\theta - p\sin\theta\left\{\frac{G^{rst^2}\sqrt{1+\beta^2}}{G_2^{rst}+\beta G_3^{rst}}\right\} + \left\{\frac{G^{rst^4}-G_1^{rst^4}}{4}\right\}\left\{\frac{\sqrt{1+\beta^2}}{G_2^{rst}+\beta G_3^{rst}}\right\}^2 \leq 0 \qquad 4.20$$

Now the values of $p \sin \theta$ satisfying 4.20 lie between the two values given by:

$$p \sin \theta = \frac{\sqrt{1+\beta^2}}{2(G_2^{rst}+ G_3^{rst})}\left[G^{rst^2} \pm 2G_1^{rst^2}\right] \qquad 4.21$$

Because we require that both G_1^{rst} and t_1 be positive, one of the limits given by 4.21 is redundant. This is best appreciated by referring to diagram 4.1 (which represents the special case of $\underline{G}^{rst}$ lying in the plane of incidence). We have assumed that G_1^{rst} is positive, in which case elementary geometry shows that taking the positive sign in 4.21 gives the value $p'' \sin \theta''$ on the diagram, where $t_1 = G_1^{rst}$. Taking the negative sign in 4.21 gives $p \sin \theta$ on the diagram. Incidentally it is also easy to show that the value mid-way between those of 4.21 corresponds to $p' \sin \theta'$ in the diagram, that is, $t_1 = 0$. Thus for our purposes, the inequality 4.5 is best expressed as:

$$\left.\begin{array}{l} p \sin \theta \text{ lies bestween the values } \dfrac{\sqrt{1+\beta^2}}{2(G_2^{rst}+\beta G_3^{rst})}\left[G^{rst^2} - 2G_1^{rst^2}\right] \\ \text{and } \dfrac{\sqrt{1+\beta^2}}{2(G_2^{rst}+\beta G_3^{rst})} \cdot G^{rst^2} \text{ with } G_1^{rst} > 0 \end{array}\right\} 4.22$$

Before proceeding to apply this simple theory to the results of McRae and Caldwell, we just point out that our discussion of Taylor's results in Chapter II was an application of this theory for normal incidence.

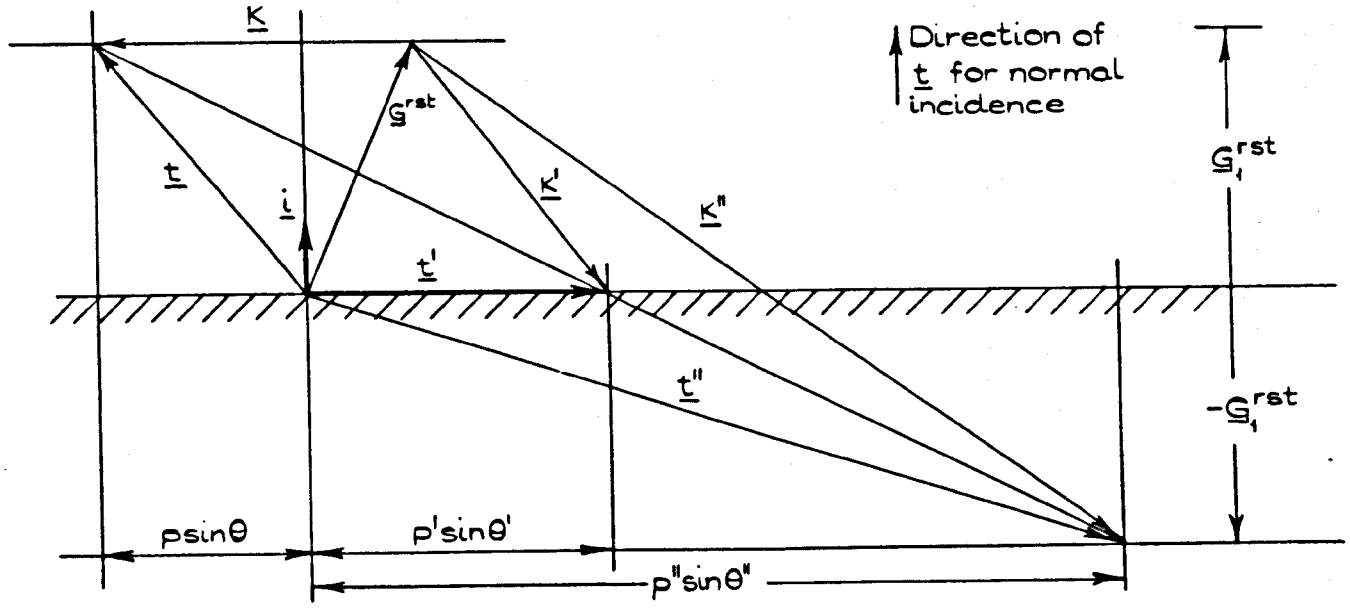
K
G^rst
Direction of
t for normal
incidence
t
i
K'
K''
G_1^rst
t'
t''
-G_1^rst
psinθ
p'sinθ'
p''sinθ''

DIAGRAM 4.1

We proceed now to apply this simple theory to some experimental results.

B. Interpretation of experimental data obtained for NaF and LiF

(i) Preliminaries

The diagrams 4.2, 4.3 and 4.4 reproduce McRae and Caldwell's results for LiF (1) and NaF (2). Throughout, the crystal surface exposed to the incident electrons is the (100) face. For both types of specimen measurements were made for two azimuthal angles corresponding to $\beta = 0$ and 1 in our notation. In all cases the results show the detailed structure in the specular reflectivity in the region of enhanced intensity associated with the Bragg peak of order two. For future reference we have indicated and labelled what appear to be sequencies of peaks on these results.

In our investigation of these results we use the dimensionless units employed in Chapter III. We also use 3.5 while 3.8 and 3.9 give the conversion factors to electron volts from our units of energy.

By a similar process to that used in section A(ii) of Chapter III, we find that in order to interpret McRae's results, we require a knowledge of those reciprocal lattice vectors for which:

$$|\underline{G}_{rst}|^2 \leq 27 \qquad 4.24$$

For the (100) face of the face-centred cubic direct lattice we have:

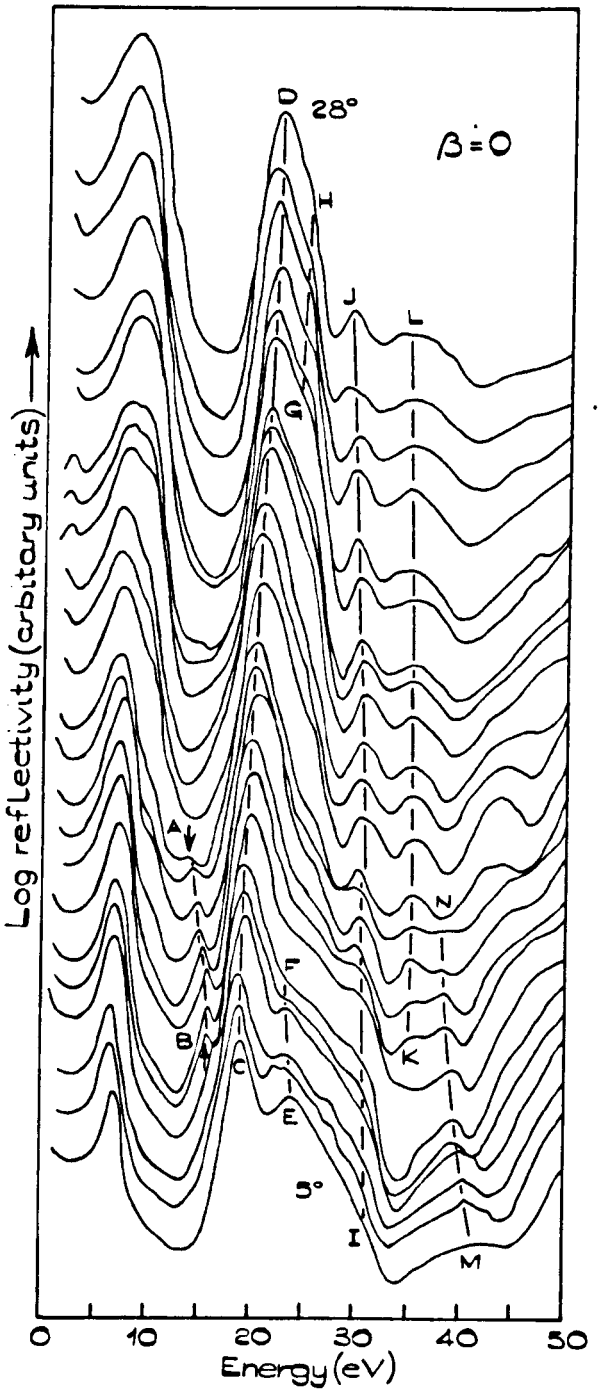

Reflectivity curves for NaF(100) obtained by McRae & Caldwell. The angles of incidence for the top and bottom curves are shown, the remaining curves were obtained at one degree increments in the angle of incidence. Successive curves are displaced upwards for clarity. The arrows indicate the sequence of peaks that are interpreted as surface resonance peaks by McRae & Caldwell.

DIAGRAM 4.2.

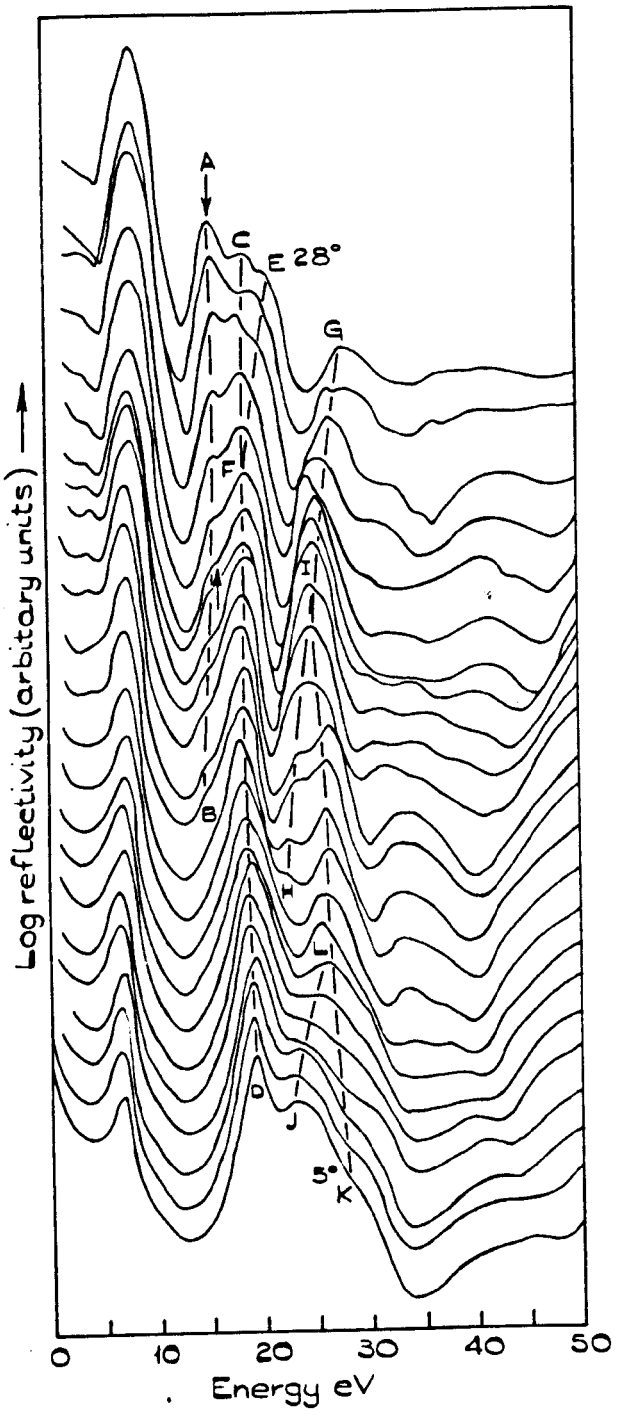

Reflectivity curves obtained by McRae & Caldwell for NaF(100) with $\beta = 1$.

DIAGRAM 4.3.

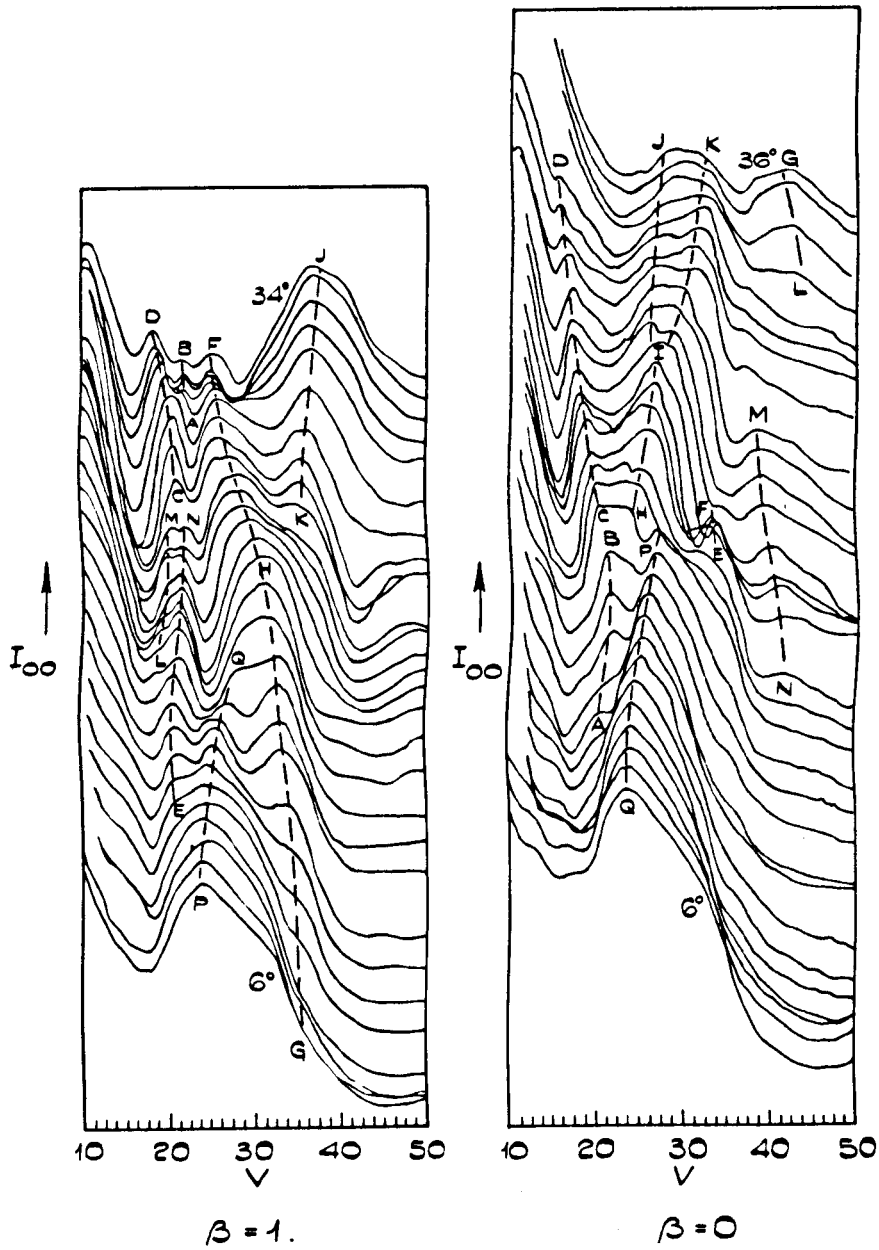

Reflectivity curves for LiF(100) obtained by McRae & Caldwell

DIAGRAM 4.4

$$E(p'') = E(-p'') \qquad 4.25$$

so that we need only evaluate the curves of $(E+V_o)$ versus p" for p" positive, say. This last fact, coupled with the condition 4.22, eliminates a further set of reciprocal lattice vectors which do satisfy 4.24.

In diagram 4.5 we have tabulated those curves, 4.16, which satisfy 4.24 and which have an allowed section, by virture of 4.22, with p" positive. In diagram 4.6 these curves are plotted for $\beta = 0$, while diagram 4.7 shows the curves for $\beta = 1$. A few curves of constant angle of incidence for $V_o = 0$ are superimposed.

We note that, for the (100) faces of the face-centred cubic direct lattice, 3.74 applies to all the reciprocal lattice points.

McRae and Caldwell's results are only concerned with angles of incidence less than 36°. Therefore, in order to obtain the maximum resolution, we have enlarged the relevant portions for subsequent diagrams which are specifically concerned with McRae and Caldwell's results.

(ii) Detailed comparison with experiment

We come now to a detailed discussion of the experimental results. On diagrams 4.8 to 4.12 inclusive the results are depicted, the letters labelling the sequencies of peaks correspond to those on the diagrams

G^{rst}				$\beta = 0$		$\beta = 1$	
r s t	G_1^{rst}	G_2^{rst}	G_3^{rst}	$E+V_0$	Range of p''	$E+V_0$	Range of p''
0 0 1	1	1	-1	$2p''^2 - 3p'' + 2\frac{1}{4}$	$\frac{1}{2} \to \frac{3}{2}$	———	———
1 1 1	1	1	1	$2p''^2 - 3p'' + 2\frac{1}{4}$	$1/2 \to 3/2$	$3p''^2 - \frac{8}{\sqrt{2}}p'' + 2\frac{1}{4}$	$\frac{\sqrt{2}}{4} \to \frac{3}{4}\sqrt{2}$
0 1 1	2	0	0	$p''^2 + 1$	$-\infty \to \infty$	$p''^2 + 1$	$-\infty \to \infty$
1 2 1	2	0	2	———	———	$3/2\,p''^2 - \frac{4}{\sqrt{2}}p'' + 4$	$0 \to 2\sqrt{2}$
1 1 2	2	2	0	$2p''^2 - 4p'' + 4$	$0 \to 2$	$3/2\,p''^2 - \frac{4}{\sqrt{2}}p'' + 4$	$0 \to 2\sqrt{2}$
1 2 3	3	1	1	$\frac{10}{9}p''^2 - \frac{11}{9}p'' + \frac{121}{36}$	$-7/2 \to 11/2$	$\frac{11}{9}p''^2 - \frac{4}{\sqrt{2}}p'' + 4$	$-\frac{7}{4}\sqrt{2} \to \frac{11}{4}\sqrt{2}$
-1 1 1	3	-1	-1	$\frac{10}{9}p''^2 + \frac{11}{9}p'' + \frac{121}{36}$	$-11/2 \to 7/2$	$\frac{11}{9}p''^2 + \frac{22}{4\sqrt{2}}p'' + \frac{121}{36}$	$-\frac{11}{4}\sqrt{2} \to \frac{7}{4}\sqrt{2}$
0 1 2	3	1	-1	$\frac{10}{9}p''^2 - \frac{11}{9}p'' + \frac{121}{36}$	$-7/2 \to 11/2$	$p''^2 + \frac{121}{36}$	$-\infty \to \infty$
0 2 1	3	-1	1	$\frac{10}{9}p''^2 + \frac{11}{9}p'' + \frac{121}{36}$	$7/2 \to -11/2$	$p''^2 + \frac{121}{36}$	$-\infty \to \infty$
2 1 2	1	3	1	$10p''^2 - 33p'' + 30\frac{1}{4}$	$11/6 \to -3/2$	$9p''^2 - \frac{44}{\sqrt{2}} + 30\frac{1}{4}$	$\frac{3}{8}\sqrt{2} \to \frac{11}{8}\sqrt{2}$
2 2 1	1	1	3	———	———	$9p''^2 - \frac{44}{\sqrt{2}} + 30\frac{1}{4}$	$\frac{9}{8}\sqrt{2} \to \frac{11}{8}\sqrt{2}$
2 3 3	4	2	2	———	———	$\frac{3}{2}p''^2 \quad \frac{6}{\sqrt{2}}p'' + 9$	$3\sqrt{2} \to \sqrt{2}$
3 2 3	2	4	2	———	———	$\frac{9}{2}p''^2 - \frac{36}{\sqrt{2}}p'' + 36$	$\frac{4}{3}\sqrt{2} \to 2\sqrt{2}$
3 3 2	2	2	4	———	———	$\frac{9}{2}p''^2 - \frac{36}{\sqrt{2}}p'' + 36$	$\frac{4}{3}\sqrt{2} \to 2\sqrt{2}$
2 2 3	3	3	1	———	———	$1^8/_9 p''^2 - \frac{76}{9\sqrt{2}}p'' + 10\frac{1}{36}$	$\frac{1}{4\sqrt{2}} \to \frac{19}{4\sqrt{2}}$
2 3 2	3	1	3	———	———	$1^8/_9 p''^2 - \frac{76}{9\sqrt{2}}p'' + 10\frac{1}{36}$	$\frac{1}{4\sqrt{2}} \to \frac{19}{4\sqrt{2}}$
1 0 2	1	3	-1	$10p''^2 - 33p'' + 30\frac{1}{4}$	$11/6 \to 3/2$	———	———
2 1 3	2	4	0	$5p''^2 - 20p'' + 25$	$3/2 \to 5/2$	———	———
1 2 3	4	2	0	$5/4\,p''^2 - 5/2\,p'' + 6\frac{1}{4}$	$-4 \to 5$	$9/8\,p''^2 - \frac{5}{2\sqrt{2}}p'' + 6\frac{1}{4}$	$-4\sqrt{2} \to 5\sqrt{2}$
1 3 2	4	0	2	$p''^2 + 6\frac{1}{4}$	$-\infty \to \infty$	$9/8\,p''^2 - \frac{5}{2\sqrt{2}}p'' + 6\frac{1}{4}$	$-4\sqrt{2} \to 5\sqrt{2}$
-1 2 1	4	-2	0	$5/4\,p''^2 + 5/2\,p'' + 6\frac{1}{4}$	$-5 \to 4$	$9/8\,p''^2 + \frac{5}{2\sqrt{2}}p'' + 6\frac{1}{4}$	$-5\sqrt{2} \to 4\sqrt{2}$
-1 1 2	4	0	-2	$p''^2 + 6\frac{1}{4}$	$-\infty \to \infty$	$9/8\,p''^2 + \frac{5}{2\sqrt{2}}p'' + 6\frac{1}{4}$	$-5\sqrt{2} \to 4\sqrt{2}$
0 0 2	2	2	-2	$2p''^2 - 6p'' + 9$	$1 \to 3$	———	———
2 2 2	2	2	2	$2p''^2 - 6p'' + 9$	$1 \to 3$	$3p''^2 - \frac{12}{\sqrt{2}}p'' + 9$	$\frac{1}{\sqrt{2}} \to \frac{3}{\sqrt{2}}$
0 2 2	4	0	0	$p''^2 + 4$	$-\infty \to \infty$	$p''^2 + 4$	$-\infty \to \infty$
3 1 3	1	5	1	$26p''^2 - 135p'' + 182\frac{1}{4}$	$25/10 \to 27/10$	———	———
2 0 3	1	5	-1	$26p''^2 - 135p'' + 182\frac{1}{4}$	$25/10 \to 27/10$	———	———
3 2 2	1	3	3	———	———	$19p''^2 - \frac{114}{\sqrt{2}}p'' + 90\frac{1}{4}$	$\frac{17}{12}\sqrt{2} \to \frac{19}{2}\sqrt{2}$
3 3 3	3	3	3	———	———	$3p''^2 - \frac{54}{3\sqrt{2}}p'' + 20\frac{1}{4}$	$\frac{3}{4}\sqrt{2} \to \frac{27}{12}\sqrt{2}$
1 3 3	5	1	1	———	———	$\frac{27}{25}p''^2 - \frac{27}{25}\sqrt{2}p'' + 20\frac{1}{4}$	$\frac{27}{4}\sqrt{2} \to \frac{23}{4}\sqrt{2}$

DIAGRAM 4.5

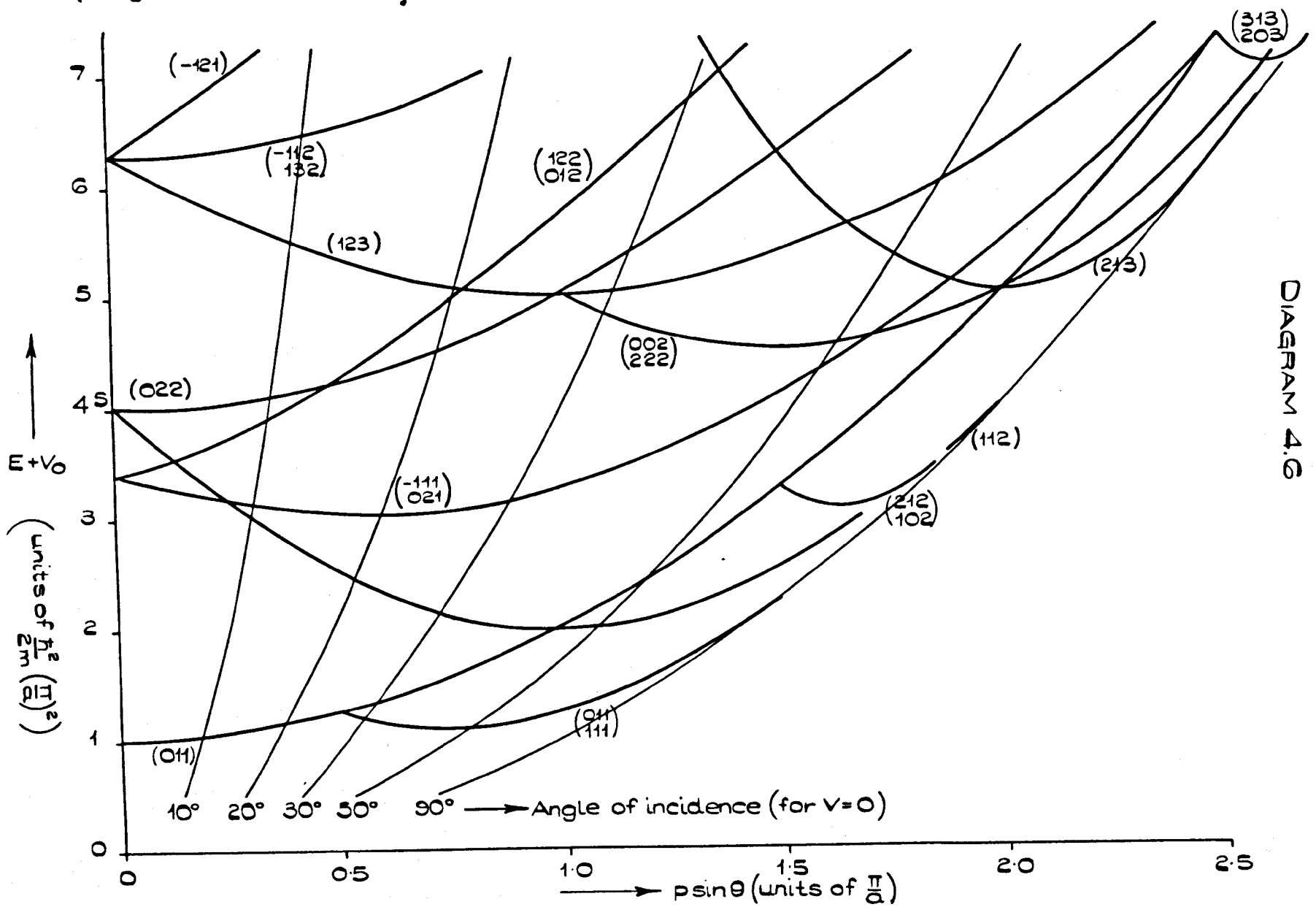
(E+V0) VERSUS p SIN θ FOR FACE-CENTRED DIRECT LATTICE FOR β=0.
(-121)
(-112 / 132)
(122 / 012)
(123)
(313 / 203)
(213)
(002 / 222)
(022)
(112)
(-111 / 021)
(212 / 102)
(011 / 111)
(011)
10° 20° 30° 50° 90° → Angle of incidence (for V=0)
E+V0
(units of ħ²/2m (π/a)²)
psinθ (units of π/a)
0 0·5 1·0 1·5 2·0 2·5
0 1 2 3 4 5 6 7
DIAGRAM 4.6

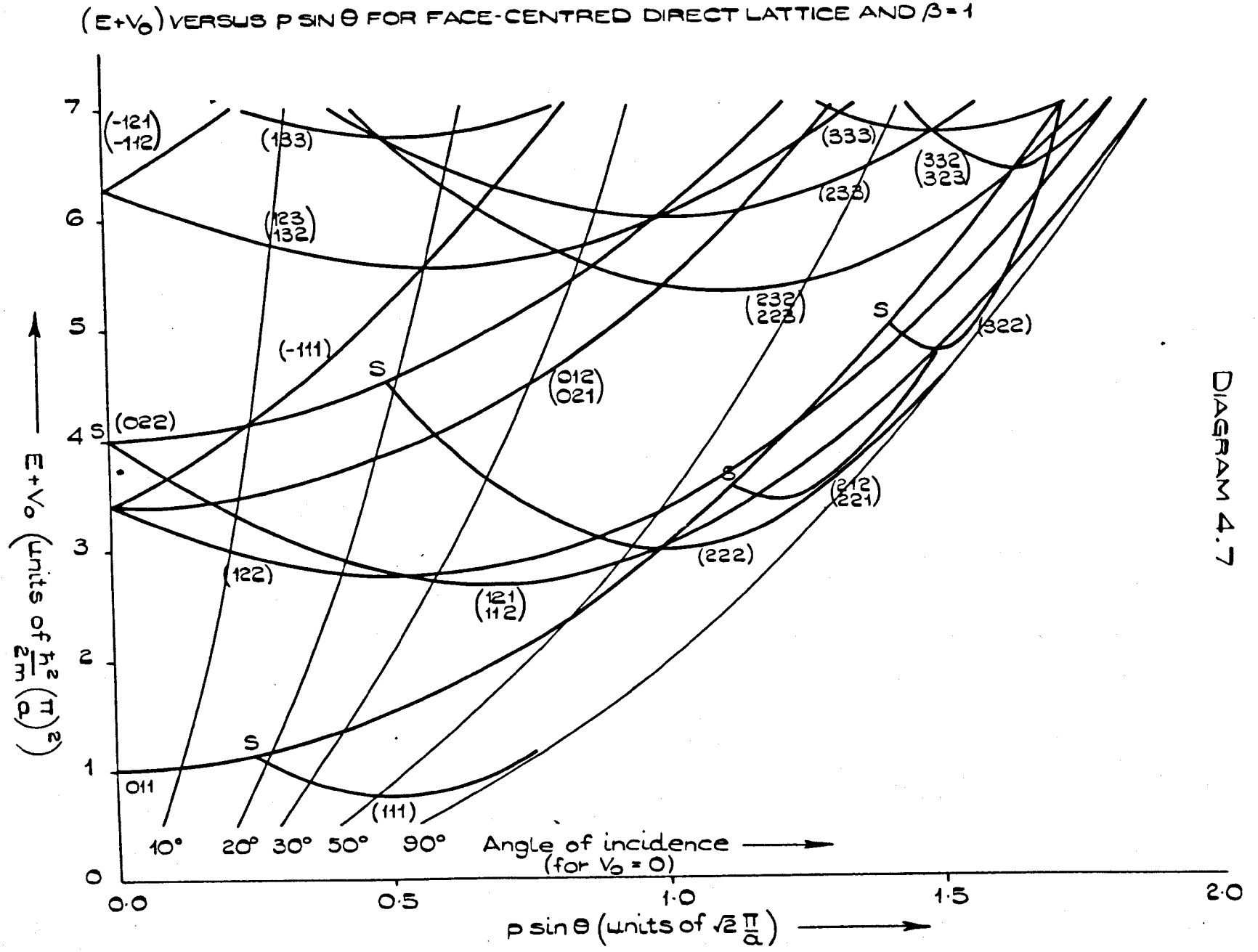
(E+V0) VERSUS p SIN θ FOR FACE-CENTRED DIRECT LATTICE AND β = 1
E+V0 (units of h²/2m (π/a)²)
p sin θ (units of √2 π/a)
Angle of incidence (for V0 = 0)
10°
20°
30°
50°
90°
(-121) (-112)
(133)
(333)
(332) (323)
(123) (132)
(233)
(232) (223)
(322)
(-111)
(012) (021)
(022)
(212) (221)
(222)
(122)
(121) (112)
011
(111)
S
0
1
2
3
4
5
6
7
0·0
0·5
1·0
1·5
2·0

DIAGRAM 4.7

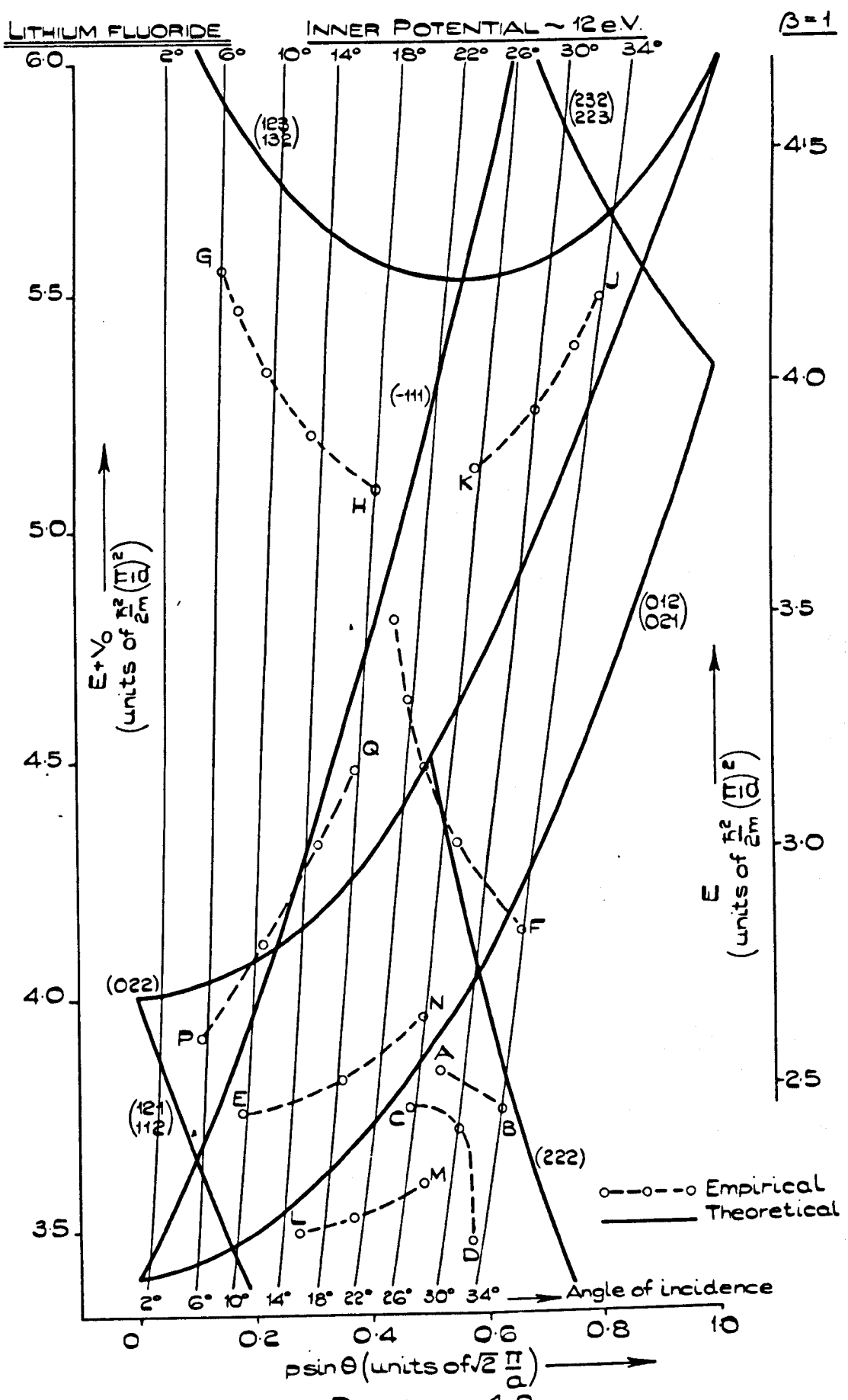
LITHIUM FLUORIDE
INNER POTENTIAL ~ 12 eV.
β = 1
2° 6° 10° 14° 18° 22° 26° 30° 34°
(123) (132)
(232) (223)
(-111)
(012) (021)
(022)
(121) (112)
(222)
G
H
K
L
Q
P
F
N
A
E
C
B
M
L
D
6·0
5·5
5·0
4·5
4·0
3·5
4·15
4·0
3·5
3·0
2·5
E+V0 (units of ħ²/2m (π/d)²)
E (units of ħ²/2m (π/d)²)
Empirical
Theoretical
Angle of incidence
0 0·2 0·4 0·6 0·8 1·0
p sin θ (units of √2 π/a)

DIAGRAM 4.8

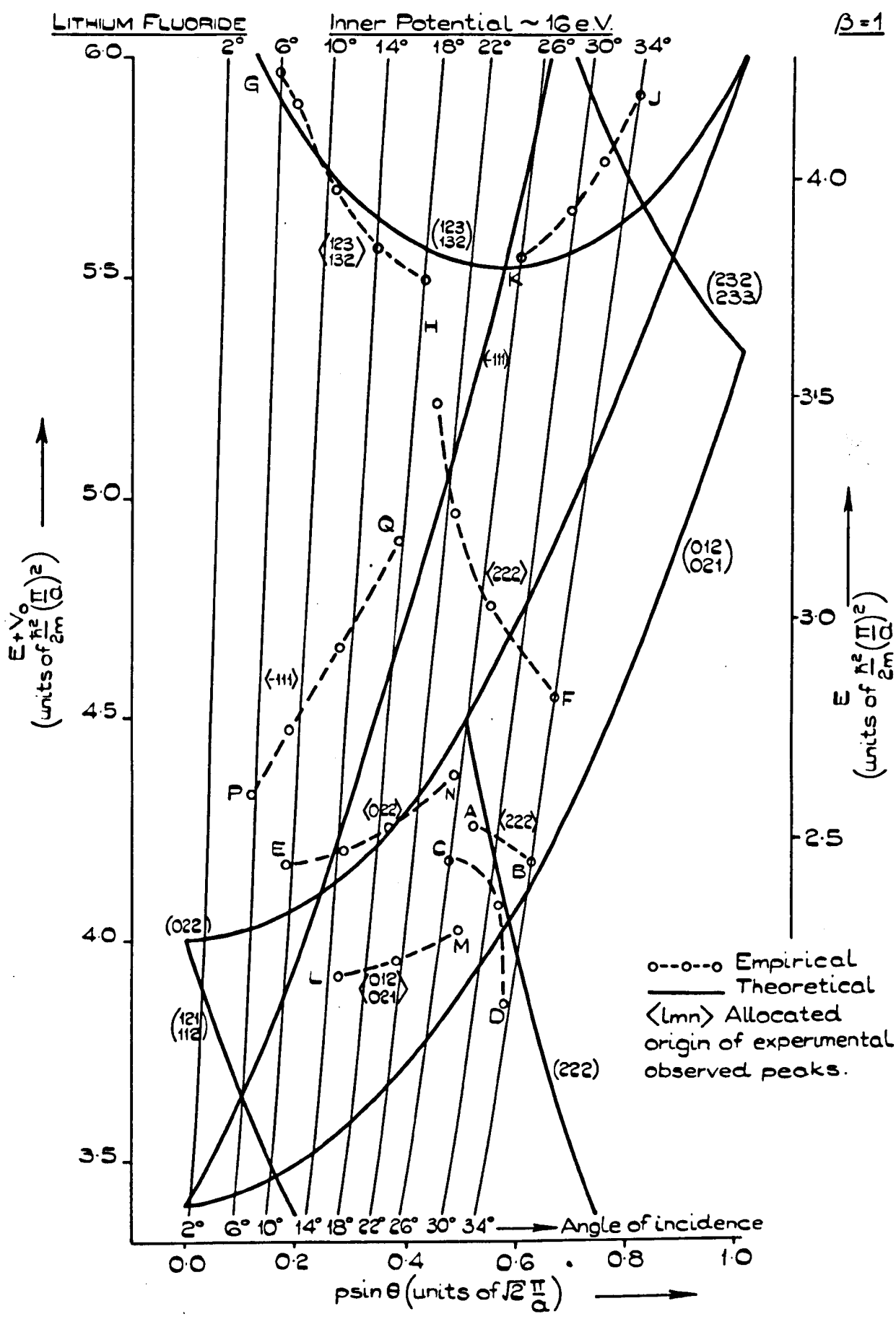
LITHIUM FLUORIDE
Inner Potential ~ 16 e.V.
β = 1
2° 6° 10° 14° 18° 22° 26° 30° 34°
6·0
5·5
5·0
4·5
4·0
3·5
4·0
3·5
3·0
2·5
G
J
K
I
(123) (132)
⟨123⟩ ⟨132⟩
(232) (233)
⟨111⟩
Q
⟨222⟩
F
(012) (021)
P
⟨022⟩
N
A
E
C
B
(022)
M
L
⟨012⟩ ⟨021⟩
D
(121) (112)
(222)
E+V₀ (units of ħ²/2m (π/a)²)
E (units of ħ²/2m (π/a)²)
2° 6° 10° 14° 18° 22° 26° 30° 34° Angle of incidence
0·0 0·2 0·4 0·6 0·8 1·0
psin θ (units of √2 π/a)
o--o--o Empirical
Theoretical
⟨lmn⟩ Allocated origin of experimental observed peaks.

DIAGRAM 4.9

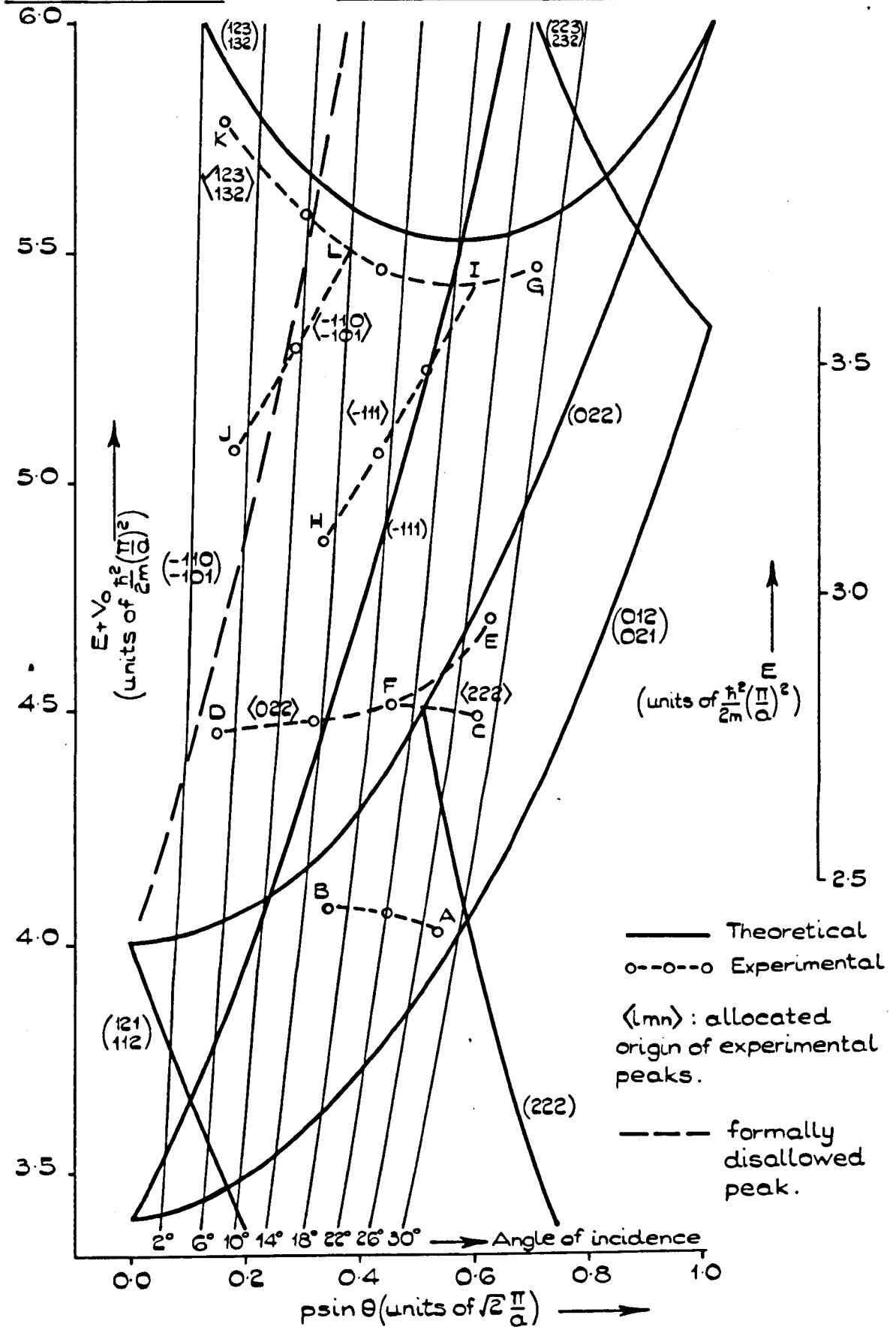
SODIUM FLUORIDE
Inner Potential ~12¼ eV
β=1
6·0
5·5
5·0
4·5
4·0
3·5
(123)/(132)
(223)/(232)
K
(123)/(132)
L
I
G
(-110)/(-101)
(-111)
(022)
J
H
(-111)
(-110)/(-101)
(012)/(021)
E
F
(222)
D
(022)
C
B
A
(121)/(112)
(222)
E+V₀ (units of ħ²/2m(π/a)²)
E (units of ħ²/2m(π/a)²)
3·5
3·0
2·5
2° 6° 10° 14° 18° 22° 26° 30° → Angle of incidence
0·0 0·2 0·4 0·6 0·8 1·0
psin θ (units of √2 π/a) →
Theoretical
o--o--o Experimental
⟨lmn⟩ : allocated origin of experimental peaks.
formally disallowed peak.

DIAGRAM 4.10

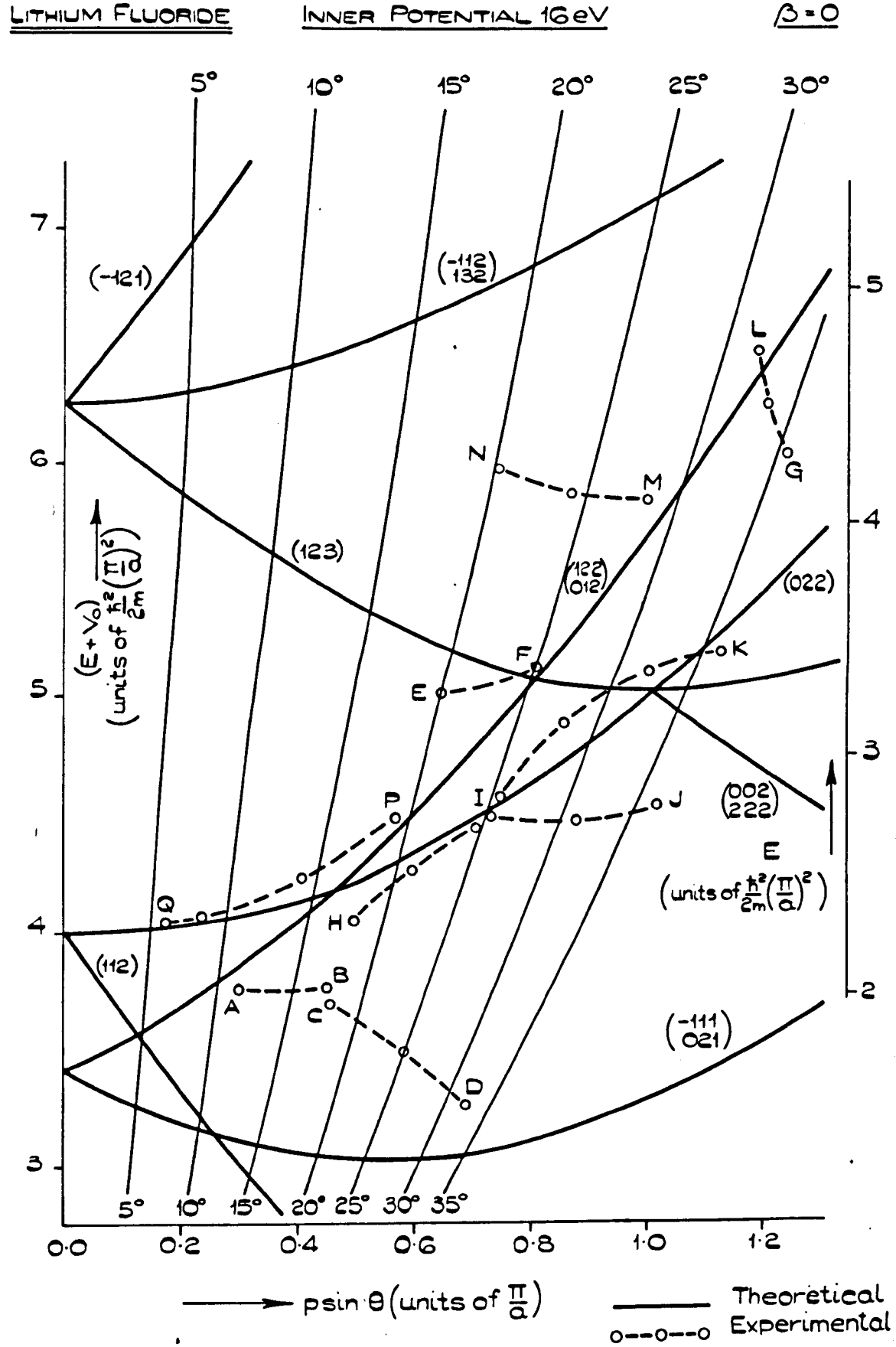
LITHIUM FLUORIDE
INNER POTENTIAL 16 eV
β = 0
5°
10°
15°
20°
25°
30°
35°
(-121)
(-112)/(132)
(123)
(122)/(012)
(022)
(002)/(222)
(-111)/(021)
(112)
A
B
C
D
E
F
G
H
I
J
K
L
M
N
P
Q
(E + V0) (units of ħ²/2m (π/a)²)
E (units of ħ²/2m (π/a)²)
psin θ (units of π/a)
0·0
0·2
0·4
0·6
0·8
1·0
1·2
3
4
5
6
7
2
3
4
5
Theoretical
Experimental

DIAGRAM 4.11

SODIUM FLUORIDE. INNER POTENTIAL ~ 9 e.V. $\beta = 0$

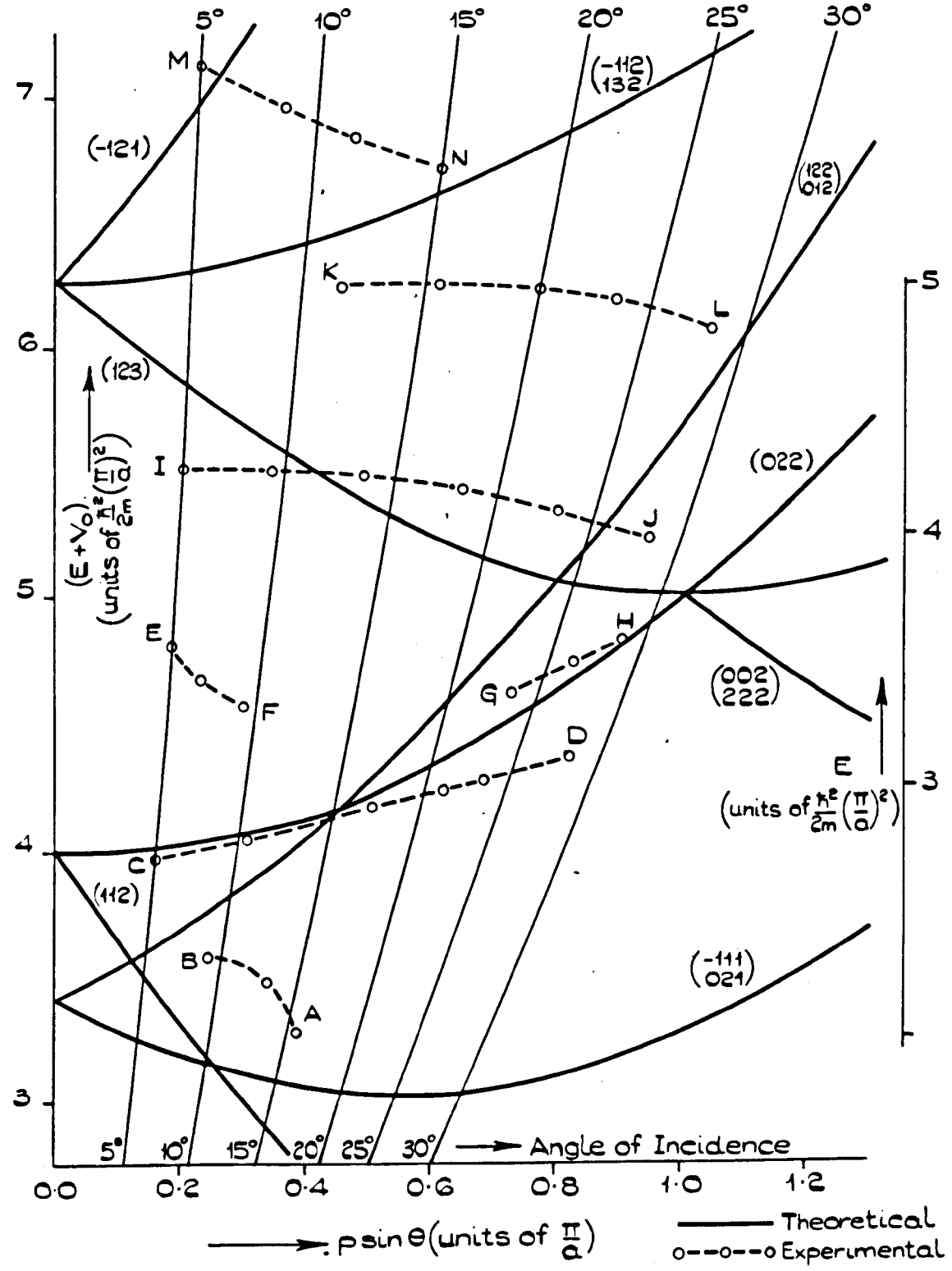

DIAGRAM 4.12

4.2 to 4.4. We now discuss the results individually.

The best apparent fit between theory and experiment is obtained with the results for $\beta = 1$, and in particular for LiF. Diagram 4.8 shows the results for LiF with $\beta = 1$ using the inner potential of .2 eV, which McRae and Caldwell (9) find provides the best value to fit the gross reflectivity structure. However, his value is not the best to fit the detailed structure. Diagram 4.9 shows the same data using an inner potential of 16 eV. This value, incidentally, does not provide a gross mismatch between the expected peak positions of the gross structure if the experimental uncertainty in the energy (~ 2 eV : McRae and Caldwell (9)) is taken into account. In any case, McRae and Caldwell's determination of the inner potential was on the basis of fitting several Bragg peaks using a constant inner potential. Using an energy dependent inner potential would require different criteria and a consequently different value at the energy of these results (see Appendix V).

On diagram 4.9 we have, perhaps tenuously, allocated the origins of the experimentally observed peaks. Some peaks which are expected theoretically are missing. This is permissible. The present theory has no pretension to predict peak heights: they may be so low as to be undetectable. There is a difficulty concerning the sequence of peaks labelled HF. At energies higher than ~ 4.5, our theory (if the allocation <222> is correct) predicts a negligible intensity. However, the sequence is fairly intense up to an energy ~ 5.2.

There is a tendency for the actual peak positions to be at greater variance with the theoretical positions where more than one Bragg condition is satisfied. One is then tempted to suggest that anomalous dispersion (Sommerfeld and Bethe (5)) is responsible for the inexact fit between theory and experiment.

Diagram 4.10 shows the results for NaF with $\beta = 1$. An inner potential of ~ 12 eV has been chosen to obtain the best fit. McRae and Caldwell (16) suggest a value of 10 eV. The results are seen to differ in detail from those for LiF. However, it is again possible to suggest, perhaps tenuously, mechanisms for the observed peaks. Unsatisfactorily, we have assigned the sequence LJ to a secondary Bragg mechanism which, according to our theory, should provide a negligible reflectivity at the energies where these peaks are observed.

Incidentally, the sequence of peaks labelled AB are interpreted as surface resonance peaks by McRae and Caldwell (16). In the absence of anomalous dispersion, we would predict a secondary Bragg peak mechanism operating through intermediate beams in the surface on the line (222) and close to the intersection with (022) in diagram 4.10. The close proximity with the sequence of peaks labelled AB provides some evidence for our remarks in the previous chapter concerning the claims of McRae and Caldwell (16) to have observed surface resonance peaks. The same remarks apply to the sequence of peaks labelled CD in diagram 4.9. Similarly, for NaF with $\beta = 0$, the sequence of peaks labelled AB in diagram 4.12 are interpreted as resonance peaks by McRae and Caldwell (16)

but lie close to (112), this corresponds to a secondary Bragg peak mechanism where, at the intersection with (022), operates through intermediate beams lying in the crystal surface.

In diagrams 4.11 and 4.12 we present the results for $\beta = 0$. We only make the comment that the interpretation of the results is even harder on the present basis than for $\beta = 1$. The most likely reason being that, for this azimuthal angle, we encounter a much greater number of points where more than one Bragg condition is satisfied. Anomalous dispersion then plays a more significant role.

We put off further discussion until the next chapter.

CHAPTER V

A Synopsis and Critique

In this chapter we present a synopsis of the more important results in this thesis and review the band structure approach to LEED. In the last section we suggest what is likely to be the most fruitful line of approach to the LEED problem in the future.

A. A synopsis of the present work

The major results of the present thesis are as follows. The band structure approach provides a good intuitive understanding of how peaks arise in the diffracted beams without recourse to a detailed knowledge of the crystal potential. The wavefunction in the crystal consists, primarily, of the specularly transmitted beam which is turned into a Bloch wave by scattering from the Bragg planes. If this Bloch wave contains any plane-wave components directed back towards the surface, then these are partially internally-reflected back into the crystal. The internally reflected components are then scattered by the Bragg planes and each is turned into a Bloch wave, and so on. The flux transmitted into the vacuum by the partial internal reflections provides the observed diffraction pattern. Apart from these processes, the specularly reflected intensity is enhanced by the partial reflection of the incident beam at the crystal surface.

If, at a particular energy and angle of incidence, the Bloch wave containing the specularly transmitted beam also contains a strongly excited, back-scattered, plane-wave component which enhances the (0,0) intensity, then we have a Bragg peak in the specularly reflected beam. Other strongly excited components of this Bloch wave, which are back-scattered, provide Bragg peaks in other diffraction spots. Secondary Bragg peaks (which may actually be observed in any of the back-reflected beams) arise when Bloch waves, apart from that containing the specularly transmitted wave, are strongly excited. These Bloch waves may contain plane wave components directed towards the surface which will enchance the intensities of certain beams forming the diffraction pattern. In certain situations, the crystal symmetry will provide that secondary Bragg peaks and/or Bragg peaks will be observed simultaneously in several of the diffraction spots. The understanding of these processes is based purely upon kinematical ideas and no recourse is made to a detailed knowledge of the crystal potential.

We have also seen how a proper account of the inner potential can affect the back-scattered intensities by providing a 'plane of potential' at the crystal surface which scatters the electrons.

We supposed, in Chapter III, that the effect of the inelastic scattering was to make the process summarised in 3.74, the most important producer of secondary Bragg peaks in the specular reflectivity. Some justification was found in the inspection of Taylor's (28) results for

the gross reflectivity structure in the (0,0) reflectivity for Cu(111). In particular, the number of peaks predicted for the specular intensity was of the same order as the number seen in practice.

We have seen that the particular secondary Bragg peak mechanism of Boudreaux and Heine (14), is very often inappropriate. In practice, we always have to contend with a non-zero inner potential and often 3.74 applies. We were also able, for our model, to confirm their remarks concerning the improbability of observing the surface resonance phenomenon when a reasonable value is assigned to the inner potential.

In Chapter IV we derived a simple theory to predict the positions of peaks in the specular reflectivity. The precise manner in which this was formulated took account of the results 3.71 to 3.75. With particular reference to 3.73 and 3.74, we believe that the similar theory due to Marcus/Jona and Jepsen (20) provides too much structure in the specular intensity. Secondary Bragg peaks of appreciable intensity in the specularly reflected beam do not as a rule accompany Bragg peaks in non-specular beams. The assumption of Marcus/Jona and Jepsen (20) was, incidentally, based on calculations (19) where 3.74 applied.

We saw in Chapter IV that the simple theory was not entirely adequate to explain detailed structure in the specular reflectivity. In the next section we discuss this.

B. Critique and suggestions for future work

The failure of our simple theory for predicting peak positions may be due to any or some of the following reasons:

(a) The crystal surfaces may have been contaminated in the experiments producing the results we used.

(b) There may have been some relaxation of the lattice near the crystal surface.

(c) We have neglected the inelastic scattering.

(d) The nearly free electron approximation may be inappropriate.

We discuss each in turn.

As far as (a) is concerned, the experimental precautions taken by McRae and Caldwell would suggest that the crystal surfaces were chemically pure. No Auger spectroscopy was used to confirm this. There may be some doubt concerning the physical disposition of the two ionic species, constituting the crystal, at the crystal surface. Palmberg and Rhodin (29) have detected increases in the partial pressure of chlorine in the LEED apparatus when using a KCℓ specimen in the LEED experiment. This suggests the possibility of dissociation at the surfaces of the alkali halides, the crystal surfaces containing a larger proportion of the metal ion than the bulk. Clearly, this would modify the diffracted intensities, possibly leading to additional peaks. The experiments of

McRae and Caldwell were performed at - 300°C; naively one might expect this to encourage dissociation. No experimental evidence is reported in these experiments.

There appears to be, as McRae and Caldwell (9) point out, some evidence for expansion of the crystal surface for NaF and LiF. We see, in Appendix V that, if anything, their estimate of the expansion is too low. Such surface expansions have been predicted for the alkali halides by Benson et. al (30). Additional peaks in the reflectivity then arise because the Fourier components of the potential required to describe such an expansion would be formally absent for the perfect surface. No account has been taken of this in the simple theory of Chapter IV.

It is difficult to see how the exclusion of inelastic scattering will modify the peak positions. We only expect its inclusion to broaden the peaks which are produced by the elastic scattering processes, and to affect the relative intensities of the diffraction spots.

The last of our reasons for the failure of the simple theory is probably the most important. The general correlation between experiment and theory in diagrams 4.8 to 4.12, although poor in detail, suggests that our physical arguments are probably along the correct lines. The indication is that the nearly free electron approximation is not good enough and that a much better job of solving the Schrödinger equation in the crystal is required. The initial step in solving our difficulties is then to obtain an accurate solution using the formalism of Chapter II

with a suitable pseudo-potential. Incidentally, Pendry (31) has discussed the application of pseudo-potentials to an elastic scattering solution of the LEED problem, he is also engaged on such a calculation for nickel (32).

We now outline some objections to pursuing the LEED problem using a band structure approach. The first objection is that a NFE-pseudo-potential calculation would be an order of magnitude more arduous than our calculations of Chapter IV, and yet we feel that all it can achieve is possibly the correct positioning of the intensity peaks in energy and angle of incidence. There is growing evidence that the inelastic scattering must be treated, from the beginning, on an equal par with the elastic scattering in order to obtain the absolute (and probably even the relative) intensities of the diffraction spots. At the moment, this evidence comes from the work of Duke and Tucker (4), the ad hoc arguments in this thesis to remove the peaks associated with high order multiple scattering processes (and similarly McRae (36) requires a small 'depth of penetration' in order that his sequence of secondary Bragg peaks characterised by t_1 is most prominent). Of course, we also have that the flat-topped peaks of the elastic-scattering calculations are supposed to be 'rounded off' by the inelastic scattering. We feel that these general observations should bear on the final approach to the LEED problem but do not remove the value of performing one or two NFE-pseudo-potential type of calculations (which are needed anyway to confirm our remarks!). In the context of our discussion at the beginning of

this chapter we feel that the band-structure approach does give a good 'physical feel' to the problem, the ardour of a more accurate calculation could be reduced by not bothering with the matching procedure. A simple inspection of the band-structure and wavefunctions should suffice to determine the occurrence of the intensity peaks.

There are, in the long run, further objections to the band-structure approach. The loss of periodicity in a direction normal to the crystal surface (due to relaxation of the surface) and the adsorption of gas layers on the surface are not easily accounted for in a band-structure approach. Also, the matching procedure is accomplished at a plane of discontinuity in the potential. This potential step is chosen so as to make the solution of the Schrödinger equations, in both regions, a relatively simple procedure. However, all the physics of the LEED problem occurs near this matching plane where we have markedly modified the real potential for mathematical convenience. We could overcome these latter difficulties by enclosing the surface region between two planes and carry out the matching procedure at both of them. Of course, on a band-structure picture, the solution of the Schrödinger equation is not easily accomplished between these planes and we still have not accounted for the inelastic scattering.

The difficulties associated with a 'selvedge' region are best dealt with in a layer by layer treatment of the scattering. Such theories as McRae's (13) and Beeby's (21) thus seem appropriate. In such treatments

the atomic layers parallel to the crystal surface need not be of identical chemical content. It should also be an easy task to incorporate irregularities in the spacing of such planes. At present no theory exists which is likely to take reasonable account of the inelastic scattering.

Duke and Tucker (4) have taken the first steps in what appears to be the best approach. However, as we indicated in Chapter I, their description of the 'electron fluid' would inhibit calculation of the intensities with any accuracy. As these authors point out, this deficiency could be partially remedied by using modified ion-core potentials near the surface and a local density dependence of the electron self-energy.

The situation reflects a fundamental ambiguity in the existing formalism of electron lattice scattering in the presence of an inhomogeneous electron fluid. Therefore, a revised formulation must be devised before any remedy, except a strictly phenomenological one, is possible. On the grounds that the energy resolution of most experiments are not sufficiently high to distinguish phonon emission events from elastic scattering events, Duke and Tucker do not consider phonon excitation. We make the point that phonon-excitation, although 'quasi-elastic', will lead to a slight redistribution of the experimentally observed 'elastically-scattered' electrons in the back-scattered beams.

It seems that it will be some years before the problem of evaluating the absolute intensities of the diffraction spots in LEED is accomplished.

Ideally, a detailed understanding of the magnitude of the intensities (supplied by a better theory) would be necessary for a proper comprehension of surface phenomena like gas adsorption and catalysis. It is in an understanding of this sort of phenomena that LEED should ultimately prove invaluable.

Appendix I

Scattering from a potential step

In Chapter II it is shown that, if the end of the wave-vector of the specularly transmitted beam does not lie near any Bragg scattering planes, then the wave-function outside the crystal, $\psi_{o,\underline{p}}$, consists of only the specularly reflected beam with the incident wave:

$$\psi_{o,\underline{p}} = A\left[e^{i\underline{p}\cdot\underline{r}} + \left(\frac{p^{\perp} - t^{\perp}}{p^{\perp} + t^{\perp}}\right) e^{i(\underline{p}'' - \underline{n}p^{\perp})\cdot\underline{r}}\right] \qquad \text{A1.1}$$

Inside the crystal, the wavefunction, $\psi_{i,\underline{p}}$, consists of a specularly transmitted wave:

$$\psi_{i,\underline{p}} = A\left[\frac{2p^{\perp}}{p^{\perp} + t^{\perp}}\ e^{i(\underline{p}'' - \underline{n}t^{\perp})\cdot\underline{r}}\right]. \qquad \text{A1.2}$$

The vector, $\underline{n}$, is a unit vector directed normally into the crystal. The electrons in all the beams have the same energy, E, determined by the incident wave:

$$E = \frac{\hbar^2}{2m} p^2 \qquad \text{A1.3}$$

so that

$$t^{\perp} = \sqrt{\frac{2m}{\hbar^2}(E + V_o) - p''^2} \qquad \text{A1.4}$$

and

$$p^{\perp} = \sqrt{\frac{2mE}{\hbar^2} - p''^2} \qquad \text{A1.5}$$

where V_o is the inner potential.

We now show that A1.1 and A1.2 are the wavefunctions appropriate for scattering from a potential step, and we also describe the reflection coefficient as a function of the energy of the incident wave and the incident angle.

We take the potential distribution for the step to be:

$$V(\underline{r}) = 0 \text{ for } x < 0$$

and

$$V(\underline{r}) = -V_o \text{ for } x > 0 \qquad \text{A1.6}$$

for all y and z, where V_o is a positive constant.

We consider a plane wave, Ψ, with energy E, incident on the step from the high potential side. A suitable solution of the Schrödinger equation:

$$-\frac{\hbar}{2m}\nabla^2\Psi = E\,\Psi \qquad \text{A1.7}$$

is:

$$\Psi = A\, e^{i\underline{p}\cdot\underline{r}} \qquad \text{A1.8}$$

where E is given by A1.3. The vector, $\underline{p}$, is real and:

$$\underline{p}\cdot\underline{n} > 0 \qquad \text{A1.9}$$

where $\underline{n}$ is a unit vector directed along the x-axis. Equation A1.9

ensures that the flux associated with A1.8 is travelling towards the step. The angle of incidence, θ, is given by:

$$\theta = \cos^{-1}\left(\frac{\underline{p}.\underline{n}}{p}\right) . \qquad \text{A1.10}$$

The incident wave, A1.8, can give rise to reflected flux in the region $x < 0$. This will be contained in plane waves of the form: $\exp i\, \underline{k}.\underline{r}$ where

$$\underline{k}.\underline{n} < 0 \qquad \text{A1.11}$$

Equation A1.11 ensures that the flux is travelling away from the boundary. These reflected waves have the same energy as the incident wave so that:

$$|\underline{k}| = |\underline{p}| . \qquad \text{A1.12}$$

The Hamiltonian, $\left(-\frac{\hbar}{2m}\nabla^2\right)$, commutes with the translation operators $T(y,z)$. Thus $\left(-\frac{\hbar}{2m}\nabla^2\right)$ and $T(y,z)$ have simultaneous eigenfunctions and the eigenvalue of $T(y,z)$, which is characterised by $\underline{k}''$, is a constant of the motion determined by the incident wave. Hence, we have:

$$\underline{p}'' = \underline{k}'' \qquad \text{A.13}$$

for all the plane waves scattered from the step as a result of the incidence of the wave A1.8.

Equations A1.11, A1.12 and A1.13, fix uniquely the wave vectors of the reflected waves. Only one wave is possible. It has the wave vector:

$$\underline{k} = \underline{p}'' - \underline{n}p^{+} \qquad \text{A1.14}$$

Thus in the region $x < 0$, the complete wave function will be:

$$\psi_{o,\underline{p}} = A\, e^{i\underline{p}\cdot\underline{r}} + B\, e^{i(\underline{p}'' - \underline{n}p^{+})\cdot\underline{r}} \qquad \text{A1.15}$$

Similarly, inside the crystal there is only one wave satisfying A1.13 and the Schrödinger equation:

$$\left(-\frac{\hbar^2}{2m}\nabla^2 - V_o\right)\psi_{i,\underline{p}} = \left(\frac{\hbar^2}{2m}p^2\right)\psi_{i,\underline{p}}. \qquad \text{A1.16}$$

It is:

$$\psi_{i,\underline{p}} = C\, e^{i(\underline{p}'' - \underline{n}t^{+})\cdot\underline{r}} \qquad \text{A1.17}$$

where

$$t^{+} = \sqrt{\frac{2m}{\hbar^2}(E + V_o) - p''^2} \qquad \text{A1.18}$$

The wavefunction must be smooth and continuous for all x. Thus a smooth joining of A1.15 on to A1.17 at $x = 0$ is a necessary requirement. This also enables us to evaluate B and C. The smooth journey is ensured by:

$$\psi_{o,\underline{p}}\Big|_{x=0} = \psi_{i,\underline{p}}\Big|_{x=0} \qquad \text{Al.19}$$

and
$$\frac{d\psi_{o,\underline{p}}}{dx}\Big|_{x=0} = \frac{d\psi_{i,\underline{p}}}{dx}\Big|_{x=0} \qquad \text{Al.20}$$

Equation Al.19 gives:

$$A + B = C$$

while Al.20 yields:

$$p^{\perp}(A - B) = -t^{\perp}C$$

from which

$$\frac{B}{A} = \frac{p^{\perp} - t^{\perp}}{p^{\perp} + t^{\perp}} \qquad \text{Al.21}$$

and
$$\frac{C}{A} = \frac{2p^{\perp}}{p^{\perp} + t^{\perp}} \qquad \text{Al.22}$$

Hence, the wavefunctions appropriate for the potential step are simply Al.1 and Al.2. Conversely the crystal behaves like a potential step when the specularly transmitted beam does not undergo Bragg reflections.

We note the following:

(a) The wave vectors of the incident ($\underline{p}$), reflected ($\underline{r}$), and transmitted ($\underline{t}$) waves lie in the same plane; see diagram Al.1.

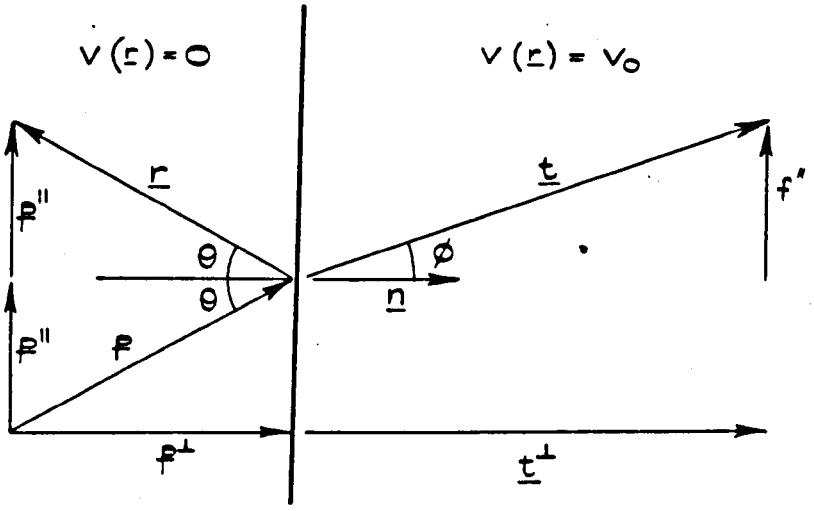

DIAGRAM A 1.1

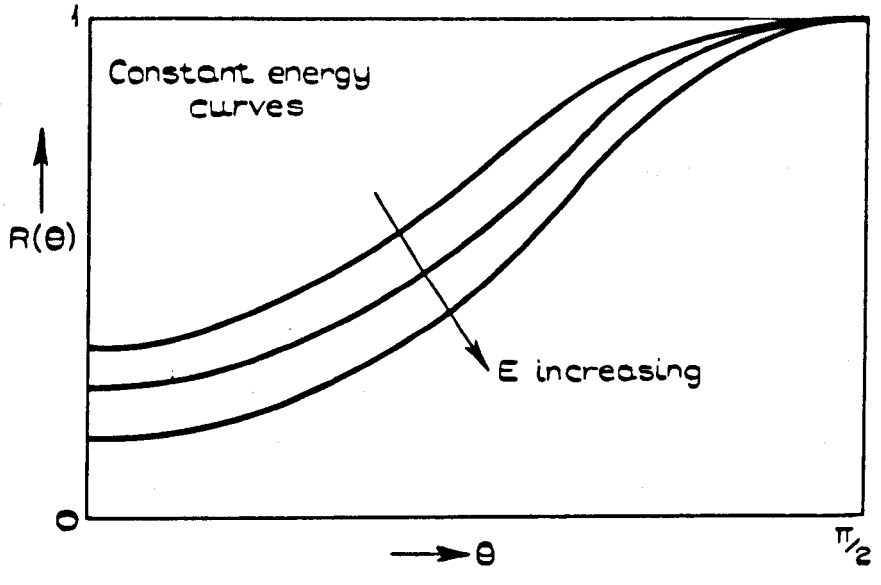

DIAGRAM A 1.2

We also have: $\frac{\sin\theta}{\sin\phi} = \frac{t}{p} = \sqrt{1 + \frac{V_o}{E}}$ which has an analogy with Snell's law.

(b) The reflection coefficient, R, is given by:

$$R = \left|\frac{B}{A}\right|^2 = \left|\frac{p^{\perp} - t^{\perp}}{p^{\perp} + t^{\perp}}\right|^2 = \left|\frac{\frac{p^{\perp}}{p''} - \frac{t^{\perp}}{p''}}{\frac{p^{\perp}}{p''} + \frac{t^{\perp}}{p''}}\right|^2 = \left|\frac{\cot\theta - \cot\phi}{\cot\theta + \cot\phi}\right|^2 .$$

Using the relationship, $\sin\theta = \sin\phi\sqrt{1 + \frac{V_o}{E}}$, we obtain

$$R = \left(\left|\frac{1 - \sqrt{1 + \frac{V_o}{E}\sec^2\theta}}{1 + \sqrt{1 + \frac{V_o}{E}\sec^2\theta}}\right|\right)^2 \qquad \text{A1.23}$$

Using equation A1.23 we find the graphical relationships sketched in diagrams A1.2 and A1.3. These represent the case of incidence on the step from the high potential side. We can make A1.23 appropriate to incidence from the low potential side by reversing the sign on V_o, then:

$$R = \left(\left|\frac{1 - \sqrt{1 - \frac{V_o}{E}\sec^2\theta}}{1 + \sqrt{1 - \frac{V_o}{E}\sec^2\theta}}\right|\right)^2 \qquad \text{A1.24}$$

Equation A1.24 shows that $R = 1$ if $V \geq E$ for all θ. If, however, $E > V$, then $R = 1$ provided $\theta \geq \sec^{-1}\sqrt{\frac{E}{V}}$. The angle, $\theta = \sec^{-1}\sqrt{\frac{E}{V}}$, is the critical angle for total internal reflection. Diagram A1.4 shows a line of constant energy, the value of which is greater than V_o.

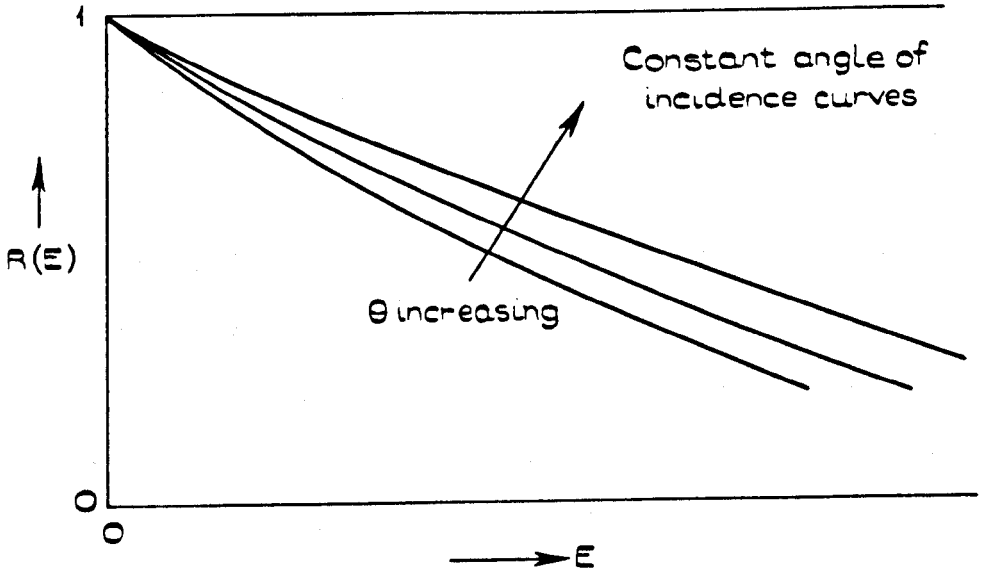

DIAGRAM A 1.3

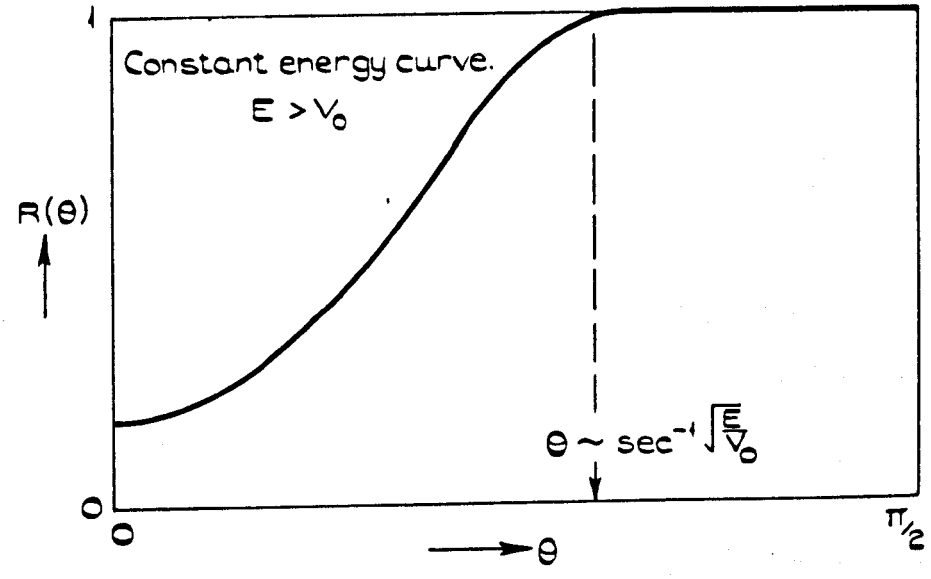

DIAGRAM A 1.4

Appendix II

Wavefunctions and energy bands as a function of the complex wave vector in the NFE approximation

In this Appendix we obtain formal expressions for the wavefunctions and energy bands for the model described at the beginning of Chapter II. We discuss how evanescent and propagating waves enter into the problem and how the energy bands and wavefunctions in the crystal might be calculated. In short, we solve the Schrödinger equation

$$\left(-\frac{\hbar^2}{2m}\nabla^2 + V(\underline{r})\right)\psi = E\psi \qquad \text{A2.1}$$

where

$$V(\underline{r}) = 0, \quad x < \alpha \qquad \text{A2.2}$$

and

$$V(\underline{r}) = \sum_{\underline{g}} e^{i\underline{g}\cdot\underline{r}} V_{\underline{g}}, \quad x > \alpha \qquad \text{A2.3}$$

where $\underline{g}$ are reciprocal lattice vectors of the crystal. As is well known (Kittel (26)) the crystal potential can, whatever its form, be expressed as the series A2.3.

In the region $x < \alpha$, the solutions of A2.1 are of the form $\exp i\,\underline{k}\cdot\underline{r}$, where $\underline{k}$ may be real or imaginary. While in the region $x > \alpha$ the solutions are of the form of Bloch waves, $u_{\underline{k}}(\underline{r}) \exp \underline{i}\cdot\underline{r}$,

where, as we shall see, $\underline{k}$ may be real or complex. All the waves that enter into the problem will have the same energy as the incident wave because we do not consider any inelastic scattering processes. The Hamiltonian in A2.1 commutes with the translation operators $T(\underline{s})$, where $\underline{s}$ are the direct lattice vectors of the crystal surface. Thus the total wavefunction obeys a two dimensional Bloch theorem for the crystal surface. Therefore, all the plane wave type of solutions in $x < \alpha$ and the Bloch wave type of solutions in $x > \alpha$ must have the same value of the reduced component of $\underline{k}$ lying in the crystal surface, which will be determined by the incident wave.

A. Solution of the Schrödinger equation in $x < \alpha$

The solutions of A2.1 in the region $x < \alpha$ are of the form $\exp i \underline{k}.\underline{r}$. We pick out the linear combination of such solutions for the scattering problem. We require an incident wave for which we take A1.8 where A1.9 and A1.10 apply. The other terms will represent flux scattered, by the crystal, into propagating plane waves and waves localised in the crystal surface, where:

$$\underline{k}.\underline{n} < 0 \qquad \text{A2.4}$$

$$k^2 = p^2 = \frac{2mE}{\hbar^2} \qquad \text{A2.5}$$

$$\underline{k}'' = \underline{p}'' + \underline{g}'' \qquad \text{A2.6}$$

Here and elsewhere $\underline{x}''$ means the component of $\underline{x}$ parallel to the crystal surface and $\underline{n}$ is a unit vector directed normally into the crystal surface. E is the incident energy. Then A2.4 ensures that the flux in the scattered waves is not directed towards the surface; A1.5 ensures that the energy of the scattered beams is the same as the incident energy; A1.6 is the result of the two-dimensional Bloch theorem. These equations give:

$$\underline{k} = \left[(\underline{p}'' + \underline{g}'') - \underline{n}\sqrt{\frac{2mE}{\hbar^2} - (\underline{p}'' + \underline{g}'')^2}\right] \qquad \text{A2.7}$$

where $\underline{g}$ is some reciprocal lattice vector of the crystal. Thus the complete acceptable wave function in the region $x < \alpha$, $\psi_{o,\underline{p}}$, is given by:

$$\psi_{o,\underline{p}} = A \exp i\, \underline{p}.\underline{r} + \sum_{\underline{g}''} A(\underline{p}'' + \underline{g}'') \exp i \left[(\underline{p}'' + \underline{g}'') - \underline{n}\sqrt{\frac{2mE}{\hbar^2} - (\underline{p}'' + \underline{g}'')^2}\right].\underline{r} \qquad \text{A2.8}$$

The amplitudes $A(\underline{p}'' + \underline{g}'')$, are determined in chapter II by matching A2.8 on to the solution of A2.1 in $x > \alpha$ at the plane $x = \alpha$.

The summation in A2.8 is over a set of propagating waves, $\frac{2mE}{\hbar^2} > (\underline{p}'' + \underline{g}'')^2$, which will be finite in number, and an infinite set of waves localised near $x = \alpha$, for which $\frac{2mE}{\hbar^2} < (\underline{p}'' + \underline{g}'')^2$. Moreover, at the plane $x = \alpha$, A2.8 represents an infinite two dimensional Fourier series satisfying the two-dimensional Bloch theorem. Thus we have a suitable complete set of functions with which to carry out the matching at $x = \alpha$.

B. Solution of the Schrödinger equation in $x > \alpha$

(i) General discussion In order to match the total wavefunction in the crystal on to the total wavefunction outside at $x = \alpha$, we require all the solutions of A2.1 in $x > \alpha$ which have the same energy and $\underline{k}''_{(\text{reduced})}$ as the incident wave. This is best accomplished by looking at the energy bands and wavefunctions in the infinite crystal, for $\underline{k}''$ fixed (equal to $\underline{p}''$), as a function of the complex variable $\underline{k}_x$. A plane of constant energy, E, will intersect the energy bands, each intersection corresponding to a Bloch wave type of solution:

$$u_{\underline{k}}(\underline{r}) \exp i\, \underline{k}.\underline{r} \qquad \text{A2.9}$$

where $\underline{k}$ may be real or its component $\underline{k}_x$ may be complex such that A2.9 is a propagating wave or localised near $x = \alpha$. In the present problem we are only interested in those waves A2.9 which are transmitted waves, that is, those for which:

$$\nabla_{\underline{k}} E(\underline{k}) > 0 \qquad \text{A2.10}$$

if $\underline{k}$ is real. If $\underline{k}$ is complex A2.9 must be bounded in $x > \alpha$, so that the imaginary part of $\underline{k}_x$, $\underline{k}_x^i$, must satisfy:

$$\underline{n}.\underline{k}_x^i < 0 \qquad \text{A2.11}$$

In this context we now summarise the results of Heine (8) on the band structure as a function of the complex variable $\underline{k}_x$. Diagram A2.1

shows a section of $E(\underline{k}_x)$ for $\underline{k}_x$ of a two-dimensional band structure in the NFE approximation. The value of k'' is about $0.4\ \frac{\pi}{a}$. Along the real $\underline{k}_x$ axis we see the familiar band structure. However, by the inclusion of the imaginary $\underline{k}_x$ axis we see that the band structure for real $\underline{k}_x$ is joined by loops on which the energy is real but $\underline{k}_x$ is complex. Another feature is that lines of real energy leave minima on the real $\underline{k}_x$ band structure and go to $\underline{k}_x^i = \pm\infty$ with decreasing energy. There are an infinite number of such lines intersecting a plane of constant energy.

In general, Heine comes to the following conclusions: two lines of real energy (complex $\underline{k}_x$) leave the real $\underline{k}_x$ axis symmetrically about real $\underline{k}_x$ at every extrema of the band structure along real $\underline{k}_x$, such that the extrema are really saddle points; these lines follow the energy monotonically and may loop back to the real axis after going round one or more branch points, otherwise they go to imaginary $\underline{k}_x = \pm\infty$ with monotonically decreasing energy. For very large negative energies the wavefunction corresponding to one of the complex $\underline{k}_x$ real energy lines is approximately given by

$$\psi = \exp i\ (\underline{k}_m + \underline{g}_m).\underline{r} \qquad \text{A2.12}$$

where $\underline{k}_x$ is complex and $\underline{g}_m$ is some reciprocal lattice vector of the crystal. If we restrict attention to those real energy lines for which A2.11 holds, then each real energy line is characterised by a particular

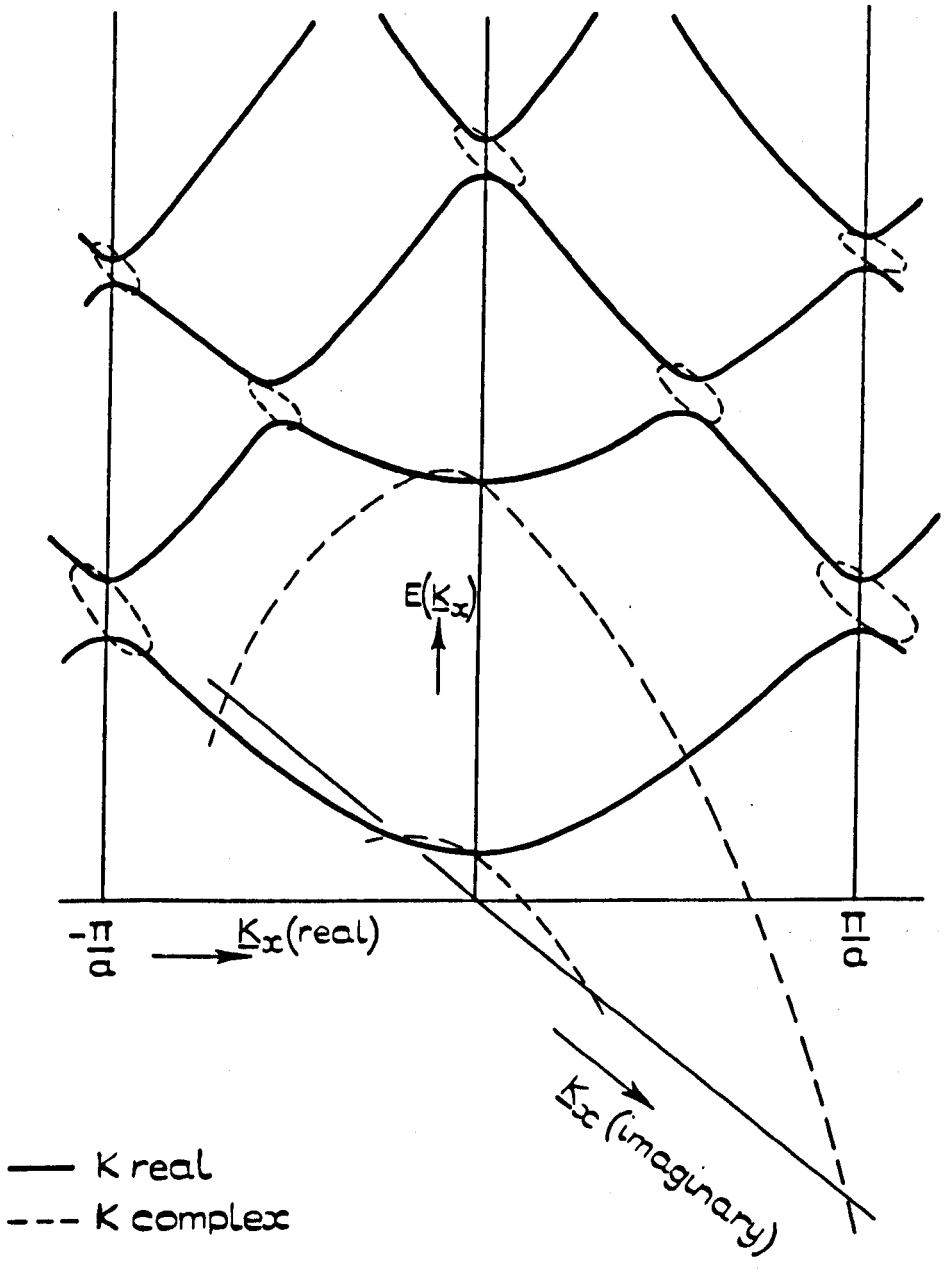

DIAGRAM A 2.1.

$\underline{g}_m$, each $\underline{g}_m$ occurring once only. Thus at a fixed large negative value of the energy we have an infinite number of the waves A2.12 satisfying A2.11 and corresponding to the infinite number of $\underline{g}$. The linear combination of all A2.12 at this energy thus gives a complete set of functions in the form of an infinite two dimensional Fourier series, which satisfies the two dimensional Bloch theorem at $x = \alpha$.

If we follow one of these real energy lines, from large negative values of the energy, in the direction of increasing energy we eventually join the band structure for real $\underline{k}_x$. We can then follow the real $\underline{k}_x$ band structure with increasing energy along a portion satisfying A2.10 until we reach another saddle point. Then we can go around that side of a loop satisfying A2.11 and so on. In this way we obtain a path along which the energy is real and which follows the energy monotonically from $-\infty$ to $+\infty$. By following all such paths the total band structure, $E(\underline{k}_x)$, satisfying A2.10 and A2.11 is covered, and each section is covered once only. We see, therefore, that a plane of constant energy, whatever its value, cuts each of the paths once and we obtain a complete set of functions which are continuously related to A2.12.

We represent the change in a wavefunction from A2.12 to A2.9, as we follow a path from a very low energy to a higher energy, by:

$$e^{i(\underline{k}_m+\underline{g}_m)\cdot\underline{r}} \longrightarrow e^{i(\underline{k}_m+\underline{g}_m)\cdot\underline{r}} u_{\underline{k}+\underline{g}_m}(\underline{r}) = e^{i\underline{k}_m\cdot\underline{r}} \sum_{\underline{g}_n} u^{\underline{g}_m}_{\underline{g}_n} e^{i\underline{g}_n\cdot\underline{r}} \qquad \text{A2.13}$$

The expansion of $u_{\underline{k}+\underline{g}_m}(\underline{r})$ is consistent with reference (26), and $u^{\underline{g}_m}_{\underline{g}_m}$ will be the largest coefficient in the summation (although at certain energies other coefficients may become equal to it).

At a given energy, the total wavefunction in the crystal, $\psi_{i,\underline{p}}$, appropriate to our scattering problem will be a summation over all the paths (each characterised by a particular $\underline{g}_m$) satisfying A2.10 and A2.11, thus:

$$\psi_{i,\underline{p}} = \sum_{\underline{g}''_m} D(\underline{p}'' + \underline{g}''_m)\ e^{i\underline{k}_m \cdot \underline{r}} \sum_{\underline{g}_n} u^{\underline{g}_m}_{\underline{g}_m}\ e^{i\underline{g}_n \cdot \underline{r}} \qquad \text{A2.14}$$

The coefficients $D(\underline{p}'' + \underline{g}''_m)$ are only labelled, for later convenience, by the components of $(\underline{k}_m + \underline{g}_m)$ parallel to the crystal surface. Given $(\underline{p}'' + \underline{g}''_m)$ we can always find $(\underline{k}_m + \underline{g}_m)$ uniquely through the energy. In chapter I the coefficients, $D(\underline{p}'' + \underline{g}''_m)$, are found by matching A2.14 smoothly on to A2.8 at $x = \alpha$.

One other point is worth noting. If we choose the unit cell in reciprocal space in a certain way, then it may contain more than one line for which $\underline{k}''$ is constant. This is best illustrated by an example shown in Diagram A2.2. The diagram shows a two-dimensional hexagonal reciprocal lattice. If we choose the Brillouin zone, ABCDEF, as our unit cell, we see that it contains two lines, XY and Y'Z', for which $\underline{k}''$ is constant, and along which the band structure $E(\underline{k}_x)$ will be of interest. However, if we choose the unit cell to be AGHF, then (YX being equivalent to X'Y') we

have only one line along which $\underline{k}''$ is a constant. Heine (8) has shown how to choose the unit cell in a general way so that it contains only one line of $\underline{k}''$.

(ii) NFE energy bands and wavefunctions In this section we derive the energy bands and wavefunctions in the crystal in the NFE approximation. We start with the free electron bands and then treat the potential, $V(\underline{r})$, as a perturbation.

(a) Free electron bands and wavefunctions

The free electron bands consist of the parabolas

$$\frac{2m}{\hbar^2}(E_n + V_o) = (\underline{k} + \underline{g}_n)^2 \qquad \text{A2.15}$$

where $\underline{k}$ lies within the unit cell in $\underline{k}$-space and $\underline{k}''= \underline{p}''$. V_o is the coefficient of the $\underline{g} = \underline{0}$ term in A2.3. The energy, A2.15, must be real, while $\underline{k}$ can be complex. We substitute:

$$\underline{k} = \underline{k}_r + i\,\underline{k}_i \qquad \text{A2.16}$$

into A2.15:

$$\frac{2m}{\hbar^2}(E_n + V_o)^2 = (\underline{K}_r + \underline{g}_n)^2 - k_i^2 + 2i\,\underline{k}_i.(\underline{k}_r + \underline{g}_n)^2, \qquad \text{A2.17}$$

so that we require:

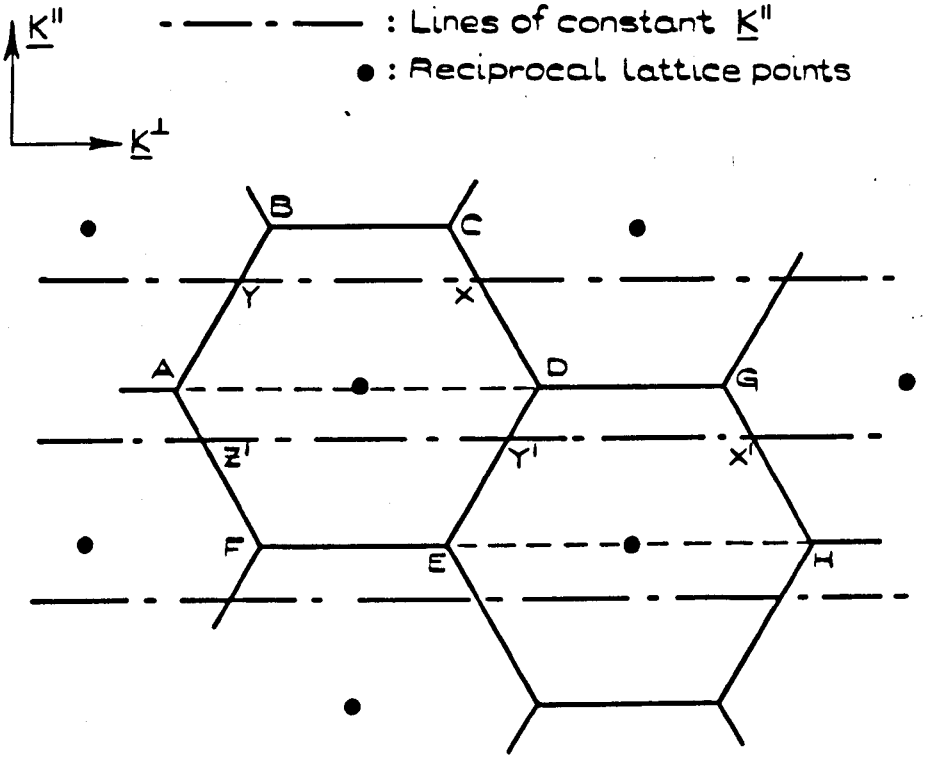

DIAGRAM A2.2

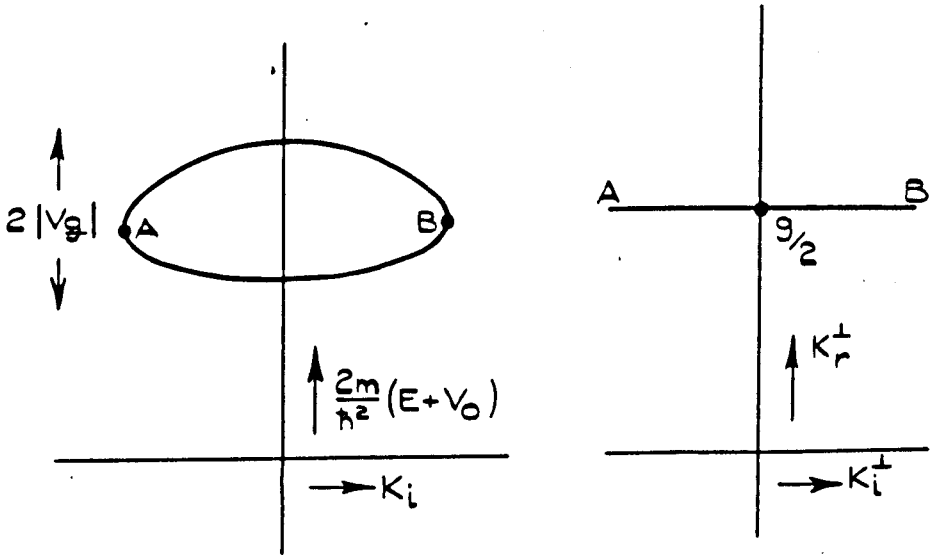

DIAGRAM A2.3

$$\underline{k}_i \cdot (\underline{k}_i + \underline{g}_n) = k_i (\underline{k}_r + \underline{g}_n)^{\perp} = 0 \qquad \text{A2.18}$$

for A2.15 to be real. The first equality in A2.18 comes about because $\underline{k}_i$ must lie along the $\underline{k}_x$ direction in order that the wavefunction be bounded in $x > a$. Hence the energy associated with the free electron bands is real for:

$$k_i = 0, \text{ then, } \frac{2m}{\hbar^2}(E_n + V_o) = (\underline{k}_i + \underline{g}_n)''^2 + (\underline{k}_i + \underline{g}_n)^{\perp 2} \qquad \text{A2.19}$$

$$(\underline{k}_i + \underline{g}_n)^{\perp} = 0, \text{ then, } \frac{2m}{\hbar^2}(E_n + V_o) = (\underline{k}_i + \underline{g}_n)''^2 - k_i^2 \qquad \text{A2.20}$$

Equations A2.19 and A2.20 are parabolic functions of $\underline{k}^{\perp}$; A2.20 join on to A2.19 on the $\underline{k}_r$ axis whenever A2.19 have minima such that

$$\frac{2m}{\hbar^2}(E + V_o) = (\underline{k}_i + \underline{g})''^2; \quad k_i = 0; \quad k_r^{\perp} = -g_n^{\perp} \qquad \text{A2.21}$$

are saddle points. Thus the free electron bands consist of paths, which we have described in the general case, along which the energy changes monotonically from $-\infty$ to $+\infty$. The free electron wavefunctions are:

$$\psi = \exp i\, \underline{k} \cdot \underline{r} \qquad \text{A2.22}$$

where, for A2.19

$$\underline{k} = (\underline{k}_r + \underline{g}_n)'' + (\underline{k}_r + \underline{g}_n)^{\perp} \qquad \text{A2.23}$$

while for A2.20

$$\underline{k} = (\underline{k}_r + \underline{g}_n)'' \pm i\, \underline{k}_i \,, \qquad \text{A2.24}$$

at the saddle points A2.21, the waves A2.22, are surface waves for which

$$\underline{k} = (\underline{k}_r + \underline{g}_n)'' \qquad \text{A2.25}$$

We see, then, that the free electron bands are consistent with the general picture already outlined except that we have no loops along which the energy is real but $\underline{k}$ complex. We will see that the most important effect that $V(\underline{r})$ produces, when it is treated as a perturbation, is the creation of such loops.

We note one other point. If we impose the restrictions A2.10 and A2.11 on our free electron bands A2.19 and A2.20, we remove exactly half of them. Then each intersection of the real energy bands with a plane of constant energy is characterised by a particular $\underline{g}_n$. Each $\underline{g}_n$ occurs once only. Thus we have a singly infinite two-dimensional set of matching functions at $x = a$. The additional free electron waves acquired by relaxing A2.10 and A2.11, are just those extra waves we would require in our scattering problem if the crystal were of finite width.

(b) $V(\underline{r})$ as a perturbation on the free electron bands and wave functions

We now treat the crystal potential as a perturbation. Before doing so, we note that the wavefunctions so obtained are continuously

related to the free-electron functions as we gradually "turn on" $V(\underline{r})$. It follows that we will always have a complete set of matching functions.

As is well known, the effect of the crystal potential is to turn the plane-wave solutions, A2.22, into Bloch waves, A2.13. We note that in A2.13, $\underline{k}_m$ in general can be complex. We now proceed to evaluate the energy bands and wavefunctions to first order in the perturbation. It is not possible to draw immediately on the standard results of perturbation theory because here we are concerned with plane wave expansions in which $\underline{k}$ can be complex. However we can start with the first order non-degenerate perturbation equation of Schiff (23), which in our notation is:

$$\sum_n u^{(1)}_{\underline{k}+\underline{g}_m}(\underline{g}_n)\, H_o e^{i(\underline{k}+\underline{g}_n)\cdot\underline{r}} + H^1 e^{i(\underline{k}+\underline{g}_n)\cdot\underline{r}}$$

$$= E_{\underline{g}_m} \sum_n u^{(1)}_{\underline{k}+\underline{g}_m}(\underline{g}_n)\, e^{i(\underline{k}+\underline{g}_n)\cdot\underline{r}} + W_1 e^{i(\underline{k}+\underline{g}_m)\cdot\underline{r}} \qquad \text{A2.26}$$

where $H_o \equiv \left(-\frac{\hbar^2}{2m}\nabla^2 - V_o\right)$

$$H^1 \equiv \sum_{\underline{g}\neq 0} V_{\underline{g}} \exp i\, \underline{g}\cdot\underline{r}$$

Unperturbed wavefunction: $e^{i(\underline{k}+\underline{g}_m)\cdot\underline{r}}$ ⟶ perturbed: $\sum_n u^{(1)}_{\underline{k}+\underline{g}_m}(\underline{g}_n)\, e^{i(\underline{k}+\underline{g}_n)\cdot\underline{r}}$

where we assume $u_{\underline{k}+\underline{g}_m}(\underline{g}_m) \gg u_{\underline{k}+\underline{g}_m}(\underline{g}_n)$ A2.27

also we have $E_{\underline{g}_m} = \frac{\hbar^2}{2m}(\underline{k}+\underline{g}_m)^2 - V_o$

The first order correction to the energy is W_1. We immediately resolve the difficulty associated with the non-orthogonal nature of the exp i $(\underline{k} + \underline{g}_n).\underline{r}$ in A2.26 by dividing through by exp i $\underline{k}.\underline{r}$. We can then multiply through by $(\exp i\ \underline{g}_\ell.\underline{r})^*$ and integrate over all $\underline{r}^3$ to obtain

$$u^{(1)}_{\underline{k}+\underline{g}_n}(\underline{g}_\ell)\ [E_{\underline{g}_m} - E_{\underline{g}_\ell}] + W_1 = \int_{\underline{r}^3} e^{i\underline{g}_m.\underline{r}}\, H^1 e^{-i\underline{g}_\ell.\underline{r}}\, d^3\underline{r} \qquad \text{A2.28}$$

Using H^1 from A2.27 the R.H.S. of A2.28 becomes $V_{\underline{g}_\ell - \underline{g}_m}$. Then, taking $\ell = m$:

$$W_1 = 0 \qquad \text{A2.29}$$

while for $\ell \neq m$:

$$u^{(1)}_{\underline{k}+\underline{g}_m}(\underline{g}_\ell) = \frac{V_{\underline{g}_\ell - \underline{g}_m}}{E_{\underline{g}_m} - E_{\underline{g}_\ell}} \qquad \text{A2.30}$$

Where non-degenerate perturbation theory holds in our free electron band structure, equation A2.29 shows that the free electron bands are, to first order not changed as $V(\underline{r})$ is switched on.

In those regions of the free electron band structure where:

$$\left|E_{\underline{g}_m} - E_{\underline{g}_\ell}\right| \leq \left|V_{(\underline{g}_\ell - \underline{g}_m)}\right| \qquad \text{A2.31}$$

we see that the initial assumption that $u^{(1)}_{\underline{k}+\underline{g}_m}(\underline{g}_\ell)$ be small compared with $u_{\underline{k}+\underline{g}_m}$ is invalid and the perturbation theory developed so far is not adequate. If we write $\underline{k} = \underline{k}_r + i\,\underline{k}_i$, the condition A2.31 becomes:

$$\left|(\underline{k}_r + \underline{g}_i)^2 - (\underline{k}_r + \underline{g}_m)^2\right| \lesssim \left|V_{(\underline{g}_i - \underline{g}_m)}\right| \qquad \text{A2.32}$$

and

$$\left|2k_i(\underline{g}_\ell - \underline{g}_m)^{\perp}\right| \lesssim \left|V_{\underline{g}_\ell - \underline{g}_m}\right| \qquad \text{A2.33}$$

Equations A2.32 and A2.33 have to be satisfied simultaneously if we are to use degenerate perturbation theory. Equation A2.32 corresponds to the plane-wave, with wave-vector $(\underline{k} + \underline{g}_\ell)$, lying near a Bragg condition associated with the reciprocal lattice vector $(\underline{g}_\ell - \underline{g}_m)$. Equation A2.33 shows that the use of degenerate perturbation theory will be limited to:

$$\left|k_i\right| \lesssim \left|\frac{V_{\underline{g}_\ell - \underline{g}_m}}{2(\underline{g}_\ell - \underline{g}_m)^{\perp}}\right| \qquad \text{A2.34}$$

The case that $(\underline{g}_\ell - \underline{g}_m)^{\perp} = 0$ corresponds to $\underline{k}'' = \frac{\underline{g}_\ell - \underline{g}_m}{2}$, that is $\underline{k}^{\perp}$ runs along a symmetry line in the Brillouin zone for our present purposes we restrict ourselves to a general $\underline{k}''$, how to deal with all cases will become apparent.

So far we have seen, to first order in the perturbation, that the free electron bands A2.19 and A2.20, are unaltered as we switch on

$V(\underline{r})$ except near a Bragg condition and then the bands are modified for $|\underline{k}_i|$ lying within the limit A2.34. Incidentally, A2.34 also shows that the only lines of real energy and large $\underline{k}_i$ are, to first order approximation, those obtained for the free electron bands, A2.20.

Suppose that at a particular energy and wave-vector, n of the free electron bands are degenerate, or quasi degenerate in the sense that

$$|u_{\underline{k}+\underline{g}_m}(\underline{g}_\ell)| > \beta \qquad \text{A2.35}$$

where the $u_{\underline{k}+\underline{g}_m}(\underline{g}_\ell)$ are determined by A2.30 and β is an arbitrarily small real number. We can then approximate the perturbed wavefunctions, $\psi_{\underline{k}}(\underline{r})$, by:

$$\psi_{\underline{k}}(\underline{r}) = e^{i\underline{k}\cdot\underline{r}} \sum_{\underline{g}_n} u_{\underline{k}}(\underline{g}_n)\, e^{i\underline{g}_n\cdot\underline{r}} \qquad \text{A2.36}$$

where only those $(\exp i(\underline{k}+\underline{g}_n)\cdot\underline{r})$ terms, whose coefficients, $u_{\underline{k}+\underline{g}_n}(\underline{g}_\ell)$, in the non-degenerate perturbation theory satisfy A2.35, are included. That is, A2.36 contains n terms. We substitute A2.36 into the Schrödinger equation:

$$\left[-\frac{\hbar^2}{2m}\nabla^2 + \sum_{\underline{g}} V_{\underline{g}}\, e^{i\underline{g}\cdot\underline{r}}\right] e^{i\underline{k}\cdot\underline{r}} \sum_n u_{\underline{k}}(\underline{g}_n) e^{i\underline{g}_n\cdot\underline{r}} = E\, e^{i\underline{k}\cdot\underline{r}} \sum_n u_k(\underline{g}_n) e^{i\underline{g}_n\cdot\underline{r}} \qquad \text{A2.37}$$

where E is the perturbed energy. Now:

$$\left(-\frac{\hbar^2}{2m}\nabla^2 - V_o\right) e^{i(\underline{k}+\underline{g}_n)\cdot\underline{r}} = \left(\frac{\hbar^2}{2m}(\underline{k}+\underline{g}_n)^2 - V_o\right) e^{i(\underline{k}+\underline{g}_n)\cdot\underline{r}} = E_{\underline{g}_n}\, e^{i(\underline{k}+\underline{g}_n)\cdot\underline{r}}$$

so that A2.37 becomes, after dividing through by exp $i\underline{k}.\underline{r}$:

$$\sum_n (E_{\underline{g}_n} - E)\, u_{\underline{k}}(\underline{g}_n) e^{i\underline{g}_n \cdot \underline{r}} + \sum_{\underline{g} \neq 0} V_{\underline{g}}\, e^{i\underline{g}\cdot\underline{r}} \sum_n u_{\underline{k}}(\underline{g}_n)\, e^{i\underline{g}_n \cdot \underline{r}} = 0 \qquad \text{A2.38}$$

Now we multiply through by $(\exp i\, \underline{g}_\ell . \underline{r})^*$ and integrate over all $\underline{r}$:

$$(E_{\underline{g}} - E)\, u_{\underline{k}}(\underline{g}) + \sum_{n \neq \ell} u_{\underline{k}}(\underline{g}_n)\, V_{\underline{g} - \underline{g}_n} = 0 \qquad \text{A2.39}$$

Equation A2.39 represents a set of n-coupled equations, in matrix form:

$$\begin{vmatrix} (E_{\underline{g}_1} - E), & V_{\underline{g}_1 - \underline{g}_2}, & \cdots\cdots, & V_{\underline{g}_1 - \underline{g}_n} \\ V_{\underline{g}_2 - \underline{g}_1}, & (E_{\underline{g}_2} - E) & \cdots\cdots, & \\ \cdot & \cdot & \cdot & \cdot \\ \cdot & \cdot & \cdot & V_{\underline{g}_{n-1} - \underline{g}_n} \\ V_{\underline{g}_n - \underline{g}_1}, & \cdots\cdots\cdots\cdots, & V_{\underline{g}_n - \underline{g}_{n-1}}, & (E_{\underline{g}_n} - E) \end{vmatrix} \begin{vmatrix} u_{\underline{k}}(\underline{g}_1) \\ u_{\underline{k}}(\underline{g}_2) \\ \\ \\ u_{\underline{k}}(\underline{g}_n) \end{vmatrix} = 0 \qquad \text{A2.40}$$

We write A2.40 as:

$$|A|\ |u| = 0 \qquad \text{A2.41}$$

The necessary condition that A2.41 has a non-trivial solution for the $u_{\underline{k}}(\underline{g}_n)$ is that:

$$\det |A| = 0 \qquad \text{A2.42}$$

If we now fix the energy, E, in A2.42, and vary $\underline{k}$ (which may be complex), we will determine the n zeros A2.42. By repeating the procedure with

different values of E we then generate the band structure in the region of the n-fold quasi-degeneracy.

We can now determine the wave-functions, i.e. the $u_{\underline{k}}(g_n)$ for a given E and $\underline{k}$ satisfying A2.42. Equation A2.39 shows that any of the $u_{\underline{k}}(g_n)$ can be expressed as a linear combination of the others. Thus there are only (n-1) linearly independent solutions of the n equations. We divide A2.39 by any of the $u_{\underline{k}}(g_n)$, say $u_k(g_k)$ and denote the (n-1) solutions by:

$$\frac{u_{\underline{k}}(g_1)}{u_{\underline{k}}(g_k)}, \frac{u_{\underline{k}}(g_2)}{u_{\underline{k}}(g_k)}, \ldots\ldots \frac{u_{\underline{k}}(g_{k-1})}{u_{\underline{k}}(g_k)}, \frac{u_{\underline{k}}(g_{k+1})}{u_{\underline{k}}(g_k)}, \ldots\ldots \frac{u_{\underline{k}}(g_n)}{u_{\underline{k}}(g_k)} \qquad \text{A2.43}$$

A necessary condition that a square matrix be singular is that its rows be linearly dependent; thus A2.42 shows that we can reduce the number of the equations A2.39, we remove the k^{th} equation say, and obtain (n-1) equations in the (n-1) unknowns A2.43:

$$|A|_{kk} \; |u'_r| = - |a'_{mk}| \qquad \text{A2.44}$$

The quantity $|A|_{kk}$ denotes the cofactor of the element in the k^{th} row and k^{th} column of $|A|$; $|u'_r|$ is the column matrix with elements A2.43; $|a'_{mk}|$ denotes the k^{th} column of $|A|$ and the k^{th} row missing. Then we have:

$$|u'_r| = - |A|^{-1}_{kk} \; |a'_{mk}| = - \left| \frac{||A|_{kk}|_{mr}}{\det A_{kk}} \right|^T |a'_{mk}| \qquad \text{A2.45}$$

where $||A|_{kk}|_{mr}$ means the cofactor of the element in the m^{th} row and r^{th} column (of $|A|$) in $|A|_{kk}$, and T denotes the transpose of a matrix. Thus:

$$|u'_r| = - \left| \sum_m \frac{||A|_{kk}|_{mr} a_{mk}}{\det |A|_{kk}} \right| \qquad \text{A2.46}$$

but, $$\left|\left|A\right|_{kk}\right|_{mr} = -\left|\left|A\right|_{kr}\right|_{mk}$$

and $$\det\left|A\right|_{kr} = \sum_{m}\left|\left|A\right|_{kr}\right|_{mk} a_{mk}$$

so that A2.46 becomes:

$$\left|u'_r\right| = \left|\frac{\det\left|A\right|_{kr}}{\det\left|A\right|_{kk}}\right| . \qquad \text{A2.47}$$

That is:

$$\frac{u_{\underline{k}}(g_r)}{u_{\underline{k}}(g_k)} = \frac{\det\left|A\right|_{kr}}{\det\left|A\right|_{kk}} \qquad \text{A2.48}$$

Thus for a given E and $\underline{k}$ satisfying A2.42 we can determine all the $u_{\underline{k}}(g_r)$ in terms of $u_{\underline{k}}(g_k)$ using A2.48. It may happen that, for $\underline{k}$ at some symmetry points, $u_{\underline{k}}(g_k)$ will be zero, in which case we just determine the $u_{\underline{k}}(g_r)$ in terms of $u_{\underline{k}}(g_s)$ say:

$$\frac{u_{\underline{k}}(g_r)}{u_{\underline{k}}(g_s)} = \frac{\det\left|A\right|_{sr}}{\det\left|A\right|_{ss}} .$$

Using A2.48 obviously leaves $u_{\underline{k}}(g_k)$ undetermined. We could determine this coefficient by normalising the wavefunction but this is an unnecessary procedure in the scattering problem. Instead we simply include the $u_{\underline{k}}(g_k)$ into the coefficient $D(\underline{p}''+\underline{g}''_m)$ of equation A2.14.

We again make the point that having determined the wavefunctions in the manner described and so having obtained the series A2.14 at a particular energy, we reject those wavefunctions not satisfying A2.10 and A2.11.

One other point is worth noting. By solving the perturbation problem only at points of degeneracy in the free electron bands, we cannot hope that the bands obtained will join up smoothly between points of degeneracy. We could overcome this by including in A2.40 all the plane waves at a given $\underline{k}$ over the whole energy range of interest. We will still encounter discontinuities, however, because, as we move along a particular band, the condition A2.35 will "switch in or out" certain plane wave components of the wavefunctions. In the next appendix we show how we can join up the bands between points of degeneracy by means of expanding about them in a power series in $\underline{k}$ which has arbitrary coefficients determined by requiring that the bands join smoothly and are coincident with $\underline{k}.\underline{p}$ perturbation theory near the points of degeneracy.

(c) An example of the procedure outlined in B(ii)(b)

We consider the two free electron bands

$$\frac{2m}{\hbar^2}(E_{\underline{o}}+V_o) = \underline{k}^2 \qquad \text{A2.49}$$

and

$$\frac{2m}{\hbar^2}(E_{\underline{g}}+V_o) = (\underline{k}+\underline{g})^2, \qquad \text{A2.50}$$

where for simplicity we take $\underline{g}$ to be parallel to $\underline{k}_x$. Then we require to find the energy bands and wavefunctions at the energy for which

$$E_{\underline{o}} = E_{\underline{g}} \qquad \text{A2.51}$$

and we imagine that, within the criterion A2.35, no other bands are quasi-degenerate with $E_{\underline{o}}$ and $E_{\underline{g}}$ at the energy for which A2.51 holds. In this

situation the set of equations A2.40 become:

$$\begin{vmatrix} (E_{\underline{o}}-E), & V_{\underline{g}} \\ V_{-\underline{g}}, & (E_{\underline{g}}-E) \end{vmatrix} \begin{vmatrix} u_{\underline{k}}(\underline{o}) \\ u_{\underline{k}}(\underline{g}) \end{vmatrix} = 0 \qquad \text{A2.52}$$

Thus $$|A| = \begin{vmatrix} (E_{o}-E), & V_{\underline{g}} \\ V_{-\underline{g}}, & (E_{\underline{g}}-E) \end{vmatrix} \qquad \text{A2.53}$$

Equation A2.42 thus gives for A2.53:

$$E = \left(\frac{E_{\underline{o}}+E_{\underline{g}}}{2}\right) \pm \sqrt{\left(\frac{E_{\underline{o}}-E_{\underline{g}}}{2}\right)^2 + V_{\underline{g}}^2} \qquad \text{A2.54}$$

where we have taken account of

$$V_{\underline{g}} = V_{-\underline{g}}.$$

Now, $$E_{\underline{o}} = \frac{\hbar^2}{2m}\underline{k}^2 - V_o$$

and $$E_{\underline{g}} = \frac{\hbar^2}{2m}(\underline{k}+\underline{g})^2 - V_o$$

so that A2.54 becomes:

$$\frac{2m}{\hbar^2}(E+V_o) = (k^2 - \underline{k}.\underline{g} + \frac{g^2}{2}) \pm \sqrt{\left(\underline{k}.\underline{g} - \frac{g^2}{2}\right)^2 + V_{\underline{g}}^2} \qquad \text{A2.55}$$

If we now write:

$$\underline{k} = \underline{k}_r + i\,\underline{k}_i, \qquad \text{A2.56}$$

A2.55 becomes

$$\frac{2m}{\hbar^2}(E+V_o) = \left(k_r^2 - k_i^2 - \underline{k}_r\cdot\underline{g} + \frac{g^2}{2}\right) + i\,\underline{k}_i\cdot(2\underline{k}_r - \underline{g})$$

$$\pm\left(\left\{\underline{k}_r\cdot\underline{g} - \frac{g^2}{2}\right\} + i\,\underline{k}_i\cdot\underline{g}\right)^2 + \ldots \qquad \text{A2.57}$$

Along the $\underline{k}_r$ axis, $\underline{k}_i = o$, and A2.57 is real, giving us the familiar splitting of the free electron bands. A band gap of $2|V_g|$ results at $\underline{k}_r = \frac{g}{2}$; if we keep $\underline{k}_r$ constant at this value and allow $\underline{k}_i$ to be finite we have:

$$\frac{2m}{\hbar^2}(E+V_o) = \left(k''^2 + \frac{g^2}{2} - k_i^2\right) \pm\sqrt{(V_g^2 - \{k_i g\}^2)} \qquad \text{A2.58}$$

where account has been taken of $\underline{g}$ and $\underline{k}_i$ being parallel to $\underline{k}_x$. We see that A2.58 is real provided

$$k_i \leq \left|\frac{V_g}{g}\right| \qquad \text{A2.59}$$

As k_i approaches the limit A2.59, we see that the two roots A2.58 approach the same value. In fact if we plot A2.58 in the $\frac{2m}{\hbar^2}(E+V_o)/k_i$ plane we find a loop along which the energy is real.

This is sketched in diagram A2.3. The points A and B indicate where the bands A2.58 take on the same energy. By writing:

$$\sqrt{V_g^2 - (k_i g)^2} = \sqrt{(V_g + k_i g)(V_g - k_i g)}$$

we see immediately that A and B are branch points. Moreover the energy is real at these points. The loop of real energy joins the band structure on the $\underline{k}_r$ axis where extrema occur along this axis. Thus the points

$$\underline{k}_r^{\pm} = \frac{\underline{g}}{2} \; ; \quad \frac{2m}{\hbar^2}(E+V_{\underline{o}}) = k''^2 + \left(\frac{\underline{g}}{2}\right)^2 \pm V_{\underline{g}}$$

are saddle points.

The wavefunctions associated with the bands A2.54 are found using A2.48. In this situation

$$\frac{u_{\underline{k}}(\underline{o})}{u_{\underline{k}}(\underline{g})} = \frac{\det |A|_{\underline{g},\underline{o}}}{\det |A|_{\underline{g},\underline{g}}} = \frac{V_{-\underline{g}}}{-(E_{\underline{g}}-E)} \qquad \text{A2.60}$$

Substituting A2.54 into A2.60 we obtain

$$\frac{u_{\underline{k}}(\underline{o})}{u_{\underline{k}}(\underline{g})} = \frac{V_{\underline{g}}}{\frac{E_{\underline{o}}-E_{\underline{g}}}{2} \pm \sqrt{\left(\frac{E_{\underline{o}}-E_{\underline{g}}}{2}\right)^2 + V_{\underline{g}}^2}} \qquad \text{A2.61}$$

and thus, to within a normalisation constant, we have found the wavefunctions associated with the bands A2.54.

Appendix III

A method for obtaining continuous and smooth energy bands and wavefunctions in the zero order energy perturbation approximation

One of the difficulties of calculating the energy bands and wavefunctions to zero order in the energy perturbation, as described in Appendix II, is that they will contain discontinuities as we pass along a particular band joining two points of what would be degeneracies in the free electron bands. In this appendix we suggest a method of joining the energy bands and wavefunctions smoothly between two such points.

From Chapter II we expect the structure of the elastically backscattered intensities in LEED to be sensitively dependent upon the energy band gaps, which come from points of degeneracy in the free electron bands, and not particularly sensitive to $E(\underline{k})$ linking up such points. As far as LEED is concerned we might then only accurately determine $E(\underline{k})$ and the wavefunctions around such band gaps and then require that they vary smoothly and continuously with $\underline{k}$ between such points.

We proceed as follows: the perturbation matrices linking the degenerate states at all points of degeneracy, $\underline{k}_n$ say, in the free electron bands, are diagonalised. We then expand the energy and wavefunctions as a power series in $\underline{k}$ about such points; for the m^{th} band at $\underline{k}_n$ we have:

$$E_m(\underline{k}_n+\delta\underline{k}_n) = E_m(\underline{k}_n) + \delta\underline{k}_i.\underline{G}_m^{m,\underline{k}_n} + \delta k_n^2 \; E_m^{\underline{k}_n} + \ldots. \qquad \text{A3.1}$$

$$\psi_m(\underline{k}_n+\delta\underline{k}_n) = e^{i\delta\underline{k}_n\cdot\underline{r}}\left[\psi_m(\underline{k}_n) + \delta\underline{k}_n\cdot\sum_{\ell\neq m}\underline{G}_\ell^{m,\underline{k}_n}\psi_\ell(\underline{k}_n) + \delta k_n^2\psi_m^{\underline{k}_n} + \ldots\right] \quad \text{A3.2}$$

It will become apparent why the coefficients in A3.1 and A3.2 have been written in this manner. The coefficients of $\delta\underline{k}_n$ are chosen so that A3.1 and A3.2 are coincident with $\underline{k}\cdot\underline{p}$ perturbation theory near $\underline{k}_n$. We will require that $E_m(\underline{k}_n+\delta\underline{k}_n)$ and $\psi_m(\underline{k}_n+\delta\underline{k}_n)$ go smoothly over to $E_m(\underline{k}_\ell+\delta\underline{k}_\ell)$ and $\psi_m(\underline{k}_\ell+\delta\underline{k}_\ell)$ at $\left(\frac{\underline{k}_\ell+\underline{k}_m}{2}\right)$, where $\underline{k}_\ell$ is the next point of degeneracy on the m^{th} band for free electron bands. We can use the free electron bands and, after carrying out the energy perturbation at $\underline{k}_n$ and $\underline{k}_\ell$, the compatability relations, to determine which is the m^{th} band at $\underline{k}_\ell$ given which is the m^{th} band at $\underline{k}_n$. If we terminate A3.1 and A3.2 after the terms in δk_n^2 we will retain enough flexibility in $E_m(\underline{k})$ and the wavefunctions to ensure a smooth joining at $\left(\frac{\underline{k}_\ell+\underline{k}_n}{2}\right)$, which will determine $E_m^{\underline{k}_n}$ and $\psi_m^{\underline{k}_n}$, while avoiding the possibility of introducing extrema apart from those already at $\underline{k}_n$ and $\underline{k}_\ell$.

We now establish, using $\underline{k}\cdot\underline{p}$ perturbation theory, the coefficients of $\delta\underline{k}_n$ in A3.1 and A3.2. If we write $\psi_m(\underline{k})$ in the Bloch function form:

$$\psi_m(\underline{k}) = e^{i\underline{k}\cdot\underline{r}}\, u_m(\underline{k}) \quad \text{A3.3}$$

we can easily see from the Schrödinger equation

$$\left[-\frac{\hbar^2}{2m}\nabla^2 + V(\underline{r})\right]\psi_m(\underline{k}) = E_m(\underline{k})\,\psi_m(\underline{k}) \quad \text{A3.4}$$

that $u_m(\underline{k})$ satisfies the equation:

$$\left[-\frac{\hbar^2}{2m}\nabla^2 - \frac{i\hbar^2}{m}\underline{k}\cdot\nabla + V(\underline{r}) + \frac{\hbar^2k^2}{2m}\right]u_m(\underline{k}) = E_m(\underline{k})\,u_m(\underline{k}). \quad \text{A3.5}$$

If now we write

$$\underline{k} = \underline{k}_n + \delta\underline{k}_n \qquad \text{A3.6}$$

in A3.5, we obtain

$$(P_o+P)\, u_m(\underline{k}_n+\delta\underline{k}_n) = E_m(\underline{k}_n+\delta\underline{k}_n)\, u_m(\underline{k}_n+\delta\underline{k}_n) \qquad \text{A3.7}$$

where

$$P_o = \left[-\frac{\hbar^2}{2m}\nabla^2 - \frac{i\hbar^2}{m}\underline{k}_n\cdot\underline{\nabla} + V(\underline{r}) + \frac{\hbar^2}{2m}\,k_n^2\right] \qquad \text{A3.8}$$

and

$$P = \left[-\frac{i\hbar^2}{m}\,\underline{\nabla}\cdot\delta\underline{k}_n + \frac{\hbar^2}{m}\,\underline{k}_n\cdot\,\delta\underline{k}_n + \frac{\hbar^2}{2m}\,\delta k_n{}^2\right] \qquad \text{A3.9}$$

Now we know the solutions of:

$$P_o\, u_m(\underline{k}_n) = E_m(\underline{k}_n\, u_m(\underline{k}_n) \qquad \text{A3.10}$$

by diagonalising the energy perturbation matrix at $\underline{k}_n$. If we now take $\delta\underline{k}_n$ to be small, we can treat P as a perturbation in A3.7. The first order correction to the energy at $(\underline{k}_n+\delta\underline{k}_n)$ which we must add to $E(\underline{k}_n)$ is P_{mm}:

$$P_{mm} = \int u_m^*(\underline{k}_n)\, P\, u_m(\underline{k}_n)\,d^3\underline{r} \qquad \text{A3.11}$$

Using A3.9 and A3.3, A3.11 becomes:

$$P_{mm} = \frac{\hbar^2}{2m}\,\delta k_n^2 + \frac{\hbar}{m}\,\delta\underline{k}_n\cdot\int \psi_m^*(\underline{k}_n)(-i\hbar\underline{\nabla})\,\psi_m(\underline{k}_n)\,d^3\underline{r} \qquad \text{A3.12}$$

The second term in A3.12 is linear in $\delta\underline{k}_n$ and it is easily shown that higher order $\underline{k}.\underline{p}$ perturbation corrections do not contain terms linear in

$\underline{k}_n$. We thus have obtained the coefficient $\underline{G}_m^{m,\underline{k}_n}$ of equation A3.1:

$$\underline{G}_m^{m,\underline{k}_n} = \frac{\hbar}{m} \int \psi_m^*(\underline{k}_n)(-i\hbar\underline{\nabla})\ \psi_m(\underline{k}_n)d^3\underline{r} \qquad \text{A3.13}$$

Similarly the first order correction to the wavefunction, $e^{i\delta\underline{k}_n\cdot\underline{r}}\psi_m(\underline{k}_n)$, at $(\underline{k}_n+\delta\underline{k}_n)$ is

$$\sum_{\ell\neq m} \frac{P_{\ell m}\ \psi_\ell(\underline{k}_n)}{E_m(\underline{k}_n)-E_\ell(\underline{k}_n)}\ e^{i\delta\underline{k}_m\cdot\underline{r}} \qquad \text{A3.14}$$

where

$$P_{\ell m} = \int u^*(\underline{k}_n)Pu_m(\underline{k}_n)d^3\underline{r} \qquad \text{A3.15}$$

again, using A3.3 and A3.9, A3.15 becomes

$$P_{\ell m} = \frac{\hbar}{m}\,\delta\underline{k}_n\cdot \int \psi_\ell^*(\underline{k}_n)(-i\hbar\underline{\nabla})\psi_m(\underline{k}_n)d^3\underline{r} \qquad \text{A3.16}$$

which is linear in $\delta\underline{k}_n$. No other terms linear in $\delta\underline{k}_n$ come from higher order $\underline{k}\cdot\underline{p}$ perturbation corrections. Thus we have obtained the coefficients $\underline{G}_\ell^{m,\underline{k}_n}$ of equation A3.2:

$$\underline{G}_\ell^{m,\underline{k}_n} = \frac{\hbar}{m}\ \frac{\int\psi_\ell^*(\underline{k}_n)(-i\hbar\underline{\nabla})\psi_m(\underline{k}_n)d^3\underline{r}}{E_m(\underline{k}_n) - E_\ell(\underline{k}_\ell)} \qquad \text{A3.17}$$

We now evaluate $E_m^{\underline{k}_n}$ and $\psi_m^{\underline{k}_n}$ of A3.1 and A3.2 by joining $E_m(\underline{k}+\delta\underline{k}_n)$ and $\psi_m(\underline{k}_n+\delta\underline{k}_n)$ smoothly on to:

$$E_m(\underline{k}_\ell+\delta\underline{k}_\ell) = E_m(\underline{k}_\ell) + \delta\underline{k}_\ell\cdot\underline{G}_m^{m,\underline{k}_\ell} + \delta k_\ell^2\, E_m^{\underline{k}_\ell} \ldots \qquad \text{A3.18}$$

$$\psi_m(\underline{k}_\ell+\delta\underline{k}_\ell) = e^{i\delta\underline{k}_\ell\cdot\underline{r}}\left[\psi_m(\underline{k}_\ell) + \delta\underline{k}_\ell\cdot\sum_{s\neq m}\underline{G}_m^{m,\underline{k}_\ell}\psi_s(\underline{k}_\ell) + \delta k_\ell^2\,\psi_m^{\underline{k}_\ell}\ldots\right] \qquad \text{A3.19}$$

at $(\underline{k}_\ell+\delta\underline{k}_\ell) = \left(\frac{\underline{k}_n+\underline{k}_\ell}{2}\right) = (\underline{k}_n+\delta\underline{k}_n)$; that is at:

$$\delta\underline{k}_n = \frac{\underline{k}_\ell-\underline{k}_n}{2} = -\,\delta\underline{k}_\ell \qquad \text{A3.20}$$

we require:

$$E_m(\underline{k}_n+\delta\underline{k}_n) = E_m(\underline{k}_\ell+\delta\underline{k}_\ell) \qquad \text{(i)}$$

$$\frac{d\,E_m(\underline{k}_n+\delta\underline{k}_n)}{d(\delta\underline{k}_n)} = -\,\frac{d\,E_m(\underline{k}_\ell+\delta\underline{k}_\ell)}{d(\delta\underline{k}_\ell)} \qquad \text{(ii)} \qquad \text{A3.21}$$

and $\psi_m(\underline{k}_n+\delta\underline{k}_n) = \psi_m(\underline{k}_\ell+\delta\underline{k}_\ell)$ (i)

$$\frac{d\psi_m(\underline{k}_n+\delta\underline{k}_n}{d(\delta\underline{k}_n)} = -\,\frac{d\psi_m(\underline{k}_\ell+\psi\underline{k}_\ell)}{d(\delta\underline{k}_\ell)} \qquad \text{(ii)} \qquad \text{A3.22}$$

The negative signs enter A3.21 (ii) and A3.22 (ii) because $\delta\underline{k}_n$ and $\delta\underline{k}_\ell$ are measured in opposite directions at the point A3.20. Equation A3.21(i) gives:

$$\{E_m(\underline{k}_n) - E_m(\underline{k}_\ell)\} + \left(\frac{\underline{k}_\ell-\underline{k}_n}{2}\right).\left\{G_m^{m,\underline{k}_n} + G_m^{m,\underline{k}_\ell}\right\} + \left(\frac{\underline{k}_\ell-\underline{k}_n}{2}\right)^2\left\{E_m^{\underline{k}_n} - E_m^{\underline{k}_\ell}\right\} = 0 \qquad \text{A3.23}$$

while A3.21(ii) gives

$$\left(\frac{\underline{k}_\ell-\underline{k}_n}{2}\right).\left\{\frac{G_m^{m,\underline{k}_n} - G_m^{m,\underline{k}_\ell}}{2}\right\} + \left(\frac{\underline{k}_\ell-\underline{k}_n}{2}\right)^2\left\{E_m^{\underline{k}_n} + E_m^{\underline{k}_\ell}\right\} = 0 \qquad \text{A3.24}$$

If we add and substract A2.23 and A3.24 we obtain, respectively:

$$E_m^{\underline{k}_n} = \frac{\{E_m(\underline{k}_\ell)-E_m(\underline{k}_n)\} + \left(\frac{\underline{k}_n-\underline{k}_\ell}{4}\right).\left\{3\underline{G}_m^{m,\underline{k}_n}+\underline{G}_m^{m,\underline{k}_\ell}\right\}}{2\left(\frac{\underline{k}_\ell-\underline{k}_n}{2}\right)^2} \qquad \text{A3.25}$$

$$\text{and } E_m^{\underline{k}_\ell} = \frac{\{E_m(\underline{k}_n)-E_m(\underline{k}_\ell)\} + \left(\frac{\underline{k}_\ell-\underline{k}_n}{4}\right).\left\{3\underline{G}_m^{m,\underline{k}_\ell}+\underline{G}_m^{m,\underline{k}_n}\right\}}{2\left(\frac{\underline{k}_n-\underline{k}_\ell}{2}\right)^2} \qquad \text{A3.26}$$

which, as expected, are symmetrical under an interchange of $\underline{k}_n$ and $\underline{k}_\ell$.

Equation A3.22(i) gives:

$$\left\{\text{expi}(\underline{k}_\ell-\underline{k}_n).\underline{r} \quad \psi_m(\underline{k}_n) - \psi_m(\underline{k}_\ell)\right\}$$
$$+ \left\{\text{expi}(\underline{k}_\ell-\underline{k}_n).\underline{r} \sum_{\ell\neq m} \underline{G}_\ell^{m,\underline{k}_n} \psi_m(\underline{k}_n) + \sum_{s\neq m} \underline{G}_s^{m,\underline{k}_\ell} \psi_s(\underline{k}_\ell)\right\} . \left(\frac{\underline{k}_\ell-\underline{k}_n}{2}\right)$$
$$+ \left\{\text{expi}(\underline{k}_\ell-\underline{k}_n).\underline{r} \quad \psi_m^{\underline{k}_n} - \psi_m^{\underline{k}_\ell}\right\}\left(\frac{\underline{k}_\ell-\underline{k}_n}{2}\right)^2 = 0 \qquad \text{A3.27}$$

while A3.22(ii) gives:

$$\left\{\text{expi}(\underline{k}_\ell-\underline{k}_n).\underline{r} \sum_{\ell\neq m} \underline{G}_\ell^{m,\underline{k}_n} \psi_\ell(\underline{k}_n) - \sum_{s\neq m} \underline{G}_s^{m,\underline{k}_\ell} \psi_s(\underline{k}_\ell)\right\} \quad \left(\frac{\underline{k}_\ell-\underline{k}_n}{2}\right)$$
$$+ \left\{\text{expi}(\underline{k}_\ell-\underline{k}_n).\underline{r}\ \psi_m^{\underline{k}_n} - \psi_m^{\underline{k}_\ell}\right\}\left(\frac{\underline{k}_\ell-\underline{k}_n}{2}\right) = 0 \qquad \text{A3.28}$$

Adding and subtracting A3.27 and A3.28 give, respectively:

$$\overset{\underline{k}_n}{\psi_m} = \frac{2}{(\underline{k}_\ell - \underline{k}_n)^2}\left[\{\exp i(\underline{k}_n - \underline{k}_\ell)\cdot\underline{r}\ \psi_m(\underline{k}_\ell) - \psi_m(\underline{k}_n)\}\right.$$

$$\left. + \left(\frac{\underline{k}_n - \underline{k}_\ell}{4}\right)\cdot\left\{3\sum_{\ell\neq m} \underline{G}_\ell^{m,\underline{k}_n}\psi_\ell(\underline{k}_n) + \exp i(\underline{k}_n - \underline{k}_\ell)\cdot\underline{r}\sum_{s\neq m}\underline{G}_s^{m,\underline{k}_\ell}\ s(\underline{k}_\ell)\right\}\right] \qquad \text{A3.29}$$

and

$$\overset{\underline{k}_\ell}{\psi_m} = \frac{2}{(\underline{k}_\ell - \underline{k}_n)^2}\left[\{\exp i(\underline{k}_\ell - \underline{k}_n)\cdot\underline{r}\ \psi_m(\underline{k}_n) - \psi_m(\underline{k}_\ell)\}\right.$$

$$\left. + \left(\frac{\underline{k}_n - \underline{k}_\ell}{4}\right)\cdot\left\{3\sum_{s\neq m} G_s^{m,\underline{k}_\ell}\ \psi_s(\underline{k}_\ell) + \exp i(\underline{k}_\ell - \underline{k}_n)\cdot\underline{r}\sum_{\ell\neq m}\underline{G}_\ell^{m,\underline{k}_n}\psi_\ell(\underline{k}_n)\right\}\right] \qquad \text{A3.30}$$

Thus A3.1, A3.2, A3.18 and A3.19 give smooth and continuous functions of $\underline{k}$ for $E_m(\underline{k})$ and $\psi_m(\underline{k})$ between $\underline{k}_n$ and $\underline{k}_\ell$. The method of appendix II will always give discontinuities in $E_m(\underline{k})$ and $\psi_m(\underline{k})$ unless an infinite number of plane waves are used to build up the Bloch function, $\psi_m(\underline{k})$, and then, of course, the problem is insoluble. The present method gives smooth functions whatever the accuracy we calculate $E_m(\underline{k})$ and $\psi_m(\underline{k})$ to at points such as $\underline{k}_n$ and $\underline{k}_\ell$.

Appendix IV

Fourier Expansion of the potential due to ions in a NaCℓ type structure

The lattice consists of positively charged ions at $\underline{r}_{\ell mn}$ and negatively charged ions at $\underline{r}'_{\ell mn}$. The vectors $\underline{r}_{\ell mn}$ and $\underline{r}'_{\ell mn}$ are defined by 3.2 and 3.3. We shall be essentially concerned with the alkali halides; their highly ionic nature leads us to represent the ions by point charges. The potential an electron in the lattice then feels is:

$$V(\underline{r}) = \frac{Ze^2}{4\pi\epsilon_o} \sum_{\ell mn} \left[\frac{1}{|\underline{r}+\underline{r}_{\ell mn}+a(\underline{i}+\underline{j}+\underline{k})|} - \frac{1}{|\underline{r}+\underline{r}_{\ell mn}|} \right] \qquad A4.1$$

where e, the modulus of the charge of the electron, is also the modulus of the charge on each ion. If $|\underline{r}|$, $|\underline{r}_{\ell mn}|$ and a are measured in metres, $|e|$ in coulombs and $\epsilon_o = 8.85 \times 10^{-12}$ farads/metre then A4.1 gives $V(\underline{r})$ in Joules. We divide A4.1 by the magnitude of the electronic charge to obtain $V(\underline{r})$ in electron volts and write:

$$V(r) = A \sum_{\ell mn} f(\underline{r}+\underline{r}_{\ell mn}) \quad \text{e.V.} \qquad A4.2$$

where

$$A = \frac{Ze}{4\pi\epsilon_o} \qquad A4.3$$

and

$$f(\underline{r}+\underline{r}_{\ell mn}) = \left[\frac{1}{|\underline{r}+\underline{r}_{\ell mn}+a(\underline{i}+\underline{j}+\underline{k})|} - \frac{1}{|\underline{r}+\underline{r}_{\ell mn}\ell|} \right] \qquad A4.4$$

We require now to expand A4.2 in the form:

$$V(\underline{r}) = \sum_{rst} V_{rst} e^{i\underline{g}_{rst}\cdot\underline{r}} \qquad A4.5$$

where $\underline{g}_{rst}$ are the reciprocal lattice vectors given by equation (5) of Chapter III. We now imagine the whole direct lattice to consist of unit cells each of which we denote by a set of integers such that cell(u,v,w) means that unit cell obtained by placing the primitive vectors $\underline{a}_1$, $\underline{a}_2$ and $\underline{a}_3$, given by 3.1, at $\underline{r}_{uvw}$. By equating A4.2 and A4.5, multiplying by $(\exp i\, \underline{g}_{uvw}.\underline{r})^*$ and integrating over cell (ooo) we obtain:

$$V_{uvw} = \frac{A \int_{cell(ooo)} e^{-\underline{i}_{uvw}.\underline{r}} \sum_{\ell mn} f(\underline{r}+\underline{r}_{\ell mn})\, d^3\underline{r}}{\int_{cell\ (ooo)} d^3\underline{r}} \qquad A4.6$$

The denominator in A4.6 is just the volume of the unit cell, Ω:

$$\Omega = a(\underline{j}+\underline{k}).a(\underline{i}+\underline{k})\times a(\underline{i}+\underline{j}) = 2a^3 \qquad A4.7$$

where 2a is the length of the direct lattice cube's edge.

We define $I_{\ell mn}(ooo)$ by:

$$I_{\ell mn}(ooo) = \int_{cell\ (ooo)} e^{-i\underline{g}_{uvw}.\underline{r}} f(\underline{r}+\underline{r}_{\ell mn})\, d^3\underline{r} \qquad A4.8$$

In terms of A4.8, A4.6 becomes:

$$V_{uvw} = \frac{A}{2a^3} \sum_{\ell mn} I_{\ell mn}(ooo) \qquad A4.9$$

If we write:

$$\underline{r}' = \underline{r}+\underline{r}_{\ell mn}$$

then

$$d^3\underline{r}' = d^3\underline{r}$$

and $\exp(-i\underline{g}_{uvw}.\underline{r}) = \exp(-i\underline{g}_{uvw}.\underline{r}')$

because $\quad \underline{g}_{uvw} \cdot \underline{r}_{\ell mn} = 2n\pi$

where n is an integer. We see that A4.8 becomes:

$$I_{\ell mn}(ooo) = \int_{\text{cell } (\ell mn)} e^{-i\underline{g}_{uvw}\cdot\underline{r}'} f(\underline{r}')d^3\underline{r}' = I_{ooo}(\ell mn) \qquad \text{A4.10}$$

The range of integration changes to the cell (ℓmn) because if $\underline{r}$ is in cell (ooo) then $\underline{r}'$ will be in the corresponding position in cell (ℓmn). From A4.9 and A4.10 we have:

$$V_{uvw} = \frac{A}{2a^3} \sum_{\ell mn} I_{ooo}(\ell mn)$$

$$= \frac{A}{2a^3} \int_{\text{all cells}} e^{-i\underline{g}_{uvw}\cdot\underline{r}'} f(\underline{r}')\, d^3\underline{r}'$$

i.e.

$$V_{uvw} = \frac{A}{2a^3} \int_{\text{all space}} e^{-i\underline{g}_{uvw}\cdot\underline{r}} \left[\frac{1}{|\underline{r}+a(\underline{i}+\underline{j}+\underline{k})|} - \frac{1}{|\underline{r}|}\right] d^3\underline{r} \qquad \text{A4.11}$$

If we denote I_1 and I_2 by:

$$I_1 = \int_{\text{all space}} e^{-i\underline{g}_{uvw}\cdot\underline{r}} \frac{1}{|\underline{r}|}\, d^3\underline{r} \qquad \text{A4.12}$$

and $$I_2 = \int_{\text{all space}} e^{-i\underline{g}_{uvw}\cdot\underline{r}} \frac{1}{|\underline{r}+a(\underline{i}+\underline{j}+\underline{k})|}\, d^3\underline{r} \qquad \text{A4.13}$$

and in A4.13 let:

$\underline{r} + a(\underline{i}+\underline{j}+\underline{k}) = \underline{\gamma}$ then we see that

$$I_2 = e^{i\underline{g}_{uvw}\cdot a(\underline{i}+\underline{j}+\underline{k})} \int_{\text{all space}} e^{-i\underline{g}_{uvw}\cdot\underline{\gamma}} \frac{1}{|\underline{\gamma}|}\, d^3\underline{\gamma}$$

$$\text{i.e.} \quad I_2 = e^{ig_{uvw}\cdot a(\underline{i}+\underline{j}+\underline{k})} I_1 = (-1)^{u+v+w} I_1 \qquad \text{A4.14}$$

From A4.12, A4.13, A4.14 and A4.11, we obtain:

$$V_{uvw} = \frac{A}{2a^3}\left[(-1)^{u+v+w} - 1\right] \int_{\text{all space}} \frac{e^{-ig_{uvw}\cdot\underline{r}}}{|\underline{r}|} d^3\underline{r} \qquad \text{A4.15}$$

We now evaluate I:

$$I = \int_{\text{all space}} \frac{e^{-ig_{uvw}\cdot\underline{r}}}{|\underline{r}|} d^3\underline{r}$$

changing to spherical polar co-ordinates:

$$I = \int_0^\infty \int_0^{2\pi} \int_0^{\pi} \frac{e}{r}^{-ig_{uvw}r\cos\theta} r^2 \sin\theta \, d\theta \, d\phi \, dr \qquad \text{A4.16}$$

$$= 2\pi \int_0^\infty \int_0^{\pi} e^{-ig_{uvw}r\cos\theta} r \sin\theta \, d\theta \, dr$$

$$= 2\pi \int_{-1}^{1} \int_0^{\pi} e^{-ig_{uvw}r\cos\theta} r \, dr \, d(\cos\theta)$$

$$\text{i.e. } I = \frac{4\pi}{g_{uvw}} \int_0^\infty \sin g_{uvw} r \, dr \qquad \text{A4.17}$$

If we define $I(\alpha) = \int_0^\infty e^{-\alpha r} \sin g_{uvw} r \, dr$, then

$$I = \frac{4\pi}{g_{uvw}} I(o) \text{ , where } I(o) = \lim_{\alpha \to o} I(\alpha)$$

$$\text{now} \quad I(\alpha) = \frac{g_{uvw}}{\alpha^2 + g_{uvw}^2}$$

so that

$$I(o) = \frac{1}{g_{uvw}}$$

and thus $I = \frac{4\pi}{g_{uvw}^2}$

and so finally A4.15 becomes:

$$V_{uvw} = \left(\frac{z|e|}{2a^3\varepsilon_o}\right) \cdot \frac{[(-1)^{u+v+w}-1]}{g_{uvw}^2} \text{ e.V.} \qquad \text{A4.18}$$

where

$$g_{uvw}^2 = \left(\frac{\pi}{a}\right)^2 \left[(-u+v+w)^2 + (u-v+w)^2 + (u+v-w)^2\right] \qquad \text{A4.19}$$

From A4.18 we see that the even coefficients (i.e.(u+v+w) is an even integer) of the Fourier expansion of $V(\underline{r})$ vanish. The effect of this on the band structure of the alkali Halides is to remove a large number of band-gaps which would exist if these coefficients did not vanish. In particular, we consider those band gaps which give rise to Bragg peaks in the specularly reflected spot for incidence on the (100) faces of the alkali halides; these correspond to reciprocal lattice vectors g_{onn}. According to A4.18, $V_{g_{onn}}$ are zero, and thus no such Bragg peaks should be observed. In general they are observed, and in particular we see them in the results of McRae and Caldwell (9) for Lithium Fluoride. Clearly we need to modify A4.18.

The true potential interaction is very complicated, but there is no reason to expect the Lithium and Fluorine ion interactions with the electrons simply to differ only in sign. Hence additional band gaps will appear. Since we will only be interested in qualitative results, we

simulate this difference by a difference of charge. To avoid the formal difficulty of dealing with a charged crystal, we introduce a uniform charge background which makes the whole crystal neutral. We assume this effects nothing but the inner potential.

Taking differenct charges, A4.18 becomes:

$$V_{uvw} = \left[\frac{(-1)^{u+v+w} - \left(\frac{q^+}{q^-}\right)}{g_{uvw}^2}\right], \text{ where } A = \left(\frac{Za^-}{2a^3\varepsilon_o}\right) \qquad \text{A4.20}$$

and q^+ and q^- are, respectively, the moduli of the charges on the positive and negative ions.

No great qualitative differences will occur if A4.20 is used as opposed to the potential obtained by screening the coulomb potentials of the different ions differently. We can see this as follows. Instead of A4.1, we write:

$$V(\underline{r}) = \frac{Ze^2}{4\pi\varepsilon_o} \sum_{\ell mn} \left[\frac{e^{-\lambda_1|\underline{r}+\underline{r}_{\ell mn}+a(\underline{i}+\underline{j}+\underline{k})|}}{|\underline{r}+\underline{r}_{\ell mn}+a(\underline{i}+\underline{j}+\underline{k})|} - \frac{e^{-\lambda_2|\underline{r}+\underline{r}_{\ell mn}|}}{|\underline{r}+\underline{r}_{\ell mn}|}\right] \qquad \text{A4.21}$$

Then instead of A4.18 we obtain

$$V_{uvw} = \left(\frac{Z|e|}{2a^3\varepsilon_o}\right)\left[\frac{(-1)^{u+v+w}}{\lambda_1^2+g_{uvw}^2} - \frac{1}{\lambda_2^2+g_{uvw}^2}\right] \qquad \text{A4.22}$$

i.e.

$$V_{uvw} = \left(\frac{Z|e|}{2a^3\varepsilon_o}\right)\left[\frac{(-1)^{u+v+w} - \left(\frac{\lambda_1^2+g_{uvw}^2}{\lambda_2^2+g_{uvw}^2}\right)}{(\lambda_1^2+g_{uvw}^2)}\right] \qquad \text{A4.23}$$

Now A4.23 can be easily compared with A4.20. We expect the calculations of Chapter III to give details only of the qualitative behaviour of the reflected intensities. As far as this is concerned we can be satisfied if the potential gives the energy bands in a qualitatively correct manner. From this point of view, we can easily see that A4.20 and A4.23 will give us, qualitatively, the same behaviour of $E(\underline{k})$; there is one proviso: in order that the sign of the even coefficients given by A4.20 and A4.23 are the same, the condition:

$$\lambda_1 > \lambda_2 \qquad \text{(i)}$$

must imply A4.24

$$q^+ > q^- \qquad \text{(ii)}$$

(and, of course, $\lambda_1 < \lambda_2$ must imply $q^+ < q^-$). The screening parameter, λ, is inversely proportional to the screening length so that A4.24(i) is the situation where the negative ion is the most effectively screened. In a sense A4.24(ii) implies the same thing: for fixed $\underline{r}$ the coulomb potential is proportional to q so that A4.24(ii) means that the potential due to the negative ion is weaker.

Thus, as far as the objective of the calculations of chapter III are concerned, it will not matter which of A4.20 and A4.23 we choose. In fact, the simpler form A4.20 is used.

Appendix V

Inner potential as a function of energy for ionic crystals

From the outset we stress that the following analysis is only a rough approach to the problem of evaluating the behaviour of the inner potential as a function of energy. We only hope to obtain a feel for the sort of behaviour that might be anticipated.

For our purposes the crystal can be regarded as a set of independent oscillators which are polarised by an electron traversing the lattice. The self energy of the electron in the resulting field is the inner potential.

If the oscillator is to respond fully to a change in the polarising field, the change occurring in a time $\frac{1}{\omega_n}$ (where ω_n is the oscillator frequency) must be small. When the field is due to an electron travelling with velocity v, we require therefore that:

$$\frac{1}{(d + \frac{V}{\omega_n})^2} \approx \frac{1}{d^2} \qquad \text{A5.1}$$

where d is the distance of the oscillator from the electron. That is, we require:

$$\frac{V}{\omega_n} \ll d \qquad \text{A5.2}$$

Thus, for an order of magnitude estimate of the self energy, we can say that the oscillators within a range $\left(\frac{V}{\omega_n}\right)$ contribute nothing to the self

energy, while those at a greater distance make the same contribution as for a static electron.

The gain in self energy due to the polarisation of the n^{th} oscillator is:

$$S_n = \frac{1}{8\pi} \int (\underline{D}.\underline{E}-D^2)\, d\tau = \frac{1}{8\pi}\left(\frac{1}{\xi_n} - 1\right)\int D^2 d\tau \qquad A5.3$$

where ξ_n is the dielectric constant arising from the oscillator polarisation. From A5.3 and the ideas of the previous paragraph:

$$S_n = \left(\frac{1}{\xi_n} - 1\right) \frac{e^2}{2} \int_{V/\omega_n}^{\infty} \frac{1}{R^2}\, dR$$

i.e.

$$S_n = \frac{e^2\omega_n}{2v}\left(\frac{1}{\xi_n} - 1\right) \qquad A5.4$$

Adding the contributions from all the oscillators, we have for the self energy, S:

$$S = \frac{e^2}{2v} \sum \omega_n \left(\frac{1}{\xi_n} - 1\right) \qquad A5.5$$

Thus the inner potential is inversely proportional to the velocity, i.e. proportional to $E^{-\frac{1}{2}}$.

At sufficiently small velocities the above considerations break down since the electron cannot be localised to better than a de Broglie wavelength, $\frac{\hbar}{mv}$. Hence, for velocities less than the value given by:

$$\frac{\hbar}{mv} = \frac{v}{\omega}$$

i.e.

$$v = \left(\frac{\hbar\omega}{m}\right)^{\frac{1}{2}} \qquad A5.6$$

- our expression is not even roughly valid. The maximum value of $\hbar\omega$ likely to be important is that associated with the plasma oscillations, $\hbar\omega_p$.

Thus, for energies greater than $\hbar\omega_p$, we have:

$$S \propto E^{-\frac{1}{2}} \qquad \text{A5.7}$$

while for energies less than $\hbar\omega_p$ we have

$$S - \text{constant} \qquad \text{A5.8}$$

The values of $\hbar\omega_p$ can be found in the literature, typically: $\hbar\omega_p$ - 10 eV. We fix the proportionality constant in A5.7 as follows. Using a modified Bragg's law, the inner potential (i.e. S), can be determined at the energy of an observed Bragg peak of known order in the specular reflectivity. Then S is known for all energies.

We obtain the modified Bragg's law as follows. In Appendix I we obtained the refractive index:

$$\frac{\sin\theta}{\sin\phi} = \sqrt{1 + \frac{V_o}{E}} \qquad \text{A5.9}$$

while for Bragg peaks in the (0,0) spot:

$$2d\cos\phi = n\lambda' = \frac{n\lambda}{\sqrt{1 + \frac{V_o}{E}}} \qquad \text{A5.10}$$

where d is the spacing of direct lattice planes parallel to the crystal surface, while λ' and λ are respectively the wave lengths in the crystal and the vacuum. Eliminating ϕ from A5.9 and A5.10, we obtain the modified

Bragg's law:

$$2d \cos \theta = \lambda \sqrt{n^2 - \frac{8md^2V_o}{h^2}} \qquad \text{A5.11}$$

For our purposes a more useful form of A5.11 is:

$$E + V_o = \frac{h^2}{2m} \left(\frac{n}{2d \cos \theta} \right)^2 \qquad \text{A5.12}$$

Now, $$\frac{h^2}{2m} = 149.96 - 150 \text{ eV } \mathring{A}^2 \qquad \text{A5.13}$$

so that, if $(E+V_o)$ is measured in eV and d in $\mathring{A}$, we have:

$$(E+V_o) = 150 \left(\frac{n}{2d \cos \theta} \right)^2 \qquad \text{A5.14}$$

Thus, knowing d and n, an appropriate measurement of E determines V_o at that energy.

Well above the plasma energies, $\hbar\omega_p$, the proportionality constant in A5.7, which we denote by A, should indeed approach a constant value if the theory is substantially correct. From A5.7 and A5.14:

$$A = \left\{ 150 \left(\frac{n}{2d \cos \theta} \right)^2 - E \right\} E^{\frac{1}{2}} \qquad \text{A5.15}$$

A suitable test for this simple theory would thus be to check the degree to which A5.15 is constant. We evaluate A for the Bragg peaks of orders 2, 3 and 4 as measured by McRae and Caldwell (9) for LiF, and for the Bragg peaks of orders 3, 4, 5 and 6 as measured by Markland and Andersson (34) for NaCl. The former results were obtained at an angle of incidence of 12°, the latter at 4°. Our results are tabulated in diagram A5.1, where we have evaluated A for normal incidence.

LITHIUM FLUORIDE

Order of Peak	n	Observed Energy	Calculated A		
			$d = 4.02$ Å	$d^* = 4.10$ Å	$d^{**} = 4.15$ Å
2	4	25 ± 2eV	59	54	50
3	6	68 ± 2	128	101	85
4	8	132 ± 2	189	123	85

d : value for an unrelaxed surface

d^* : value used by the experimentalists to obtain the best fit with theory for a constant inner potential (11e.V. for LiF and 8 e.V. for NaF).

d^{**}: value required to obtain the best fit with the theory of this appendix.

SODIUM FLUORIDE

Order of Peak	n	Observed Energy	A $d^{**} = 5.8$ Å	Energy used to obtain the best fit
3	6	33 ± 2eV	51	31.0 e.V
4	8	65 ± 2	57	64.2
5	10	105 ± 2	57	106.0
6	12	156 ± 2	57	156.0

$d = 5.63$ Å $\qquad$ $d^* = 5.77$ Å

DIAGRAM A5.1

We see that our theory can be used to predict the inner potential satisfactorily. The resolution of the experiments is such that either a constant value for the inner potential or the present theory can be used. The essential difference being that our theory requires a larger value of the parameter d. This being the case suggests that the experimentalists have underestimated the surface expansion.

The Bragg peaks of order two for LiF, and of order three for NaF may not occur sufficiently far above the plasma energies for A5.7 to be appropriate. This would explain why the calculated values of A for these peaks are not compatible with the other values. According to Best (33), $\hbar\omega_p$ - 14.5 eV for LiF, while $\hbar\omega_p$ - 16 eV for NaF.

REFERENCES

(1) C. J. Davisson and L. H. Germer, Phys.Rev. 29 (1927) 908 and subsequent papers.

(2) J. J. Lander, Progr.Solid State Chem.2 (1965) 26.

(3) E. G. McRae, Lecture notes: Ghent Summer School on "Fundamental Processes in Semiconductor Surfaces"; University of Ghent, Belgium (1968).

(4) C. B. Duke and C. W. Tucker Jr., PREPRINT: to appear in Surface Science.

(5) A. Sommerfeld and H. Bethe, Handbuch d. Phys.Zeveite Anflage 24/2 (1932) 486.

(6) H. Bethe, Ann.d.Physik 87 (1928) 55.

(7) P. M. Morse, Phys.Rev. 35 (1930) 1310.

(8) V. Heine, Proc.Phys.Soc. 81 (1963) 300.

(9) E. G. McRae and C. W. Caldwell, Surf.Sci. 2 (1964) 509.

(10) G. Gafner, Surf.Sci. 2 (1964) 319.

(11) A. U. MacRae, Surf.Sci. 1 (1964) 319.

(12) J. J. Lander and J. Morrisson, J.Appl.Phys. 36 (1965) 1706.

(13) E. G. McRae, 1966: Journal of Chem.Phys. 45/9 (1966) 3258.
1968a: Surf.Sci. 11 (1968) 479.
1968b: Surf.Sci. 11 (1968) 492.

(14) D. S. Boudreaux and V. Heine, Surf.Sci. 8 (1967) 426.

(15) G. Capart, Surf.Sci. 13 (1969) 361.

(16) E. G. McRae and C. W. Caldwell, Surf.Sci. 7 (1967) 41.

(17) P. J. Estrup and J. Anderson. Surf.Sci. 8 (1967) 101.

(18) K. Kambe, Z. Naturforsch, 23a, (1968) 1280.

(19) P. M. Marcus and D. W. Jepsen: Phys.Rev.Letters 20 (1968) 925, and also notes from the Cornell Conference on LEED (1968).

(20) P. M. Marcus/F. Jona and D. W. Jepsen, I.B.M. Research Publication, R.C. 2326.

(21) J. L. Beeby, J.Phys.Chem. (Proc.Phys.Soc.) Ser.2 1 (1968) 82.

(23) L. I. Schiff, Quantum Mechanics, McGraw-Hill Book Company Inc., (1955) Sec.25, Equation at the top of page 153.

(24) J. J. Quinn, Phys.Rev. 126 (1962) 1455.

(25) C. G. Darwin, Phil.Mag. 27 (1914) 315.

(26) C. Kittel, Quantum Theory of Solids, John Wiley and Sons Inc., (1963) Equation (7) Chapter 1.

(28) N. J. Taylor, Surf.Sci. 4 (1966) 161.

(29) C. W. Palmberg and T. N. Rhodin: to be published in J.Phys.Chem. Solids.

(30) G. C. Benson, P. I. Freeman and E. Dempsey, Solid State Surfaces and the Gas Solid Interface (Advances in Chemistry Series, 33 1961) p26.

(33) P. E. Best, Proc.Phys.Soc. 507 (1962) 133.

(34) I. Markland and S. Andersson, Surf.Sci. 5, (1966) 197.

(35) M. Lax, Rev. Mod. Phys. 23 (1951) 287 and Phys.Rev. 85 (1952) 621.

(36) E. G. McRae, Fundamentals of Gas-Surface Interactions, Academic Press Inc. (1967) 116.

ERRATA

(31) J. B. Pendry. Preprint: The application of pseudo-potentials to LEED: I Calculation of the potential and inner potential.

(32) J. B. Pendry. Private communication.